DISSOLUTION, HYDROLYSIS AND DEHYDRATION OF CELLULOSIC BIOMASS INTO VALUABLE CHEMICALS BY DEEP EUTECTIC SOLVENTS

A dissertation submitted in fulfilment of the requirement for the degree

Master of Science in Chemistry

Joy Salome Dotse

University of Johannesburg

Supervisor: Dr. Banothile C. E. Makhubela

November 2020

DECLARATION

I hereby declare that the thesis: Dissolution, hydrolysis and dehydration of cellulosic biomass into valuable chemicals by deep eutectic solvents: is my original work and has never been presented for the award of any degree in any other university. All information, references and sources used and/or quoted have been duly acknowledged by means of complete physical references.

I grant the University of Johannesburg free license to reproduce the dissertation in whole or in-part for the purpose of research.

Name: Joy Salome Dotse

Signature…….. Date…….

DEDICATION

This dissertation is dedicated to my mom, Madam Emma Zotoo, and my sister, Goodness Dotse.

Thank you both so much for the prayers and immense support and encouragement.

ACKNOWLEDGEMENT

My heartfelt appreciation goes to the Almighty God, to whom is ascribed all the glory, praise, and honor for His everlasting love and guidance in my life.

To my dearest mom and sister, thank you for all your sacrifices towards the success of my education and this thesis.

I specially acknowledge and appreciate my supervisor, Dr. Banothile C. E. Makhubela for her immense support, advice and contribution during the entire project period. She has been a great blessing.

My gratitude also goes to Dr. Leah Matsinha for her brilliant contributions and expertise in proof reading my proposal and thesis. Thanks also to Mr. Novisi Oklu and Mr. Edward Ocansey for their constructive contributions and input as well as availability to help during this period.

Finally to my sponsors, The Royal Society and the African Academy of Sciences' Future Leaders-African Independent Researchers (FLAIR) Scheme for financial assistance thorough my supervisor and to the Department of Chemical Sciences, University of Johannesburg for the opportunity to study here.

The financial assistance of The Royal Society and the African Academy of Sciences' Future Leaders-African Independent Researchers (FLAIR) Scheme toward this research is hereby acknowledged. Results and conclusions attained are those of the author and not necessarily attributed to my sponsors.

TABLE OF CONTENTS

SEMINAR AND CONFERENCE CONTRIBUTIONS

July 2020-Poster presentation: *Cellulose dissolution by a new phosphonium-based deep eutectic solvent: a step towards industrial sugars production*, presented at the Green Chemistry Postgraduate Summer School online 2020, Venice, 20th July 2020.

ABSTRACT

A series of deep eutectic solvents (**DES 1**, **DES 2**, **DES 3** and **DES 4**) have been successfully synthesized and employed as alternative solvents for cellulosic biomass fractionation, dissolution and dehydration. The DESs were synthesized by firstly synthesizing the hydrogen bond acceptors (**HBA 1** and **HBA 2**) followed by mixing these with various hydrogen bond donors (HBDs). **DES 1** is a phosphonium-based DES formed from a phosphonium salt (**HBA 1**) and lactic acid in a molar ratio of 1:10. **DES 2**, **DES 3** and **DES 4** are ammonium-based and were formed from an allyl ammonium salt (**HBA 2**) and methanesulfonic acid, *p*-toluenesulfonic acid monohydrate and oxalic acid dihydrate respectively, in molar ratios of 1:1. The prepared DESs were characterized by Fourier-Transform Infrared Spectroscopy (FT-IR), Nuclear Magnetic Resonance (NMR) spectroscopy, and Elemental Analysis (EA). Some physical parameters of the synthesized DESs were measured, including, melting temperature, pH, viscosity and water content.

DES 1 was employed in the pretreatment/fractionation of raw biomass (*Arundo donax*) where the best conditions for biomass dissolution were established at a biomass loading of 5wt%, a pretreatment time of 12 hours and a temperature of 100^{0}C. Compositional analysis of the solid residue obtained from fractionation suggested that hemicellulose was mostly solubilized during the pretreatment – leaving behind mainly, undissolved lignin and cellulose fibers. The undissolved solid residues were analyzed by FT-IR spectroscopy, scanning electron microscopy (SEM) and Powder X-ray diffraction (P-XRD). **DES 1** was also used in the dissolution of cellulose at a temperature range between 80^{0}C to 120^{0}C over 24hours. The highest dissolution of cellulose was observed at 120^{0}C where 0.83wt % cellulose dissolved.

The hydrolysis of cellulose also was attempted using various catalysts (zeolites, DESs).

DES 2, **DES 3** and **DES 4** were evaluated as both solvents and catalysts in the dehydration of sugars including fructose and glucose to produce 5-HMF where the highest yield of HMF (61%) was observed for the reaction using **DES 4** at 80^0C after 45 minutes. Blackstrap molasses was also used as an alternative feedstock in 5-HMF production and gave *ca* 33% yield per 0.37g of molasses.

LIST OF ABBREVIATIONS AND MEANING OF SYMBOLS

5-CMF	5-chloro hydroxymethyl furfural
5-HMF	5-hydroxymethyl furfural
^{0}C	degrees Celsius
A. donax	*Arundo donax*
AIL	Acid Insoluble Lignin
ASL	Acid Soluble Lignin
bm	broad multiplet (NMR)
bs	broad signal (NMR)
d	doublet (NMR)
dd	doublet of doublets (NMR)
DEEAC	N, N-diethylethanolammonium chloride
DES	Deep Eutectic Solvent
C	cellulose
ca	Approximately
ChCl	Choline chloride
^{13}C {^{1}H} NMR	Carbon Nuclear Magnetic Resonance
EA	Elemental analysis
EF biomass	Extractives-free biomass
FT-IR	Fourier Transform Infrared Spectroscopy
HBA	Hydrogen Bond Acceptor
HBD	Hydrogen Bond Donor
HC	Hollocelulose

^{1}H NMR	Proton Nuclear Magnetic Resonance
IL	Ionic Liquid
J	Coupling constant
m	multiplet (NMR)
MIBK	Methyl isobutyl ketone
msa	Methanesulfonic acid
oxa	Oxalic acid dihydrate
^{31}P {^{1}H} NMR	Phosphorus Nuclear Magnetic Resonance
ptsa	Para toluenesulfonic acid monohydrate
P-XRD	Powder X-Ray Diffraction
q	quartet (NMR)
s	singlet (NMR)
SEM	Scanning Electron Microscopy
t	triplet (NMR)
TEAC	Tetraethylammonium chloride
UV-Vis	Ultra-Violet Visible Spectrophotometry

LIST OF FIGURES

LIST OF SCHEMES

LIST OF TABLES

CHAPTER ONE

Introduction and Literature review

1.1. Background

The world has seen massive development over the years through the use of fossil fuels as an efficient energy source. These energy sources have however, been known to contribute to global warming through the release of greenhouse gases into the atmosphere upon combustion.[1] Energy from fossil fuels is non-renewable and somewhat inefficient and subject to price fluctuations.[2] About one-fifth of the energy used worldwide comes from non-fossil resources, with 14% obtained from biomass, 6% from hydro-electricity and 5% from nuclear sources, depicting that 25% of the world's energy which makes little or no net atmospheric CO_2 contribution is provided by these sources (**Figure 1.1**).[3] Many developed countries of the world are therefore making considerations in terms of biomass energy as a more efficient energy supply option because it is more environmentally friendly.[4]

Biomass can generally be defined as matter originating from living organisms, including plants, animals, microorganisms, or tissues of plants, such as, stems, roots, leaves, and branches.[5] It is an inexhaustible and renewable source of energy as plants can be replaced simply by growing new ones. The use of the energy produced by biomass has the potential to be extended as long as there is the availability of the living organisms from which it is derived.

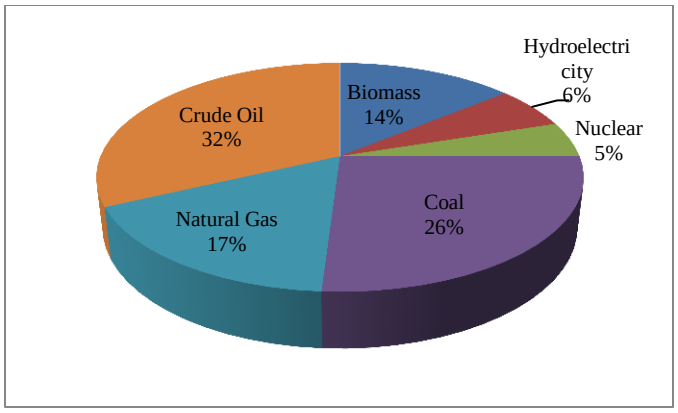

Figure 1.1: World distribution of energy use.[3]

1.2. Lignocellulosic biomass

Biomass of lignocellulose is reportedly the most plentiful renewable resource on the planet.[6] The primary composition of non-edible lignocellulosic biomass is 35-50% cellulose, 20-35% hemicellulose and 10-25% lignin.[7] These components are varied however depending on the part of the plant (**Figure 1. 2**).

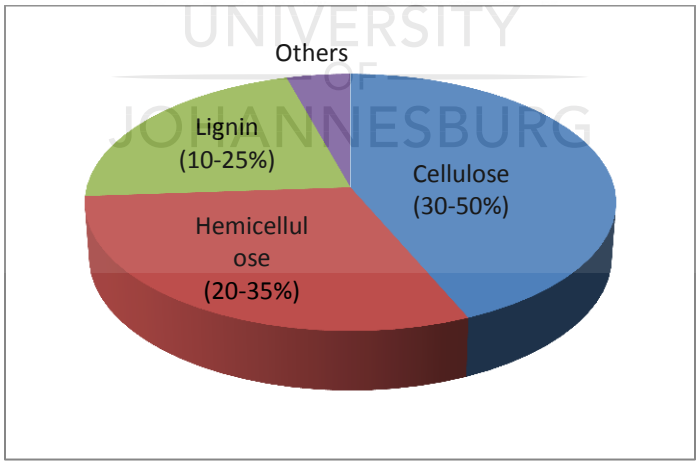

Figure 1.2: Representation of primary components of biomass.[8]

The major structural element of plant cell walls is cellulose which basically is linear chains of glucose units, strongly linked *via* β-1, 4-glycosidic linkages and is responsible for mechanical strength while, hemicellulose is a heterogeneous polymer of C6-sugars (such as galactose, glucose and mannose), pentoses (xylose, arabinose), and sugar acids.[9] Lignin which is created through a biosynthetic process and forms a protective layer around cellulose and hemicellulose is composed of three aromatic alcohols (*p*-coumaryl alcohol, coniferyl alcohol, and sinapyl alcohol and) (**Figure 1. 3**).[10,11]

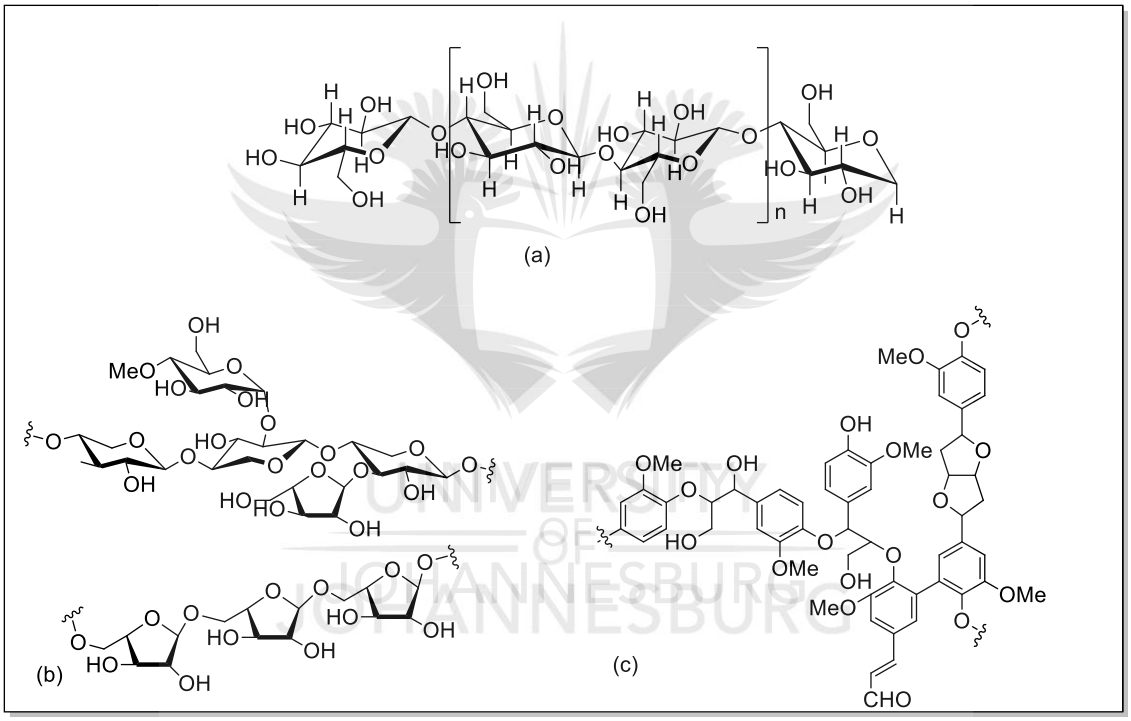

Figure 1.3: Structure of the primary components of biomass (a) Cellulose (b) Hemicellulose (c) Lignin.

1.3. Biomass as a source of various products

Lignocellulosic biomass can serve as a renewable feedstock for biochemicals and biofuels production through a variety of methods of conversion (**Scheme 1.1**). Additionally, large quantities of industrial chemicals are manufactured as by-products from the manufacturing of

biofuels. For example, glycerol which can further be used as a platform chemical for the production of various value-added chemicals and products.[12]

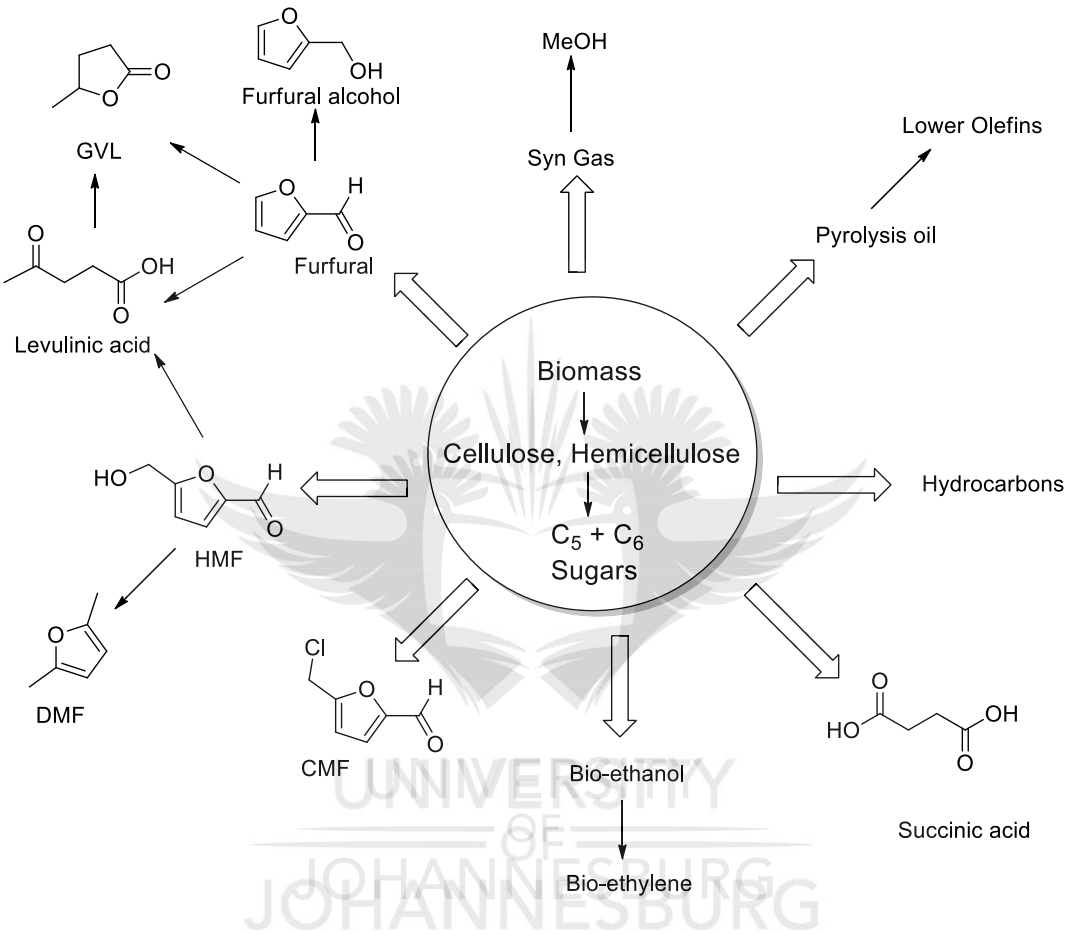

Scheme1.1: Examples of some useful platform chemicals and bio-fuels obtained from biomass.[13]

1.4. Biomass pretreatment

A number of methodologies and techniques have been considered as inexpensive methods of pretreatment for separating the components of lignocellulose to generate higher yields of sugars.[14]

Cellulose crystalline nature and the presence of lignin and acetyl groups of lignocellulosic biomass account for the need for pretreatment, so as to enhance enzymatic digestibility or acid hydrolysis into sugars for further conversion into fine chemicals and liquid fuels.[15] Valorization of lignocellulose, a material that is insoluble in most solvents, requires a method of pretreatment that involves effective solubilization of its complex and resilient structure.[16] As such leading approaches involve either biological, physical and/or chemical pre-treatment, to make it more susceptible to hydrolysis and degradation for the making of valuable products and biofuels.[17]

The roles of effective pretreatment includes very importantly, minimal heat and power requirements, the use of cost-effective reactors, the enhancing of the yields of sugar during enzyme hydrolysis, minimal formation of fermentation inhibitors , the preservation of the pentoses and lignin recovery for conversion into value-added products.[18]

1.4.1. Biological pretreatment

In biological pretreatment processes, microorganisms, usually fungi that can produce enzymes that break down lignin and hemicellulose are employed.[19] However, it has disadvantages, the most common and important being the time-consuming treatment process and the achievement of low biomass digestibility in most cases.[20] White-rot fungi show the most efficiency in degrading and mineralizing lignin and plant cell walls.[21]

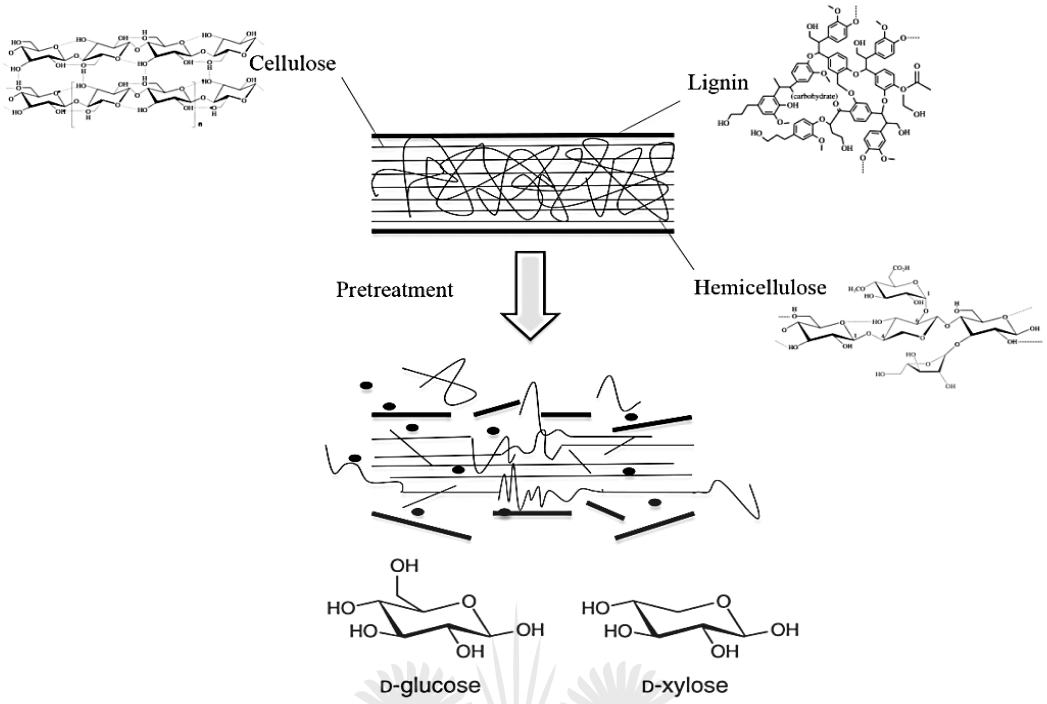

Figure 1.4: Schematic showing pretreatment of lignocellulosic biomass.[22]

1.4.2. Physical pretreatment

Physical pretreatment refers to the process of mechanical breakdown by milling, chipping or grinding in a way to reduce biomass particle size.[23,24] Reduction in biomass particle size during physical pretreatment also results in reduction in crystallinity of cellulose thereby enhancing biodegradability and subsequent hydrolysis.[11] Other physical methods of pretreatment include irradiation with microwave, gamma rays, and electron beams.[25]

Some pretreatment models are termed physicochemical because they employ both physical and chemical processes. Examples of these are steam explosion, Ammonia Fibre Explosion (AFEX) Ammonia Recycle Percolation (ARP), and pretreatment with eletrocatalysts.[26]

1.4.3. Chemical pretreatment

Chemical pretreatments using mineral acids have been applied on several biomass feedstocks including corn stover, poplar, and switchgrass. These treatments are based on the use of either dilute or concentrated mineral acids, such as hydrochloric acid or sulfuric acid.[27] The limitations of this approach is in the use of acids which results in 1) corrosion of reactors and other equipment leading to high costs as a result of frequent maintenance and/or buying special corrosive-resistant reactors;[28,29] 2) there is also the challenge of large volumes of acid effluent which arises in the process. In subsequent steps, there may be a reduced overall yield of sugars as a result of the formation of secondary products by dehydration of the sugars to furfural[30] and 5-hydroxyl-methyl furfural (5-HMF)[31] and formation of humins. These secondary reactions lead to interference in subsequent fermentation processes.

Alkali pretreatments are less expensive because they consume low-to-moderate energy. Calcium hydroxide ($Ca(OH)_2$), ammonia (NH_3), and sodium hydroxide (NaOH), are common examples of bases used.[15,32] A limitation associated with alkali pretreatment is the formation of irrecoverable salts by the conversion of some of the alkali through reactions involved in pretreatment.[23]

Another promising method of chemical pretreatment is the use of ionic liquids (ILs) and deep eutectic solvents (DESs). Pretreatment with Ionic Liquids, compared with other pretreatment models (for example, use of dilute acids), has shown a high level of delignification and reduction in cellulose crystallinity by distorting the hydrogen bonding in cellulose better than other pre-treatment techniques.[33] ILs pretreatment increases the surface area of biomass for subsequent hydrolysis and have been shown to effectively solubilize switchgrass by removing about 52.4% lignin.[34]

1.5. Ionic Liquids (ILs) and Deep Eutectic Solvents (DESs)

A different class of neoteric solvents has recently emerged since the world's search for greener and cleaner technologies in industry and academia began. The search for alternative solvents that will replace the already existing harmful and expensive ones is of utmost importance.[35] Deep eutectic solvents and ionic liquids are termed Low-Melting Mixtures (LMMs) or Low-Transition Temperature Mixtures because of their low melting temperatures.[36] They are also referred to as liquids that are close to the eutectic composition of their mixtures, i.e., the molar ratio of the components at which the lowest melting point is obtained.[37] **Figure 1.5** shows a phase behavior diagram of a two-component deep eutectic solvent system formed from a salt and a hydrogen bond donor (HBD) showing the depression in freezing point of the eutectic mixture leading to lower melting point, relative to the melting point of the starting materials. DESs can be designed according to the specific applications, consequently meeting the demands of green chemistry.

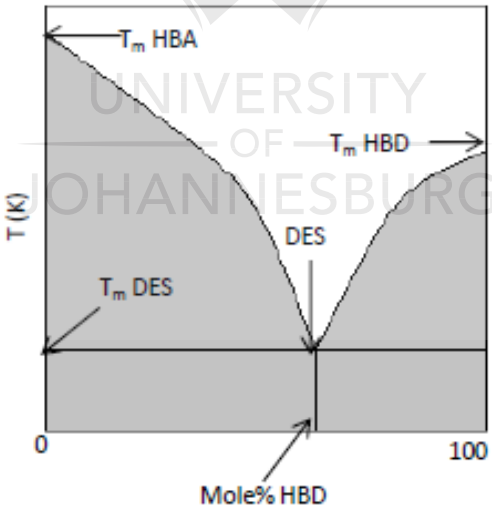

Figure 1.5: Phase behavior diagram of a two-component system showing eutectic point[38]

DESs are usually classified as analogs of ionic liquids because they share similar characteristics and properties. However, DESs cannot be completely considered as ILs because DESs may contain or be made from uncharged (non-ionic) species[39]. Ionic liquids are solvents of molten salts with a melting point below 100 degrees Celsius or at room temperature, containing organic cations and organic or inorganic anions,[40] while DESs are made from the mixing or complexation of a salt (usually formed from any ammonium, sulfonium, or phosphonium cation and a Lewis base usually a halide ion) with amines, alcohols, or carboxylic acids known as hydrogen bond donors (HBD).[41,37] The main driving force for the formation of deep eutectic solvents is hydrogen bonding and Van der Walls interactions.[42] A typical formation of a DES is shown by the interaction of choline chloride and urea in a molar ratio of 1:2. (**Scheme 1.2**)

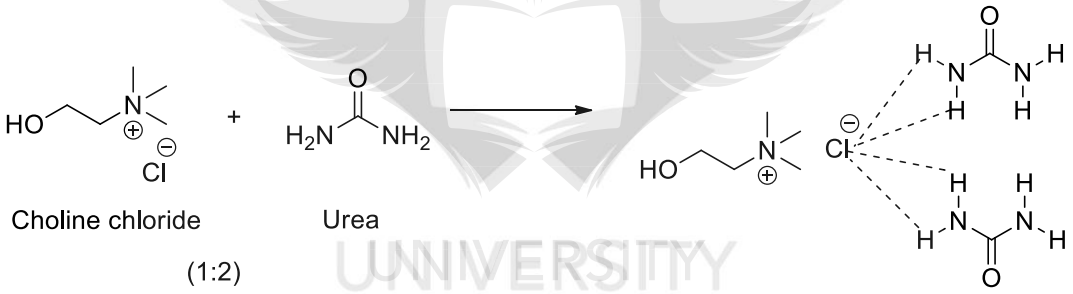

Scheme 1.2: Formation of choline chloride –urea DES[43]

Several groups of DESs have been developed and thus named and distinguished depending on the nature of their properties (for example, their diversity of acidic character), uses, and sometimes the source of their components. Examples of these groups include, DESs with a tunable acidic character, known as Acidic Deep Eutectic Solvents, (ADES) usually termed as Brönsted and Lewis acidic DES which are classified based on the nature and ratio of the complexing agents designed to replace the toxic mineral acids and the expensive and unstable solid acids employed in chemical processes.[44] Therapeutic Deep Eutectic Solvents (THEDES)

are DESs with components acting as Active Pharmaceutical Ingredients (APIs). These systems act by improving the solubility and adsorption of model APIs.[45] Natural Deep Eutectic Solvents (NADES) are also formed when primary metabolites, such as organic acids, sugars, amino acids, and urea or choline derivatives form a eutectic mixture.[46]

1.6. Preparation of deep eutectic solvents

The preparation of DES is described by the following approaches;

The most commonly used method is the method of heating which involves mixing, heating, and stirring the compounds until a clear homogenous liquid is formed.[47]

Another common method of DES preparation is the grinding method which involves forming a homogenous liquid by mixing and grinding the components in a mortar and with a pestle at room temperature.[48]

Apart from these methods, the freeze-drying method which involves the mixing of aqueous solutions of the components followed by the freezing and subsequent freeze-dry to obtain a viscous homogenous liquid is also used, however rarely because the water is seen to interact with the DES components and is not fully removed from the freeze-dried mixture.[49]

The evaporation method of DES preparation has also been developed where the components are dissolved in water using a rotary device and evaporated at 50^{0}C to obtain a homogenous liquid which is stored in a silica gel desiccator to obtain constant mass value.[47]

1.7. Classifications of deep eutectic solvents

The classification of DESs has largely depended on the nature of the complexing agents used. [50] In general, deep eutectic solvents can be defined by the formula $Cat^{+}\ X^{-}\ zY$, where Cat^{+} is

usually any ammonium, phosphonium, or sulfonium cation, X^- is a Lewis base (anion) which complexes with a *z* number of either a Lewis or Brønsted acid Y(metal salt or hydrogen bond donor, HBD) **Table 1.1**.[37] DESs are however classified by the nature of their complexing agents.

Table 1.1: Classification of deep eutectic solvents[37]

Type	General Formula	Terms
I	$Cat^+ X^- \times z\ MCl_x$ (quaternary halide + metal halide)	M = Zn^{II}, Sn^{II}, Al^{III}, Ga^{III}, In^{III}; X = Cl, Br
II	$Cat^+ X^- \times z\ MCl_x \times y\ H_2O$ (quaternary halide + metal halide hydrate)	M = Cr^{III}, Co^{II}, Cu^{II}, Fe^{II}, Ni^{II}; X = Cl, Br
III	$Cat^+ X^- \times z\ RZ$ (quaternary halide + hydrogen bond donor)	Z = $CONH_2$, COOH, OH; X = Cl, Br
IV	$MCl_x + RZ = (MCl_{x-1})^+ \times RZ + (MCl_{x+1})^-$ (metal halide hydrate + hydrogen bond donor)	M = Al^{III}, Zn^{II}; Z = $CONH_2$, OH

1.7.1 Type I: DES based on metal halides/substituted quaternary salt mixtures

Deep Eutectic Solvents that act as Lewis acid catalysts have received increasing attention especially in the electrochemistry and photochemistry fields. Until recently, research dating back to 1979 and later has focused on pyridinium cations with chloroaluminate anions. However, the sensitivity of these aluminum halide-alkylpyridinium halide-melts to water[51] has hindered their widespread applications and given way to the development of DESs with other cations and Lewis acid counterparts. It has been shown by Lin and coworkers that molten salts can be formed using zinc chlorides and imidazolium salts in their work on the electrodeposition of zinc on glassy carbon and nickel substrates[52] and the electrodeposition of copper and copper-zinc

alloys on tungsten and nickel electrodes in a zinc chloride-1-ethyl-3-methylimidazolium chloride molten salt.[53] The electrodeposition of amorphous Co-Zn alloy has also been demonstrated by Koura *et al* from an ambient temperature molten salt electrolyte, $CoCl_2$-$ZnCl_2$-1-butyl pyridinium chloride system.[54] Ionic liquid analogs (DESs) having properties such as air and water insensitivity have been developed using zinc or tin chlorides with substituted quaternary ammonium salts such as choline chloride following reports from Abbott and coworkers.[55] More recently, the team reported the chemical and electrochemical properties of ionic liquids formed by $ZnCl_2$, $SnCl_2$, and $FeCl_3$ with a variety of quaternary ammonium salts.[56]

1.7.2. Type II: DES formed from hydrated metal salts and quaternary salts

The incorporation of hydrated metal salts into ionic liquid analogs has enhanced their applications in electrochemical processes owing to the limited series of anhydrous metal salts that form DESs with quaternary ammonium salts (such as choline chloride) as demonstrated by Abbott *et al* in their work on the electrodeposition of chromium using a hydrated chromium chloride-choline chloride system ($CrCl_3.6H_2O$-ChCl).[57] Shahbaz *et al* also synthesized novel Choline chloride-Calcium chloride hexahydrate DESs and investigated their use as phase change materials.[58]

1.7.3. Type III: DES formed from quaternary salts and hydrogen bond donors

The most commonly used class of DES is formed from quaternary ammonium salts such as ChCl and hydrogen bond donors (HBD) such as urea, lactic acid, etc., and are seen to possess unique solvent properties.[59] This type of DES is the most commonly known class given that there exists a large group of HBDs (including amides, alcohols, amines, and carboxylic acids) that can be used in making them, also because of the simple process of preparation and low cost.[60] **Figure 1.7** shows some examples of common HBA and HBD used in making Type III DESs. Abbott et

al have studied and characterized mixtures of carboxylic acids such as oxalic acid, malonic acid, phenyl propionic acid, and succinic acid with choline chloride.[61] They concluded that the phase behavior and physical properties of these DESs depended on the composition of the mixture, the alkyl/aryl substituents, and the number of acid functionalities.

1.7.4. Type IV: DES formed from metal-containing anions and hydrogen bond donors

Abbott and co-workers have proven the possibility of forming deep eutectic solvents from metal salts and simple organic alcohols and amides by synthesizing a DES from $ZnCl_2$ and donor molecules such as ethylene glycol, 1,6-hexanediol, urea, and acetamide.[50] A series of lanthanide nitrate hydrate- urea deep eutectic solvents (L_n= Ce, Pr, Nd) have also been synthesized and used in the efficient combustion synthesis of lanthanide oxides by Hammond and co-workers.[62] To prove that metal halide-amide mixtures are capable of behaving as ionic liquids, Abood and colleagues synthesized a DES with $AlCl_3$ and acetamide to form a liquid of the form $[AlCl_2.nAmide]^+ AlCl_4^+$ where it was applied as a medium for the electrodeposition of aluminum and the acetylation of ferrocene.[63]

1.8. Properties of deep eutectic solvents

Eutectic mixtures share certain properties of ILs including non-volatility, biodegradability, recyclability and non-reactivity,[64] in addition to possessing lower melting points than that of the components they are made of.[65] Although DESs are advanced analogs of ILs, one factor which puts them over conventional ILs is that, the preparation of ILs requires the removal of trace amounts of impurities of synthesis reagents, whereas, with DES, no purification after synthesis is needed since no new salts are formed and purity depends on that of the individual components.[66]

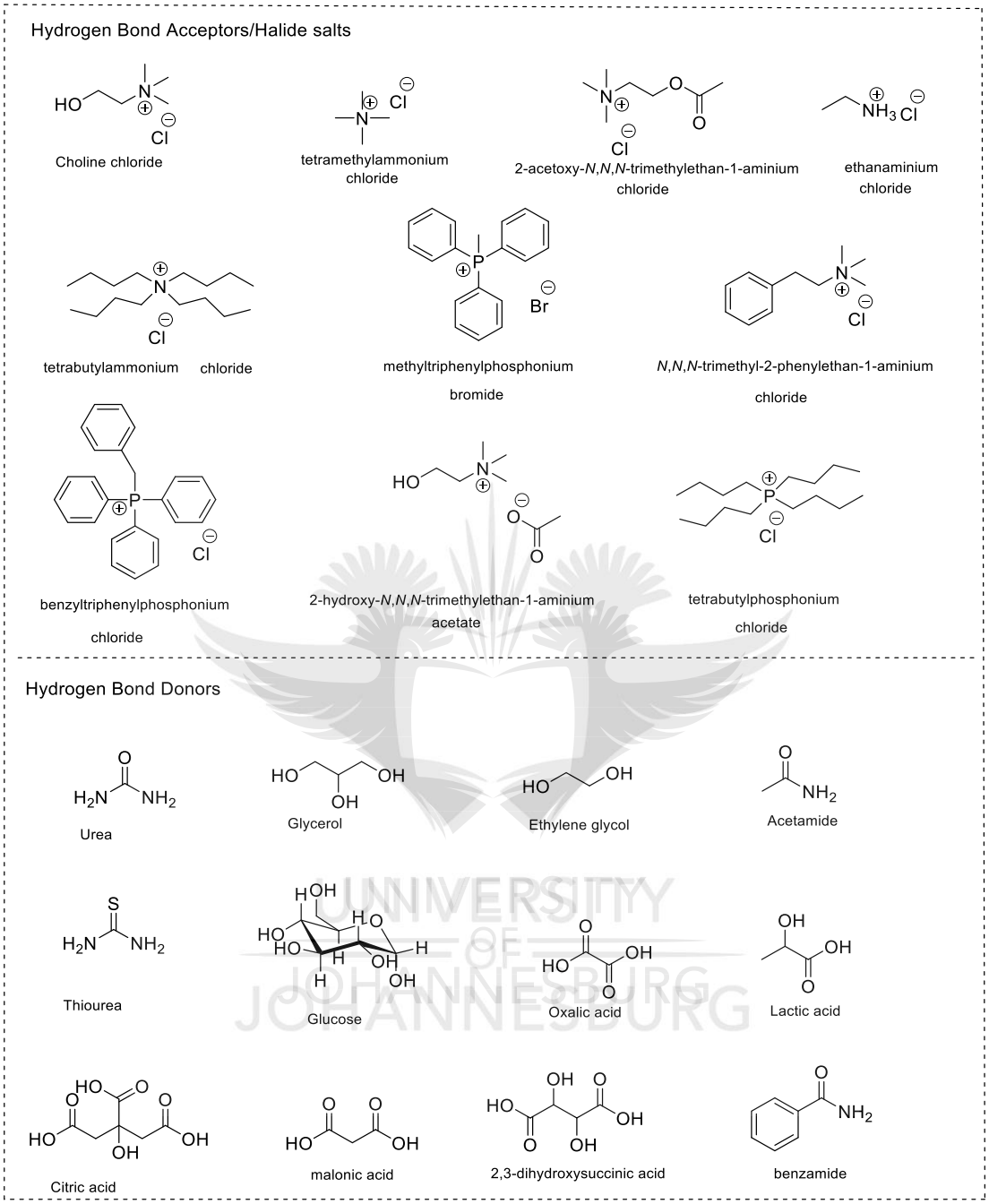

Figure 1.6: Examples of typical HBAs and HBDs for Type III DES synthesis[67, 68]

Additionally, ILs and DESs vary in their chemical properties but tend to possess similar physical properties particularly in their ability to be designed with the desired properties of freezing point,

viscosity, density and conductivity[37,39] (**Table 1.2**) among others which are seen to be related to each other and dependent on temperature, water content, HBA/HBD ratio, etc.[69]

Table 1.2: Composition and physical properties of commonly used DES at 25^{0}C (if not specified).[39,70]

HBA	HBD	Molar Ratio (HBA: HBD)	Freezing Point [^{0}C]	Density [g/cm^3]	Viscosity [cP]	Conductivity [mS/cm]
Choline chloride	Urea	1:2	12	1.24	632	0.75
Choline chloride	Ethylene glycol	1:2	-66	1.12	36	7.61
Choline chloride	Glycerol	1:2	-40	1.18	376	1.05
Choline chloride	Malonic acid	1:1	10	-	721	0.55
Choline chloride	$ZnCl_2$	1;2	-	-	-	0.06 (42^{0}C)
Methyltriphenylphosphonium bromide	Glycerol	1:3	-5.55	1.30	-	0.062
Methyltriphenylphosphonium bromide	Ethylene glycol	1:4	-49.34	1.23	-	1.092
Methyltriphenylphosphonium bromide	Triethylene glycol	1:5	-21	1.19	-	-
$ZnCl_2$	Urea	1:3.5	9	1.63	11,340	0.18 (42^{0}C)
Acetyl Choline chloride	Urea	1:2	-	1.206	2214 (40^{0}C)	0.017 (40^{0}C)
Tetra-n-butylammonium bromide	Imidazole	3:7	-	-	810 (20^{0}C)	0.24 (20^{0}C)
Choline chloride	1, 4-butanediol	1:3	-32	1.06	140 (20^{0}C)	1.64

1.8.1. Freezing point

Having established that DESs are formed from the association of molecules by hydrogen bonding, the depression in their freezing points is attributed to the organic salt/HBD ratio and the level of interaction between the HBD and the anion.[39] The decrease in DES freezing points is attributed to the delocalization of charge caused by hydrogen bonding between the halide anion of the HBA and the HBD.[71] Abbott *et al* investigated the freezing point of choline salts with urea.[59] It was observed that the freezing points of the DESs decreased in the order $F^- > NO_3^- > Cl^-$

> BF_4^- suggesting that the freezing points are indeed related to the hydrogen bonding strength of the anions.

1.8.2. Viscosity

The viscosities of DESs are reported to be higher than ILs due to lowered mobility of free species as a result of large ion size, electrostatic forces (Van der Waal), strong hydrogen bonding network between the components, and water content.[39,69] An increase in temperature, leading to increased movement of ions could hence decrease the viscosity of DESs.[39] This can be applied to the high viscosities observed for phosphonium salt-based DES compared to ammonium salt-based DES as investigated by Alomar *et al.*[72] Sugar-based DESs reportedly have higher viscosities compared to others and this can be ascribed to the strong hydrogen bonding network formed by the number of OH groups present.[73] A study by Al-Murshedi relates the viscosity of DES with the density of the hydrogen bond donor.[69] According to this study, Reline (ChCl-urea) showed the highest viscosity and hydrogen bond density (13.8 bonds nm^{-3}) followed by Glyceline, ChCl-glycerol (10.8 bonds nm^{-3}) and Ethaline, ChCl-ethylene glycol (9.4 bonds nm^{-3}).[69] The use of the Hole Theory can be applied in the formation of DES with decreased viscosities as well as increased conductivities by the use of fluorinated HBDs and small cations.[74]

1.8.3. Density

As reported by Garcia *et al*, the density of DESs is influenced also by the ratio of HBD to HBA (steric effects) as well as the strength and extension of ions-HBD.[75] By comparison with literature density data, Garcia and coworkers outline that density increases with the number of OH groups for DESs formed with HBDs with hydroxyl groups and decreases with the introduction of aromatic groups. Furthermore, density decreases with an increasing chain length

of diacid DESs (oxalic > malonic > glutaric).[75] Shahbaz *et al*, observed a decrease in the densities of nine DESs with an increase in temperature. This was ascribed to the reason that at a higher temperature, the kinetic energy of molecules increases creating more space, resulting in decreased density. They also observed that the densities of the DESs lie between that of the individual DES components used in their synthesis.[76]

1.8.4. Conductivity

The ionic conductivities of DESs are reportedly low and this is as a result of their high viscosities as previously stated. As studied by Abbott, by decreasing the size of cations as well as the surface tension of liquids to increase the size of cavities, optimal conductivities can be achieved.[74] Water plays a role in the conductivity as well as the viscosity and density of DES as reported by Azhar et al on the study of the ionic conductivities of commonly known DES, reline, glyceline, ethaline, and oxaline.[69] There is an inverse relationship observed between the viscosity and conductivity of DES. According to the group, high viscosities affect the conductivities of DES as it leads to high cell resistances. Ethaline showed the highest conductivity (and lowest viscosity) while reline showed the lowest conductivity (and highest viscosity). An increase in both temperature and water content of all the DES resulted in an increase in conductivity as a result of the decrease in viscosity.

1.8.5. Toxicity and biodegradability

In considering DESs as alternative solvents, knowledge of their toxicity and biodegradability is important for the design of environmentally friendly solvents. DESs are usually assumed to be associated with low toxicity and biodegradability because they are usually obtained from safer components. Juneidi and coworkers have evaluated the toxicity and biodegradability of 3 types of DESs on freshwater fish and fungi.[77] The DESs used were ChCl-based and N, N-diethyl

ethanol ammonium chloride-based (EAC) DES with ethylene glycol, glycerol, urea, and malonic acid as HBDs in addition to $ZnCl_2$ and Zinc nitrate hexahydrate (ZnN) as metal salts. Generally, ChCl-based DES (Type III) showed lower toxicities compared to EAC-based DES towards *Aspergillus niger*. Interestingly, higher toxicities were observed by the DES mixtures compared to their individual components. The high toxicities of EAC-ZnN and EAC-ZnCl (Type I and II) DES was attributed to the inherent toxicity of the metal salts. Similar results were observed in investigating the acute toxicities of the DESs on freshwater fish (*Cyprinus carpio*). The biodegradability test in water was more than 60% for all DESs.

1.9. Applications of deep eutectic solvents

The emergence of ionic liquids (ILs) as potential alternative solvents in industrial applications stems from many reasons. Some physical properties of ILs that make them promising solvents in synthesis include: (1) their ability to solubilize a wide range of inorganic and organic materials, (2) they possess the potential to have high polarities since they are entirely composed of ions yet are non-coordinating solvents, (3) they are capable of forming non-aqueous bi-phasic systems with many organic solvents as they are immiscible and more importantly (4) they measure negligible vapor pressures (are non-volatile).[78]

As equivalents of ionic liquids, an advantage DESs have over conventional solvents is their wide application in numerous fields of science due to their tunability, recyclability, biodegradability, non-toxicity, and low cost as previously stated.

Deep eutectic solvents have been reported to play multiple roles not only as reaction media or solvents but also simultaneously as catalysts and reagents[79] for many reactions. They have been employed in many aspects of chemistry including inorganic reactions involving the synthesis of

inorganic materials,[80] electrochemistry, and electrodeposition,[81,82] solubility of metal oxides,[83] organic reactions including acid and base-catalyzed reactions,[84] polymerization reactions,[36] biomass processes,[85] etc. Properties of deep eutectic solvents such as the dissolution of reactants and catalysts, recovery of reaction products, recycling of catalysts as well as their ability to be conserved in various reactions make them a preferred choice over many conventional solvents as reaction media.[86]

1.9.1. Application of DESs in biomass processes (cellulose dissolution and biomass fractionation)

The intricate structure of biomass and the presence of glycosidic linkages in the structure of biomass fractions such as cellulose encourage the formation of hydrogen bonds between cellulose chains which makes it challenging for chemical or biological (enzymes or bacteria) atcion, depolymerization, and further processing into value-added products.[87] The use of DESs has been reported to be promising methods of biomass conversion and valorization because they are capable of forming hydrogen bonds with molecules by accepting and donating protons hence promoting the solubilization of biopolymers.[88]

In 2011, Zhang *et al* investigated the rapid decrystallization of microcrystalline cellulose (MCC) using ChCl-based DESs where they observed almost no solubilization of cellulose in both ChCl-Urea (1:2) and ChCl-$ZnCl_2$ (1:2) DESs.[89] Ren *et al* demonstrated the dissolution of cellulose cotton linter pulp activated by ultrasound-assisted saturated calcium chloride solution in a series of ChCl- based DESs.[90] ChCl-Im DES showed the highest solubility (2.48wt %) followed by ChCl-U (1.43wt %). The addition of a co-solvent, polyethylene glycol (PEG), which reduces the hydrophobicity of cellulose improved the dissolution of cellulose in the ChCl-Im system (4.57wt %). Thereafter, the same authors reported the dissolution of 6.48wt% of cellulose in an allyl-functionalized DES.[91]

Acidic DESs have particularly been found to be effective in selectively solubilizing lignin from biomass feedstock.

The work done by Francisco *et al* showed the high solubility of lignin (up to 14.9wt% at 100^0C in malic acid/proline DES, 1:3) compared to cellulose and starch.[92] The use of lignin-derived DES synthesized from ChCl-lignin-derived phenols (4-hydroxybenyl alcohol, catechol, vanillin, and p-coumaric acid) as HBD for the delignification of switchgrass was also reported.[93]

According to Vigier and co-workers, the strong cohesive forces in the cellulose fibrils hinder its interaction with the DES due to the strong hydrogen bonding networks in both the DES and cellulose resulting in the selective solubilization of lignin over cellulose.[88] In a two-stage DES treatment of rice straw, it showed that the malic acid-proline/ChCl-urea (MP-CU) treated biomass facilitated delignification and removal of xylan which was evident in the small amount of lignin remaining in the undissolved residue. ChCl-oxalic acid /ChCl-urea (CO-CU) treatment was effective in lignin and hemicellulose removal resulting in high content of cellulose in the residues hence increase glucose yields after hydrolysis of residues by enzymes.[94] The extraction of hemicellulose from biomass has been a challenging issue as it depends on the disintegration of lignin-carbohydrate complexes (LCC) that are formed from hydrogen bonding between lignin functional groups and hemicelluloses.[70]

1.10. Hydrolysis of celluloses and hemicelluloses

To effectively promote the conversion of lignocellulosic biomass into useful end products (platform chemicals and biofuels), the biopolymers of biomass have to be depolymerized to obtain fermentable sugars. This basically involves the breaking of the glycosidic linkages in the cellulose and hemicellulose structure. It has been well established that enzymes (e.g. cellulase

enzymes) are effective in the hydrolysis of cellulose to glucose.[95] Other methods of hydrolyzing cellulose to simple sugars include the use of mineral acids like sulphuric acid[96] and solid acids like zeolites[97], among others. Noble metal catalysts (e.g. supported ruthenium catalysts) have also recently been described to be beneficial in the hydrolysis of cellulose and the dehydration of sugars.[98]

Acidic deep eutectic solvents have been reported to behave as effective hydrolytic media for dissolving cellulosic pulp. Hu *et al*, investigated the depolymerization and subsequent dehydration of inulin, a polymer of fructose to 5-HMF using choline chloride-citric acid and choline chloride-oxalic acid DES.[99] The yield of HMF was 56% and 51% for ChCl-oxalic acid and ChCl-citric acid DESs respectively at reaction conditions of 80^{o}C over 2 hours. Sirvio and co-workers have reported the successful fabrication of cellulose nanocrystals (CNCs) using choline chloride/oxalic acid dihydrate DES.[100] More recently, Hu and co-workers have combined DES pretreatment and carbon-based solid acid catalyst in the hydrolysis of pretreated corn stover for glucose production in which hemicellulose was mostly hydrolyzed in the pretreatment process.[101]

1.11. Dehydration of sugars

As illustrated in **Figure 1.3**, it can be observed that the precursors for various value-added chemicals are furan-based which are derived from the dehydration of hexoses and pentoses (C_6 and C_5 sugars) from cellulose and hemicellulosic feedstock. For example, 5-hydroxymethylfurfural (HMF) is considered a key bio-based platform chemical due to its use as a bio-refinery building block.[102] It is useful in the production of other chemicals such as levulinic

acid.[103] Furfural, another furan-based chemical is also used worldwide in the production of furfural alcohol used in the making of polymers and plastics.[104]

A variety of acid catalysts have been reported to give notable yields of chemical intermediates such as HMF following dehydration of carbohydrates. Examples of these acid catalysts include metal chlorides (e. g. $CrCl_3$)[105], noble metal catalysts [98], homogenous acid catalysts such as acidic ionic liquids,[106] and sulphuric acid (H_2SO_4) .[107]

Subcritical/supercritical solvents can be used as catalysts for many reactions including dehydration. Water in the subcritical state acts as an effective acid and/or base catalyst and has been used in the making of HMF and lactic acid.[108] HCl in supercritical water has been employed in the dehydration of sugars as well.[109]

However, the corrosion of reactors from the use of acids coupled with other factors such as toxicity and environmental issues has directed attention towards considering green solvents (DES) and heterogeneous catalysts such as CO_2/H_2O and zeolites as alternative catalysts for the dehydration of sugars.

HMF has been produced from many DESs including Type I, II, and III DESs as well as low melting mixtures comprising of an HBA and a sugar as the HBD. Lewis acids have also been used together with the DESs in HMF production. Some yields of HMF in DES and low melting mixtures stated in the literature are reported below;

Table 1.3: Reaction conditions for 5-HMF production in DESs; [a] Biphasic system with ethyl acetate and DES. [b] 10mol% of catalyst (based on sugar) used. [c] Molar ratio of ChCl to the substrate (low melting mixtures) [d] HMF yield is calculated in g/g, 10mol% sulfuric acid used as the catalyst. [e] MCC:DES ratio (1:25), 1.42% $SnCl_4$ used. [f] biphasic system with ethyl-n-butyrate

HBA	HBD or Catalyst	Molar ratio	Temp. [^{0}C]	Time [hours]	Substrate	HMF yield	ref
ChCl	Citric acid	-	80	1	Fructose	77.6	[110]
ChCl	Citric acid	-	80	1	Fructose	91.4[a]	[110]
ChCl	Citric acid	2:1	80	2	Inulin	51	[99]
ChCl	Oxalic acid	1:1	80	2	Inulin	56	[99]
ChCl	Oxalic acid	1:1	80	2	Inulin	64[a]	[99]
ChCl	$CrCl_2$[b]	5:5[c]	100	1	Sucrose	42	[111]
ChCl	$CrCl_2$[b]	4:6[c]	110	0.5	Glucose	45	[111]
ChCl	pTsOH[b]	5:5[c]	90	1	Inulin	57	[111]
ChCl	pTsOH[b]	4:6[c]	100	0.5	Fructose	67	[111]
TEAC	$CrCl_3.6H_2O$[b]	-	130	0.167	Glucose	71.3	[112]
TEAC	$CrCl_3.6H_2O$[b]	-	130	0.167	Fructose	73.8	[112]
TEAC	$CrCl_3.6H_2O$[b]	-	130	0.167	Sucrose	76.4	[112]
TEAC	$CrCl_3.6H_2O$[b]	-	130	0.167	Cellobiose	60.7	[112]
DEAC	Ptsa	1:0.5	80	1	Fructose	84.8	[113]
ChCl	Citric acid	2:1	130	0.083	fructose	15.02[d]	[114]
ChCl[e]	Oxalic acid	1:2	160	1.5	MCC	11	[115]
ChCl[f]	Oxalic acid	-	140	2	MCC	29.8	[116]

1.12. Motivation of research

There is an increase in demand for cheaper and greener technologies to replace the use of conventional solvents for lignocellulosic biomass conversion to value-added chemicals. The recalcitrant structure of cellulose in the cell wall of lignocellulosic biomass allows the formation of strong hydrogen bonds between the cellulose network, which makes it hard for attack by chemical or biological means for its effective dissolution and hydrolysis,.[7,87] Hence, it is

desirable to develop greener and effective solvents to enable biomass conversion through its dissolution and hydrolysis ahead of further conversion to value-added platform chemicals.

The use of acids and other methods tend to be hazardous and expensive. Hence, several procedures and techniques have been evaluated for developing inexpensive pretreatment methods to generate high yields of sugars and value-added chemicals such as 5-HMF from cellulosic biomass.[14] Ionic Liquid (ILs) analogues known as Deep Eutectic Solvents (DES) offer less hazardous and in-expensive solvents for the solubilization of cellulosic biomass and they have gained popularity since their advent. They are regarded as green solvents due to their non-volatility, biodegradability, recyclability, and non-reactivity.[64]

Phosphonium-based DESs have not been seriously explored as solvents for the fractionation of biomass or the dissolution of cellulose. They have however been applied in CO_2 capture[117,118] as well as solvents for the removal of glycerol from palm oil-based biodiesel.[119] All DESs reported for the fractionation of biomass and the dissolution of cellulose are ammonium-based DESs and little is known about the efficacy of phosphonium-based DESs in biomass conversion. Considering the effect on the physical and chemical properties of DESs as a result of the type of HBA used, we explored the effect of phosphonium-based DESs in the pretreatment of biomass and the dissolution of cellulose after investigating several physical properties including viscosity, pH and water content. The DESs 2-4 have their HBAs structurally similar to choline chloride which has shown to be effective in dehydration of sugars when used with different HBDs. This work hence demonstrates the use of three allyl-ammonium-based DESs (in place of the famously used cholinium-based DES) as solvent and catalysts in the dehydration of sugars into valuable platform molecules. The results of using these DESs are expected to be different from what has been reported in the literature because of the different HBAs used in this work.

1.13. Research Aim and objectives

The main aim of this project was to design, synthesize and characterize DESs and to evaluate their ability to fractionate, dissolve, hydrolyze and dehydrate cellulosic biomass into valuable products.

1.13.1. Specific objectives

1. To synthesize and characterize quaternary phosphonium (**Figure 1.7 DES 1)** and ammonium-based (**Figure 1.7 DES 2-4)** deep eutectic solvents.

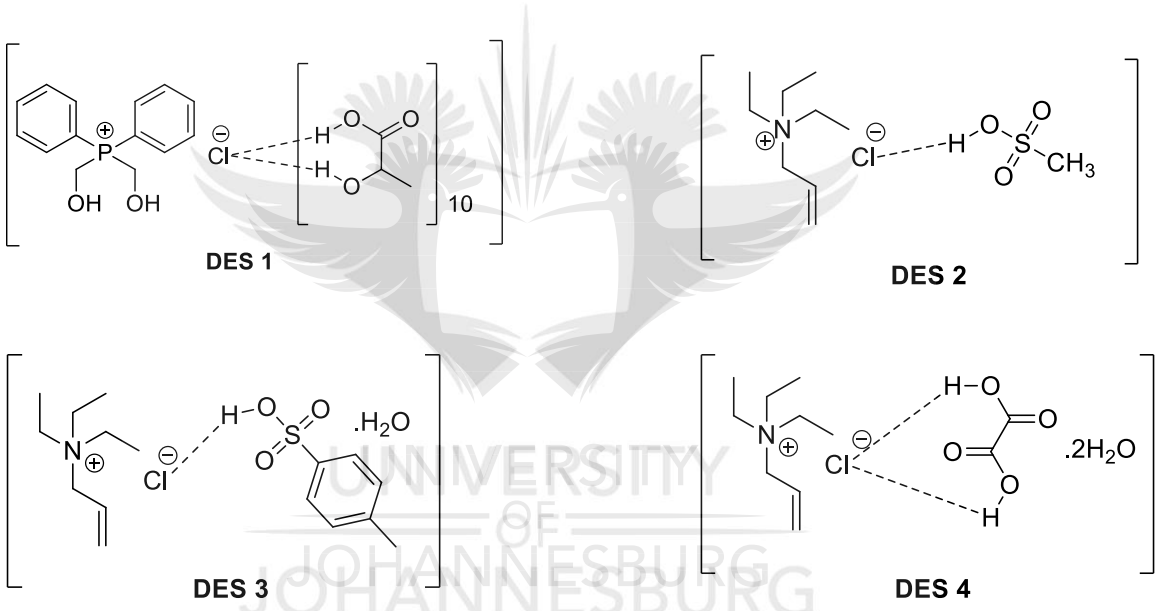

Figure 1.7: Deep eutectic solvents

2. To apply the synthesized DESs in the dissolution and pretreatment of biomass.
3. To apply the DESs in the dissolution of cellulose and its further hydrolysis. Hydrolysis by DESs and a zeolite as catalysts.
4. To dehydrate the sugars into furfural and HMF using DESs and zeolites as catalysts (**Scheme 1.4**)

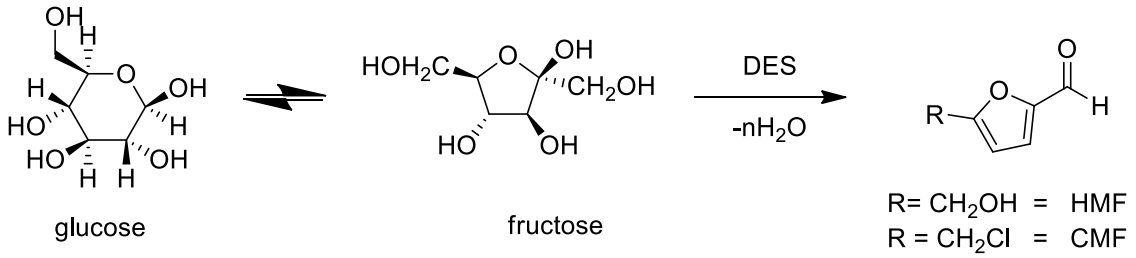

Scheme 1.3: hydrolysis of cellulose and hemicellulose to monomeric sugars

5. To characterize all synthesized products using various spectroscopic and analytical techniques.

1.14. References

1 R. E. H. Sims, W. Mabee, J. N. Saddler and M. Taylor, *Bioresour. Technol.*, 2010, **101**, 1570–1580.

2 M. K. Hubbert, *Am. Assoc. Adv. Sci.*, 1949, **109**, 103–109.

3 J. M. O. Scurlock and D. O. Hall, *Biomass*, 1990, **21**, 75–81.

4 C. W. Lewis, *Biomass*, 1981, **1**, 5–15.

5 R. A. Houghton, in *Small*, 2008, pp. 448–453.

6 E. de Jong and R. J. A. Gosselink, in *Bioenergy Research: Advances and Applications*, Elsevier, 2014, pp. 277–313.

7 A. Avci, B. C. Saha, G. J. Kennedy and M. A. Cotta, *Bioresour. Technol.*, 2013, **142**, 312–319.

8 B. C. Saha, 2009, 2–34.

9 B. C. Saha, *J. Ind. Microbiol. Biotechnol.*, 2003, **30**, 279–291.

10 F. G. Calvo-Flores and J. A. Dobado, *ChemSusChem*, 2010, **3**, 1227–1235.

11 V. Menon and M. Rao, *Prog. Energy Combust. Sci.*, 2012, **38**, 522–550.

12 M. Pagliaro, R. Ciriminna, H. Kimura, M. Rossi and C. Della Pina, *Angew. Chemie - Int. Ed.*, 2007, **46**, 4434–4440.

13 R. A. Sheldon, *Green Chem.*, 2014, **16**, 950–963.

14 B. Yang and C. E. Wyman, *Biofuels, Bioprod. Biorefining*, 2008, **2**, 26–40.

15 V. S. Chang, W. E. Kaar, B. Burr and M. T. Holtzapple, *Biotechnol. Lett.*, 2001, **23**,

1327–1333.

16 I. M. O'Hara, Z. Zhang, W. O. S. Doherty and C. M. Fellows, in *Green Chemistry for Environmental Remediation*, 2012, pp. 505–560.

17 S. Banerjee, *Biofuels, Bioprod. Biorefining*, 2009, 77–93.

18 G. Brodeur, E. Yau, K. Badal, J. Collier, K. B. Ramachandran and S. Ramakrishnan, *Enzyme Res.*, 2011, **2011**, 1–17.

19 Isroi, R. Millati, C. Niklasson, M. N. Cayanto, M. J. Taherzadeh, K. Lundquist and Others, *BioResources*, 2011, **6**, 5224–5259.

20 R. Castoldi, A. Bracht, G. R. de Morais, M. L. Baesso, R. C. G. Correa, R. A. Peralta, R. de F. P. M. Moreira, M. de L. T. de M. Polizeli, C. G. M. de Souza and R. M. Peralta, *Chem. Eng. J.*, 2014, **258**, 240–246.

21 C. Susana, M. J. Maria and M. T. Angel, *Biofuels, Bioprod. Biorefining*, 2014, **8**, 615–625.

22 M. A. Kassim, H. P. . A. Khalil, N. A. Serri, M. H. M. Kassim, M. I. Syakir, N. A. S. Aprila and R. Dungani, in *Intech*, 2016, pp. 329–355.

23 N. Mosier, C. Wyman, B. Dale, R. Elander, Y. Y. Lee, M. Holtzapple and M. Ladisch, *Bioresour. Technol.*, 2005, **96**, 673–86.

24 Y. H. Oh, I. Y. Eom, J. C. Joo, J. H. Yu, B. K. Song, S. H. Lee, S. H. Hong and S. J. Park, *Korean J. Chem. Eng.*, 2015, **32**, 1945–1959.

25 B. A. Saville, in *Plant Biomass Conversion*, 2011, pp. 199–226.

26 L. J. Chen and F. Lin, *Arch. Des Sci.*, 2012, **65**, 626–642.

27 M. von Sivers and G. Zacchi, *Bioresour. Technol.*, 1995, **51**, 43–52.

28 Z. Anwar, M. Gulfraz and M. Irshad, *J. Radiat. Res. Appl. Sci.*, 2014, **7**, 163–173.

29 C. E. Wyman, *Development*, 1999, **24**, 189–226.

30 E. R. Garrett and B. H. Dvorchik, *J. Pharm. Sci.*, 1969, **58**, 813–820.

31 Y. Sun and J. J. Cheng, *Bioresour. Technol.*, 2005, **96**, 1599–1606.

32 M. Asgher, Z. Ahmad and H. M. N. Iqbal, *Ind. Crops Prod.*, 2013, **44**, 488–495.

33 C. Li, B. Knierim, C. Manisseri, R. Arora, H. V. Scheller, M. Auer, K. P. Vogel, B. A. Simmons and S. Singh, *Bioresour. Technol.*, 2010, **101**, 4900–4906.

34 A. M. Socha, R. Parthasarathi, J. Shi, S. Pattathil, D. Whyte, M. Bergeron, A. George, K. Tran, V. Stavila, S. Venkatachalam, M. G. Hahn, B. A. Simmons and S. Singh, *Proc. Natl. Acad. Sci.*, 2014, **111**, E3587–E3595.

35 Thomas Welton, *Chem. Rev.*, 1999, **99**, 2071–2083.

36 M. Jablonsky, A. Škulcov and S. Jozef, *Molecules*, 2019, **24**, 1–33.

37 E. L. Smith, A. P. Abbott and K. S. Ryder, *Chem. Rev.*, 2014, **114**, 11060–11082.

38 A. Paiva, R. Craveiro, I. Aroso, M. Martins, R. L. Reis and A. R. C. Duarte, *ACS Sustain. Chem. Eng.*, 2014, **2**, 1063–1071.

39 Q. Zhang, K. De Oliveira Vigier, S. Royer and F. Jérôme, *Chem. Soc. Rev.*, 2012, **41**, 7108–46.

40 S. Ahrens, A. Peritz and T. Strassner, *Angew. Chemie - Int. Ed.*, 2009, **48**, 7908–7910.

41 M. A. Kareem, F. S. Mjalli, M. A. Hashim and I. M. Alnashef, *J. Chem. Eng. Data*, 2010, **55**, 4632–4637.

42 M. Espino, M. D. L. Á. Fernández, F. J. V Gomez and M. F. Silva, *Trends Anal. Chem.*, 2015, 1–27.

43 N. Azizi, S. Dezfooli and M. Mahmoodi, *Chem. Reports*, 2013, **16**, 1098–1102.

44 H. Qin, X. Hu, J. Wang, H. Cheng, L. Chen and Z. Qi, *Green Energy Environ.*, 2019, 1–47.

45 C. V Pereira, J. M. Silva, L. Rodrigues, R. L. Reis, A. Paiva, A. R. C. Duarte and A. Matias, *Sci. Rep.*, 2019, **9**, 1–11.

46 Y. H. Choi, J. Van Spronsen, Y. Dai, M. Verberne, F. Hollmann, I. W. C. E. Arends, G. Witkamp and R. Verpoorte, 2011, **156**, 1701–1705.

47 Y. Dai, J. Van Spronsen and G. Witkamp, *Anal. Chim. Acta*, 2013, **766**, 61–68.

48 T. El, S. Fourmentin and H. Greige-gerges, *J. Mol. Liq.*, 2019, **288**, 111028.

49 G. C. Maria, L. Ferrer, C. R. Mateo and F. Monte, *Langmuir*, 2009, **25**, 5509–5515.

50 A. P. Abbott, J. C. Barron, K. S. Ryder and D. Wilson, *Chem. - A Eur. J.*, 2007, **13**, 6495–6501.

51 J. Robinson and A. Osteryoung, *J. theAmerican Chem. Soc.*, 1979, **101**, 323–327.

52 Y. Lin and I. Sun, *Electrochim. Acta*, 1999, **44**, 2771–2777.

53 P. Chen, M. Lin and I. Sun, *J. Electrochem. Soc.*, 2000, **147**, 3350–3355.

54 N. Koura, T. Endo and Y. Idemoto, *J. Non. Cryst. Solids*, 1996, **205**–**207**, 650–655.

55 A. P. Abbott, G. Capper, D. L. Davies, H. L. Munro, R. K. Rasheed and V. Tambyrajah, *Chem. Commun.*, 2001, **1**, 2010–2011.

56 A. P. Abbott, G. Capper, D. L. Davies and R. Rasheed, *Inorg. Chem.*, 2004, **43**, 3447–

3452.

57 A. P. Abbott, G. Capper, D. L. Davies and R. K. Rasheed, *Chem. - A Eur. J.*, 2004, **10**, 3769–3774.

58 K. Shahbaz, I. M. Alnashef, R. J. T. Lin, M. A. Hashim, F. S. Mjalli and M. M. Farid, *Sol. Energy Mater. Sol. Cells*, 2016, **155**, 147–154.

59 A. P. Abbott, G. Capper, D. L. Davies, R. K. Rasheed and V. Tambyrajah, *Chem. Commun.*, 2003, 70–71.

60 L. S. Longo and M. V. Craveiro, *J. Braz. Chem. Soc.*, 2018, **29**, 1999–2025.

61 A. P. Abbott, D. Boothby, G. Capper, D. L. Davies and R. Rasheed, *J. Am. Chem. Soc.*, 2004, **126**, 9142–9147.

62 O. S. Hammond, D. T. Bowron and K. J. Edler, *ACS Sustain. Chem. Eng*, 2019, **7**, 4932–4940.

63 H. M. A. Abood, A. P. Abbott, D. Ballantyne and K. S. Ryder, *Chem. Commun.*, 2011, **47**, 3523–3525.

64 D. Carriazo, M. C. Serrano, M. C. Gutiérrez, M. L. Ferrer and F. Del Monte, *Chem. Soc. Rev.*, 2012, **41**, 4996–5014.

65 T. Li, G. Lyu, Y. Liu, R. Lou, L. A. Lucia, G. Yang, J. Chen and H. A. M. Saeed, *Int. J. Mol. Sci.*, , DOI:10.3390/ijms18112266.

66 J. Gorke, F. Srienc and R. Kazlauskas, *Biotechnol. Bioprocess Eng.*, 2010, **15**, 40–53.

67 V. A. Pereira, P. V. Mendonça, J. F. J. Coelho and A. C. Serra, *Polym. Chem.*, 2019, **00**, 1–11.

68 P. Xu, G. W. Zheng, M. H. Zong, N. Li and W. Y. Lou, *Bioresour. Bioprocess.*, 2017, **4**, 1–18.

69 A. Y. M. Al-Murshedi, H. F. Alesary and R. Al-Hadrawi, *J. Phys.*, 2019, **1294**, 1–20.

70 A. Satlewal, R. Agrawal, S. Bhagia and J. Sangoro, *Biotechnol. Adv.*, 2018, **36**, 2032–2050.

71 P. Domínguez de María, *J. Chem. Technol. Biotechnol.*, 2014, **89**, 11–18.

72 M. Khalid, M. Hayyan, M. Abdulhakim and S. Akib, *J. Mol. Liq.*, 2016, **215**, 98–103.

73 A. Hayyan, F. S. Mjalli, I. M. Alnashef, Y. M. Al-Wahaibi, T. Al-Wahaibi and M. A. Hashim, *J. Mol. Liq.*, 2013, **178**, 137–141.

74 A. P. Abbott, G. Capper and S. Gray, *ChemPhysChem*, 2006, **7**, 803–806.

75 G. Garcia, S. Aparicio, R. Ullah and M. Atilhan, *Energy and Fuels*, 2015, **29**, 2616–2644.

76 K. Shahbaz, F. S. Mjalli, M. A. Hashim and I. M. Alnashef, *Thermochim. Acta*, 2011, **515**, 67–72.

77 I. Juneidi, M. Hayyan and M. Ali Hashim, *RSC Adv.*, 2015, **5**, 83636–83647.

78 T. Welton, *Biophys. Rev.*, 2018, **10**, 691–706.

79 C. Ruß and B. König, *Green Chem.*, 2012, 1–14.

80 E. R. Parnham, E. A. Drylie, P. S. Wheatley, A. M. Z. Slawin and R. E. Morris, *Angew. Chemie - Int. Ed.*, 2006, **118**, 5084–5088.

81 A. P. Abbott, G. Capper, K. J. Mckenzie and K. S. Ryder, 2007, **599**, 288–294.

82 A. P. Abbott, C. J. Collins, B. I. Dalrymple, B. R. C. Harris, R. Mistry, A. F. Qiu, A. J. Scheirer and W. R. W. A, *Aust. J. Chem.*, 2009, **62**, 341–347.

83 A. P. Abbott, G. Capper, D. L. Davies, K. J. Mckenzie and S. U. Obi, *J. Chem. Eng. Data*, 2006, **51**, 1280–1282.

84 F. Ilgen and K. Burkhard, *Green Chem. Chem.*, 2009, **11**, 848–854.

85 M. Jablonsky and S. Josef, *Deep Eutectic Solvents in Biomass Valorizarion*, 2019.

86 Y. Marcus, *Sustain. Chem. Eng.*, 2017, **5**, 11780–11787.

87 S. R. Decker, J. Sheehan, D. C. Dayton, J. J. Bozell, W. S. Adney, B. Hames, S. R. Thomas, R. L. Bain, S. Czernik, M. Zhang and M. E. Himmel, *Handb. Ind. Chem. Biotechnol. Twelfth Ed.*, 2012, **2**–**2**, 1249–1322.

88 K. D. O. Vigier, G. Chatel and F. Jørôme, *ChemCatChem*, 2015, **00**, 1–12.

89 Q. Zhang, M. Benoit, K. D. O. Vigier and J. Barrault, *Chem. - A Eur. J.*, 2012, **18**, 1043–1046.

90 H. Ren, C. Chen, Q. Wang, D. Zhao and S. Guo, *BioResources*, 2016, **11**, 5435–5451.

91 H. Ren, C. Chen, S. Guo, D. Zhao and Q. Wang, *BioResources*, 2016, **11**, 8457–8469.

92 M. Francisco, A. Van Den Bruinhorst and M. C. Kroon, *Green Chem.*, 2012, **14**, 2153–2157.

93 K. H. Kim, T. Dutta, J. Sun, B. Simmons and S. Singh, *Green Chem.*, 2018, **20**, 809–815.

94 X. Hou, G. Feng, M. Ye, C. Huang and Y. Zhang, *Bioresour. Technol.*, 2017, **238**, 139–146.

95 Y. H. P. Zhang and L. R. Lynd, *Biotechnol. Bioeng.*, 2004, **88**, 797–824.

96 S. E. Jacobsen and C. E. Wyman, *Appl. Biochem. Biotechnol. - Part A Enzym. Eng. Biotechnol.*, 2000, **84**–**86**, 81–96.

97 O. Ayumu, O. Takafumi and Y. Kazumichi, *Green Chem.*, 2008, **10**, 1033–1037.

98 B. C. E. Makhubela and J. Darkwa, *Johnson Matthey Technol. Rev.*, 2018, **62**, 4–31.

99 S. Hu, Z. Zhang, Y. Zhou, J. Song, H. Fan and B. Han, *Green Chem.*, 2009, **11**, 873–877.

100 J. A. Sirviö, M. Visanko and H. Liimatainen, *Biomacromolecules*, 2016, 1–22.

101 S. Hu, F. Meng, D. Huang, J. Huang and W. Lou, *SN Appl. Sci.*, 2020, **2**, 1–12.

102 A. A. Rosatella, S. P. Simeonov, R. F. M. Frade and C. A. M. Afonso, *Green Chem.*, 2011, **13**, 754–793.

103 J. Jow, G. L. Rorrer, M. C. Hawley and D. T. A. Lamport, *Biomass*, 1987, **14**, 185–194.

104 A. Dias, A.S., Lima, S., Pillinger, M., Valente, *Ideas Chem. Mol. Sci. Adv. Synth. Chem.*, 2010, 165–186.

105 A. R. Aylak, S. Akmaz and S. N. Koc, *Part. Sci. Technol.*, 2017, **35**, 490–493.

106 A. S. Amarasekara and B. Wiredu, *Bioenergy Res.*, 2014, **7**, 1237–1243.

107 T. Horvath, L. Qi, Y. F. Mui, S. W. Lo, M. Y. Lui and G. R. Akien, *ACS Catal.*, 2014, **4**, 1470–1477.

108 F. Jin, Z. Zhou, T. Moriya, H. Kishida, H. Higashijima and H. Enomoto, *Environ. Sci. Technol.*, 2005, **39**, 1893–1902.

109 A. S. Feridoun and H. Yoshida, *Ind. Eng. Chem. Res.*, 2007, **46**, 7703–7710.

110 S. Hu, Z. Zhang, Y. Zhou, B. Han, H. Fan, W. Li, J. Song and Y. Xie, *Green Chem.*, 2008, **10**, 1280–1283.

111 F. Ilgen, D. Ott, D. Kralisch, C. Reil and K. Burkhard, *Green Chem.*, 2009, **11**, 1948–1954.

112 L. Hu, Y. Sun and L. Lin, *Ind. Eng. Chem. Res.*, 2012, **51**, 1099–1104.

113 A. Assanosi, M. M. Farah, J. Wood and B. Al-Duri, *Comptes Rendus Chim.*, 2016, **19**, 450–456.

114 W. C. Chen, Y. C. Lin, I. M. Chu, L. F. Wang, S. L. Tsai and Y. H. Wei, *Biochem. Eng. J.*, 2019, **154**, 107440.

115 H. Yang, J. Lang, J. Lu, P. Lan and H. Zhang, *BioResources*, 2020, **15**, 3344–3355.

116 J. Lang, J. Lu, P. Lan, N. Wang, H. Yang and H. Zhang, *Catalysts*, 2020, **10**, 1–12.

117 E. Ali, M. K. Hadj-kali, S. Mulyono and I. Alnashef, *Chem. Eng. Res. Des.*, 2014, **92**, 1898–1906.

118 J. Wang, H. Cheng, Z. Song, L. Chen, L. Deng and Z. Qi, *Ind. Eng. Chem. Res.*, 2019, **58**,

17514–17523.

119 K. Shahbaz, F. S. Mjalli, M. A. Hashim and I. M. AlNashef, *Energy & Fuels*, 2011, **25**, 2671–2678.

CHAPTER TWO

Synthesis and characterization of deep eutectic solvents

2.1. Introduction

Compared to ionic liquids, DESs are easily prepared with their purity depending only on the purity of their starting components.[1] Various methods of preparing deep eutectic solvents have been in recent times developed. Dai and coworkers have described the vacuum evaporation and heating methods of preparing DESs.[2] The heating method, being the most commonly used method involves the mixing and heating of the DES components while stirring until a homogenous mixture is formed. This method is usually performed to obtain DESs with a known amount of water. In the vacuum evaporation method, the components of the DES are dissolved in water, and using a rotary evaporator, the water is removed. The mixture is then stored in a desiccator until a constant weight is reached. The grinding method of preparing DESs is based on mixing the components of the DES and grinding them in a mortar with a pestle until a clear homogenous mixture is formed.[3] A newer method of DES synthesis described by Guiterrez involves the freeze-drying of the mixture of the aqueous solutions of the individual components of the DES.[4] It is notable that the amount of water and its effect in DES is important as most common DESs are hygroscopic or have hygroscopic components. Water, by itself, due to its polarity may act as a donor or acceptor of hydrogen bonding, hence may form strong interactions with the components of hygroscopic DESs.[5] The water content in DES is commonly measured by the Karl Fischer titration method. Other methods of revealing the presence of water by observing its hydrogen bonding in DES is by FT-IR spectroscopy.

In this chapter, we report the synthesis of four deep eutectic solvents, including a phosphonium-based DES (**DES 1**) and ammonium-based DESs (**DES 2-4**). These DESs are prepared by the

heating and mixing method. **DES 3** has been reported by Ren et al, who used this DES in the dissolution of cellulose.[6]

2.2. Results and discussion

The formation of a deep eutectic solvent is a result of the complexation of a hydrogen bond acceptor, (HBA) and a hydrogen bond donor (HBD). Two halide salts (phosphonium and ammonium salts) were prepared and used as HBAs with different HBDs. The deep eutectic solvents were prepared by the heating method by mixing the halide salts with the various hydrogen bond donors in different molar ratios and heating the mixture under stirring until a clear homogenous solution was formed. The mixtures were then allowed to cool at room temperature. Upon cooling, the solutions with molar compositions or ratios that remained liquid at room temperature were chosen for subsequent experiments and stored in a desiccator. The DESs are characterized by Fourier transform –infrared spectroscopy (FT-IR) and Nuclear Magnetic Resonance spectroscopy (NMR). The viscosities, pH and water content, and melting temperatures of these DES have also been measured and reported.

2.2.1. Synthesis and characterization of HBA 1 and HBA 2

To synthesize **HBA 1**, The phosphonium salt, bis(hydroxymethyl) diphenylphosphonium chloride, ($C_{14}H_{16}ClO_2P$) was prepared according to the procedure by Fawcett et al (**Scheme 2.1**).[7] The secondary phosphine, diphenylphosphine, was treated with aqueous formaldehyde and concentrated hydrochloric acid to yield white crystalline solids in 80% yield, soluble in polar solvents such as methanol and water. The melting point range of the salt was determined to be 158°-160°C. The reaction of the less basic diphenylphosphine and carbonyl compounds in concentrated hydrochloric acid under mild conditions is thought to proceed through a normal

carbonyl addition.[8] The salt was characterized by FT-IR, elemental analysis, and NMR spectroscopy.

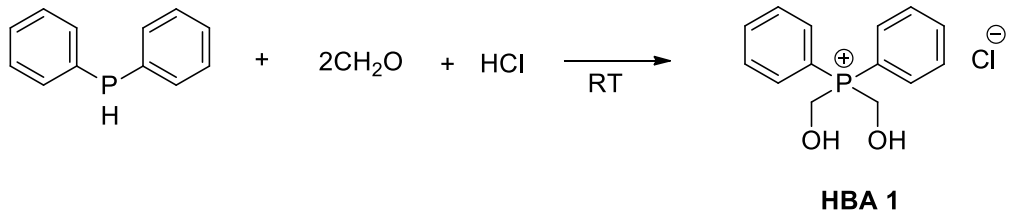

HBA 1

Scheme 2.1: Reaction scheme for the synthesis of HBA 1

In the synthesis of **HBA 2**, the synthesis of the allyl triethylammonium chloride salt ($C_9H_{18}ClN$) was performed from the procedure by Ren et al[6] by the reaction of triethylamine, and allyl chloride in acetone at 55^0C for 6hours. A white crystalline solid with a relatively low yield (14% yield) was filtered and washed with clean acetone and dried under vacuum at room temperature. The obtained salt was observed to be hygroscopic and was hence stored in an airtight container. The melting point of HBA could not be measured due to its hygroscopic nature and was found in literature to be 368°C.[6]

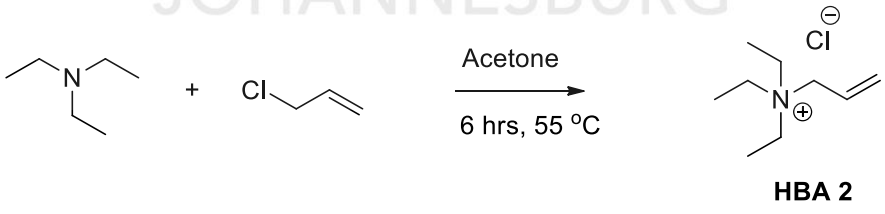

HBA 2

Scheme 2.2: Reaction scheme for the synthesis of HBA 2

2.2.2. ^{1}H NMR spectroscopy of HBA 1 and HBA 2

The formation of the phosphonium chloride salt (**HBA 1**) was confirmed by ^{1}H, ^{13}C {^{1}H} and ^{31}P-{^{1}H} NMR spectroscopy. From the ^{1}H NMR spectrum (**Figure 2.1**), the signal for the

methylene protons *(P-C<u>H₂</u>-OH)* appears at 5.01ppm as a doublet at position **a**. The splitting of the protons of the aromatic rings is also represented between 7.73-7.53ppm. The protons at **c** are observed to be magnetically different from those at **b** and **d** hence the clear splitting of the two groups. The protons at **b** are expected to be more deshielded due to proximity to the phosphorus atom.

A single phosphorus peak from the ^{31}P-{^{1}H} NMR is also observed at 16.59ppm in D_2O (**Figure 2.1**) and is comparable to that found in the literature (16.73ppm in CD_3OD).[7]

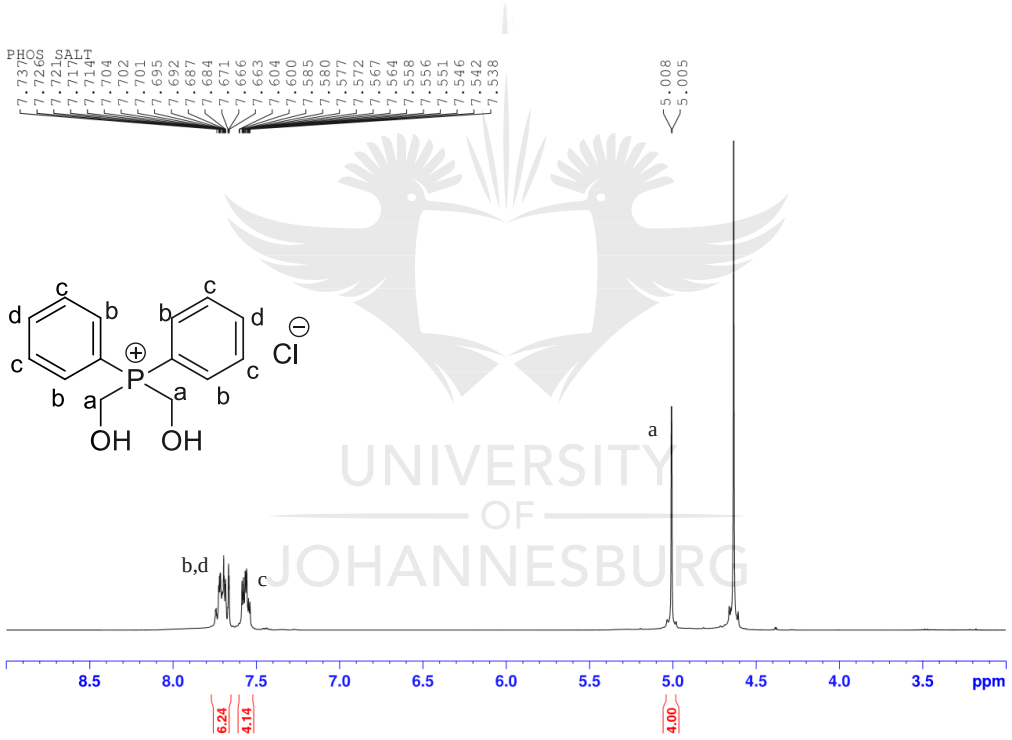

Figure 2.1: ^{1}H NMR spectrum of HBA 1 recorded in D_2O (OH protons missing from the structure of HBA1)

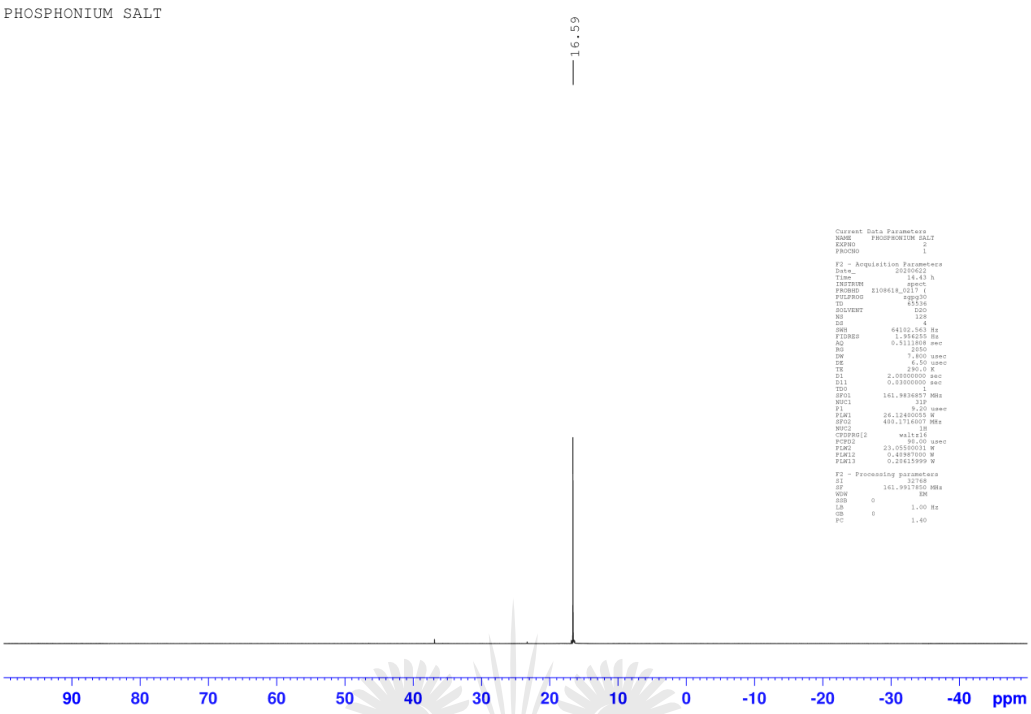

Figure 2.2: ^{31}P-{^{1}H} NMR spectrum of HBA 1 recorded in D_2O

In the ^{1}H NMR of the synthesized allyl triethylammonium chloride salt (**HBA 2**), the methyl (*C<u>H</u>$_3$)* protons of trimethylamine at position **a** are seen as a multiplet at 1.46 ppm integrating for nine protons while the corresponding methylene (*C<u>H</u>$_2$)* protons peaks at position **b** integrating for six protons are observed at 3.12ppm as a quartet. The peaks of the methylene protons labeled **c** (*N-C<u>H</u>$_2$ –CH)* appear at 3.65pmm as a doublet. The methine proton *(CH$_2$-C<u>H</u>=C)* at position **d** is seen further downfield (due to anisotropy as a result of the presence of the adjacent π system) and is split into a multiplet (as at is surrounded by protons at positions **c** and **e**) is observed at 5.79pmm. The alkene protons *(CH=C<u>H</u>$_2$)* at position **e** are also observed at different chemical environments at 5.55ppm and 5.38ppm as doublets each. The splitting patterns observed are a result of both direct and long-range coupling between atoms.

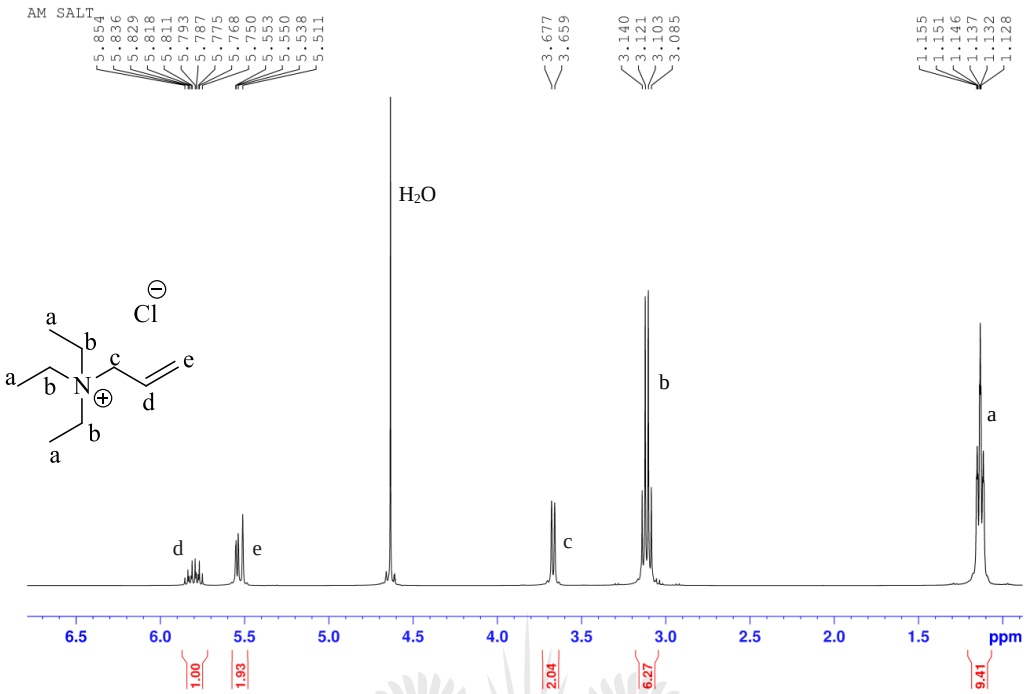

Figure 2.3: ^{1}H NMR spectrum of HBA 2 recorded in D_2O

2.3. Synthesis and characterization of deep eutectic solvents (DES 1-4)

The phosphonium-based DES (**DES 1**) was synthesized by the mixing of **HBA 1** and lactic acid in different molar ratios. Heating and stirring of the mixtures afforded a clear homogenous solution for all molar compositions. However, the molar ratio, 1:10, HBA to HBD remained a liquid at room temperature for several days while molar ratios of 1:2, 1:3, 1:5 were observed to solidify within 24hours -72hours. The composition with a molar ratio of 1:10 was hence chosen for subsequent experiments and characterization.

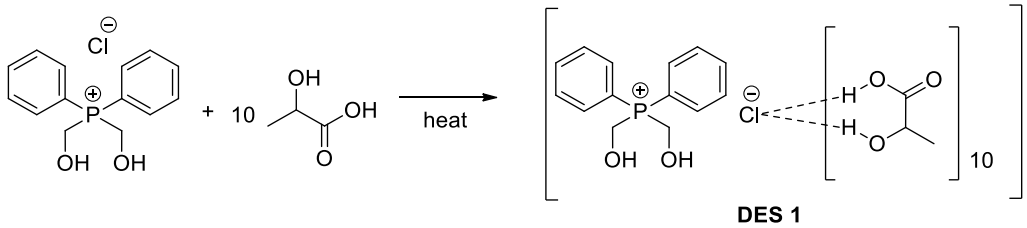

Scheme 2.3: Reaction scheme for the synthesis of DES 1

In the preparation of the ammonium-based DESs, the **HBA 2** (allyl triethylammonium chloride salt) was mixed and heated with the various HBDs in a molar ratio of 1:1 at 60^0C until a homogeneous mixture was formed. The mixtures of all three DESs remained liquid at room temperature at that molar composition. The HBDs used were methanesulfonic acid (msa), p-toluenesulfonic acid monohydrate (ptsa), and oxalic acid dihydrate (oxa). **DES 3** was first synthesized by Ren and coworkers (using anhydrous oxalic acid) and used in the dissolution of cellulose to an amount of 6.48wt%.[6]

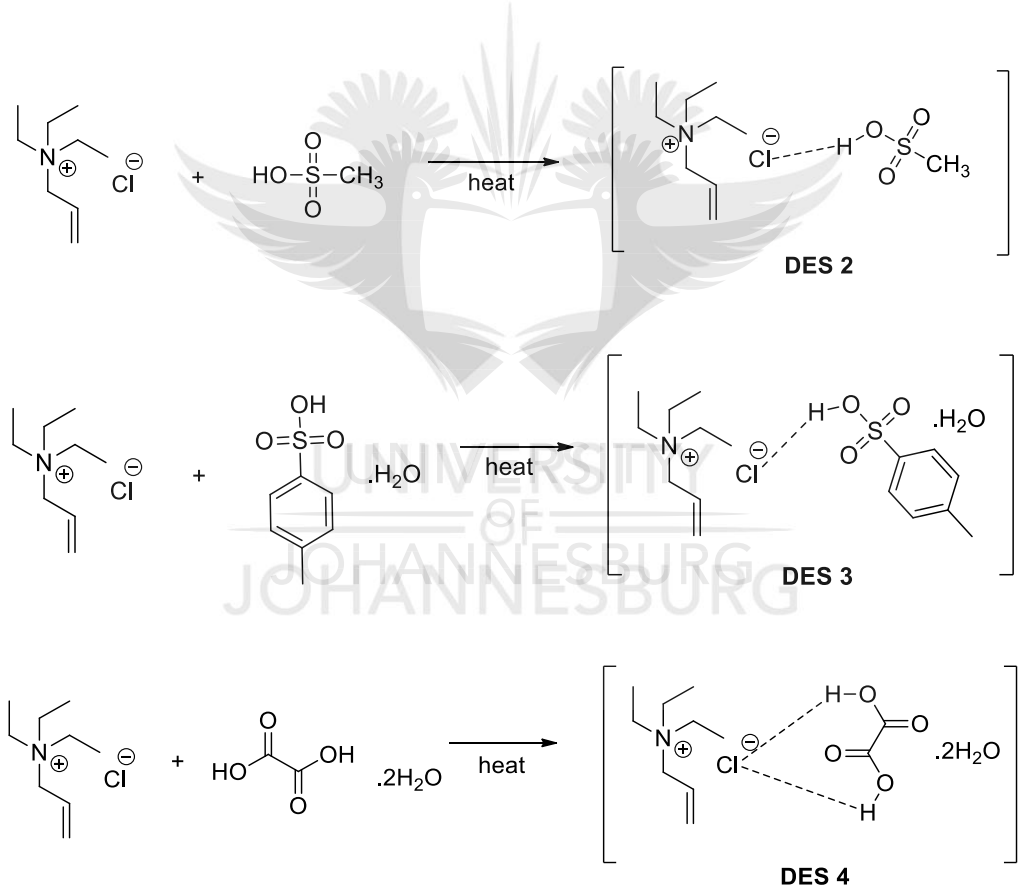

Scheme 2.4: Reaction scheme of the synthesis of DES 2, DES 3 & DES 4

2.3.1. FT-IR spectroscopy of DES 1-4

In **Figure 2.4** below, the FT-IR spectrum of the synthesized phosphonium chloride salt shows a very weak O-H stretching peak at 3325cm^{-1}. A strong sp^2 C-H stretching peak is observed at 3109cm^{-1} while a medium sp^3 C-H stretch is seen at 2877cm^{-1}. A strong C-O stretching peak is seen at 1049cm^{-1}. Medium to strong absorptions in the region of 1600cm^{-1} to 1450cm^{-1} depict the presence of aromatic rings (double bonds, C=C stretch).

The FT-IR spectrum for **DES 1** shows a broad O-H stretching peak at 3311cm-^{1}. The broadening of the O-H peak is significant in proving the formation of the DES. The presence of intermolecular hydrogen bonds between the organic salt and lactic acid results in the broad O-H stretching peak of **DES 1** as seen. The difference in the shape of the O-H stretch of the precursors (**HBA 1** and lactic acid) and **DES 1** also shows the successful synthesis of the DES. Some amount of water could be present in the DES (due to the hygroscopic nature of lactic acid) and also forming strong interactions. The water content is measured with a Karl Fischer Coulometric titrator. A C-H stretch was observed at 2985cm-^{1}. A strong C=O peak is seen at 1719cm-^{1}. The peak at 1118cm-^{1} represents the C-O stretch of the secondary alcohol of lactic acid.

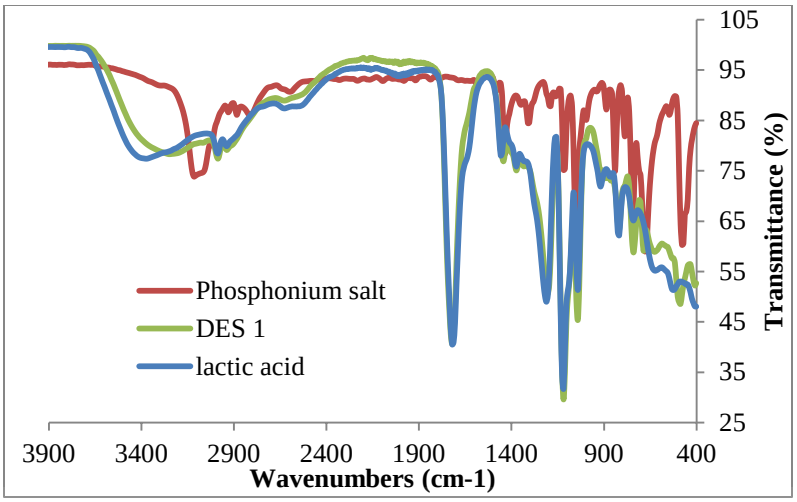

Figure 2.4: FT-IR spectrum of DES 1 showing precursors

In **Figures 2.5**, **2.6,** and **2.7**, characteristic peaks on **HBA 2** include the sp^2 C-H stretch seen quite high (possibly due to interaction with atmospheric moisture as the salt is hygroscopic) in the region of 3345cm^{-1} while the sp^3 C-H stretch appears at 2978cm^{-1}. The C=C stretching vibration is observed starting at 1650cm^{-1}. The C-N stretching vibration of the salt is also observed as medium to small peaks between 1350cm^{-1} and 1000cm^{-1}.

The spectra of the DESs all show a broadened O-H stretch in the region of 3500cm^{-1} to 3100cm^{-1}. The spectrum of all three DESs clearly looks different from the individual precursors used in their synthesis. The shape of the O-H stretch is significant in the presence of intermolecular hydrogen bonding formed between the HBA and the HBD in the samples. Again, the presence of a small amount of water could also be expected as the salt (**HBA 2**) is highly hygroscopic making the DESs also hygroscopic. The HBDs used also in the synthesis of **DES 3** and **DES 4** are also hydrated. The Karl Fischer coulometric titrator was used to measure the water content of the DESs.

The spectrum of **DES 2** (**Figure 2.5**) shows a broad and deep O-H stretch at 3400cm^{-1} signifying the formation of new hydrogen bonds in the eutectic mixture. There is a shift in the C=C stretch of **HBA 2** as seen from 1650cm^{-1} - 1635cm^{-1} possibly as a result of the inductive effect. The S=O stretch of methanesulfonic acid seen between 1350cm^{-1} and 1342cm^{-1} is also observed to disappear in the DES due to changes in the environment of the chemical bonds by complexation of the DES components.

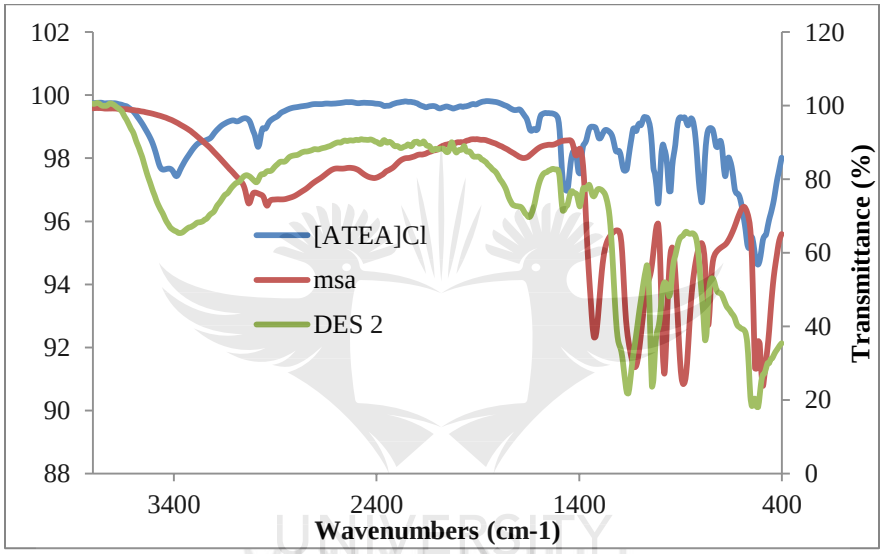

Figure 2.5: FT-IR spectrum of DES 2 showing spectra of precursors

There is a similar formation of new hydrogen bonds seen in the O-H stretch of **DES 3** (**Figure 2.6**) in the region of 3510cm^{-1} – 3024cm^{-1}. The C=C stretch of the ammonium salt also shifts from 1620cm^{-1} to 1589cm^{-1}. The aromatic overtones observed in the spectrum of p-toluenesulfonic acid (2700cm^{-1}-1712cm^{-1}) are seen to diminish as well in the DES as a result of modified chemical interactions.

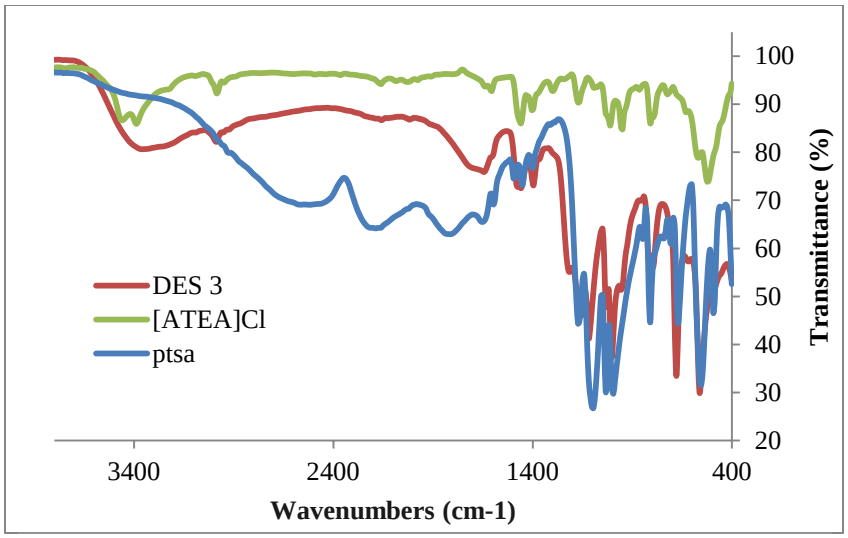

Figure 2.6: FT-IR spectrum of DES 3 showing spectra of precursors

In the spectrum of **DES 4** also, changes in the chemical interactions caused by the complexation reaction present resulted in the formation of a more intense O-H stretch in the DES at 3579cm^{-1} – 3057cm^{-1}. The C=O stretch of the carboxylic acid of oxalic acid at 1720cm^{-1} is also seen to be more intense in the DES compared to its precursor.

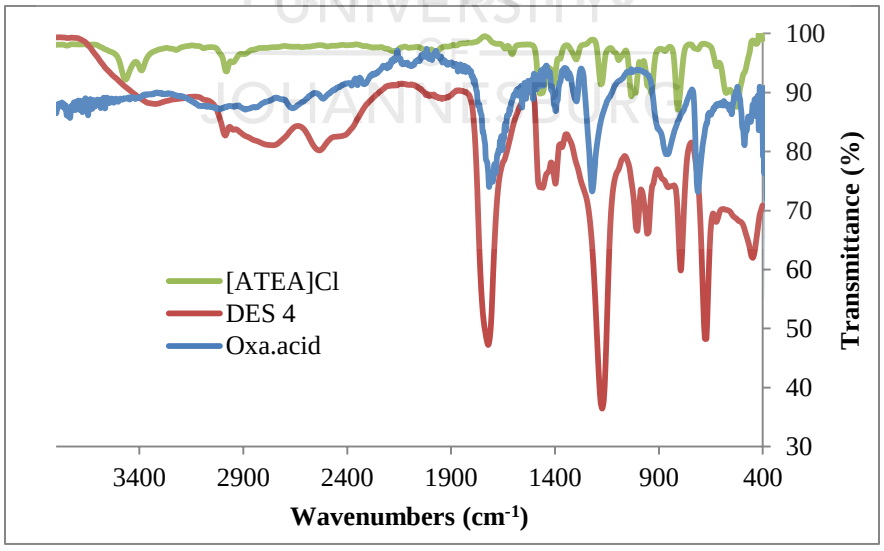

Figure 2.7: FT-IR spectrum of DES 4 showing spectra of precursors

2.3.2. ^{1}H NMR spectroscopy analysis of DES 1-4

The ^{1}H NMR of **DES 1** displays the presence of possibly, the two or three stereoisomers of lactide. The methyl protons of the lactide stereoisomers (R,R or S,S) are shown as doublets of doublets at position **f** with both sets of CH_3 protons observed between 1.23ppm-1.28ppm. The other isomer (R,S lactide) shows its CH_3 protons at around 1.38ppm-1.39ppm. Their corresponding methine protons are positioned at **e** (4.20ppm and 4.95ppm for the R,R or S,S isomers) while that of the other isomer has its methine protons at position **e** seen at 4.94ppm with multiple splitting observed. The protons of the phosphonium salt are all represented at positions **a**, **b**, **c,** and **d.**

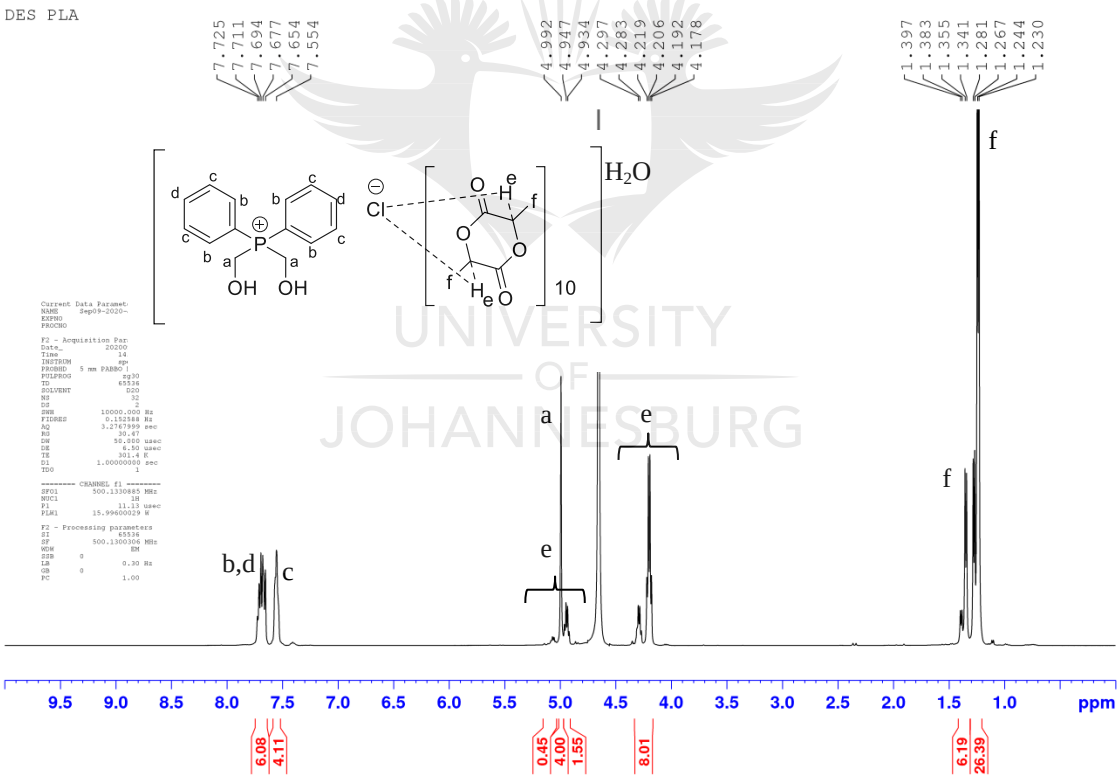

Figure 2.8: ^{1}H NMR spectrum of DES 1 recorded in D_2O

The formation of **DES 2-4** was also ascertained by ^{1}H NMR spectroscopy (**Figures 2.9, 2.10** & **2.11**). The presence of the O-H groups was unidentifiable due to proton-solvent exchange in protic solvents such as D_2O. There was however a slight shift upfield in ppm values of the DESs compared to that of the **HBA 2** in the same deuterated solvent. The shift in ppm values could be attributed to the change in the chemical environment as a result of the complexation of **HBA 2** to the various HBDs. All peaks corresponding to **HBA 2** were observed in spectra of all the DESs.

The peak for the methyl protons of methane sulfonic acid in **DES 2** was observed at 2.61ppm, slightly downfield and as a single at position **f** (**Figure 2.9**).

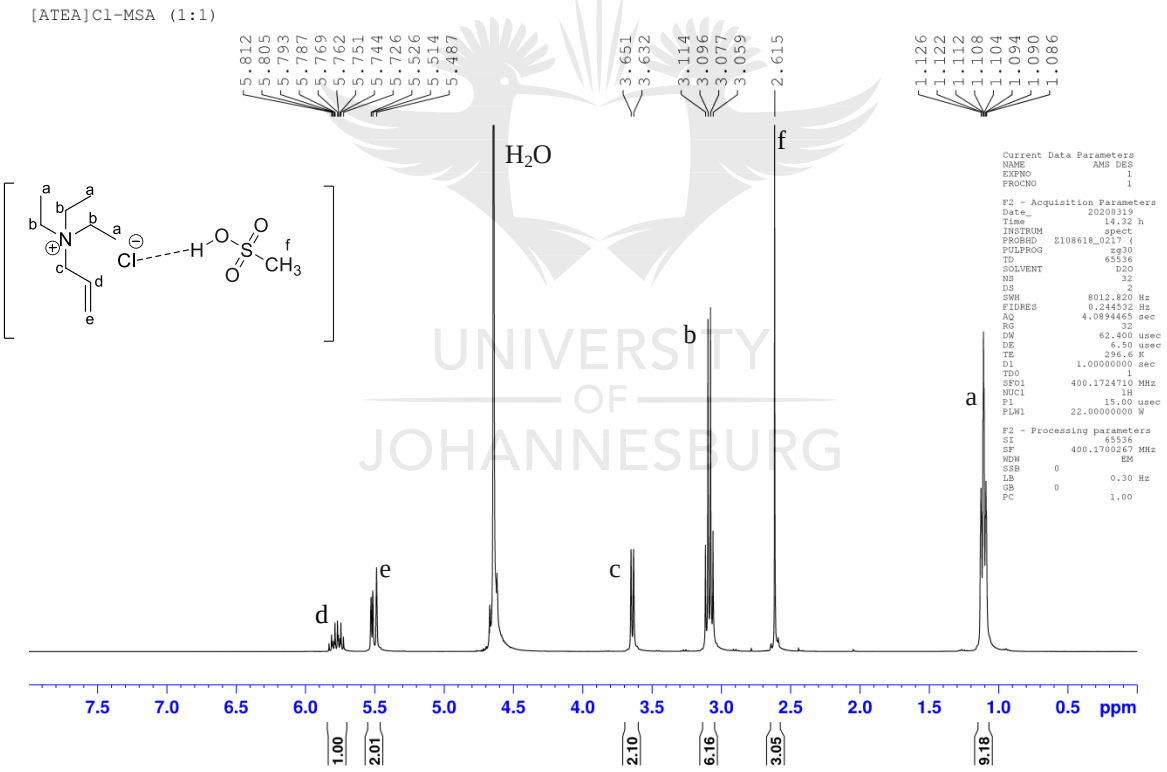

Figure 2.9: ^{1}H NMR spectrum of DES 2 recorded in D_2O

The methyl protons of p-toluenesulfonic acid in **DES 3** also show a singlet peak at 2.20ppm at position **h**. Its aromatic proton peaks at positions **g** and **f** (in chemically distinct environments), integrating for two protons each are observed at a doublet and a doublet of doublets at 7.18 and 7.50ppm respectively with the protons at position **f** being more downfield as a result of their adjacency to the electron-withdrawing oxygen atoms (**Figure 2.10**).

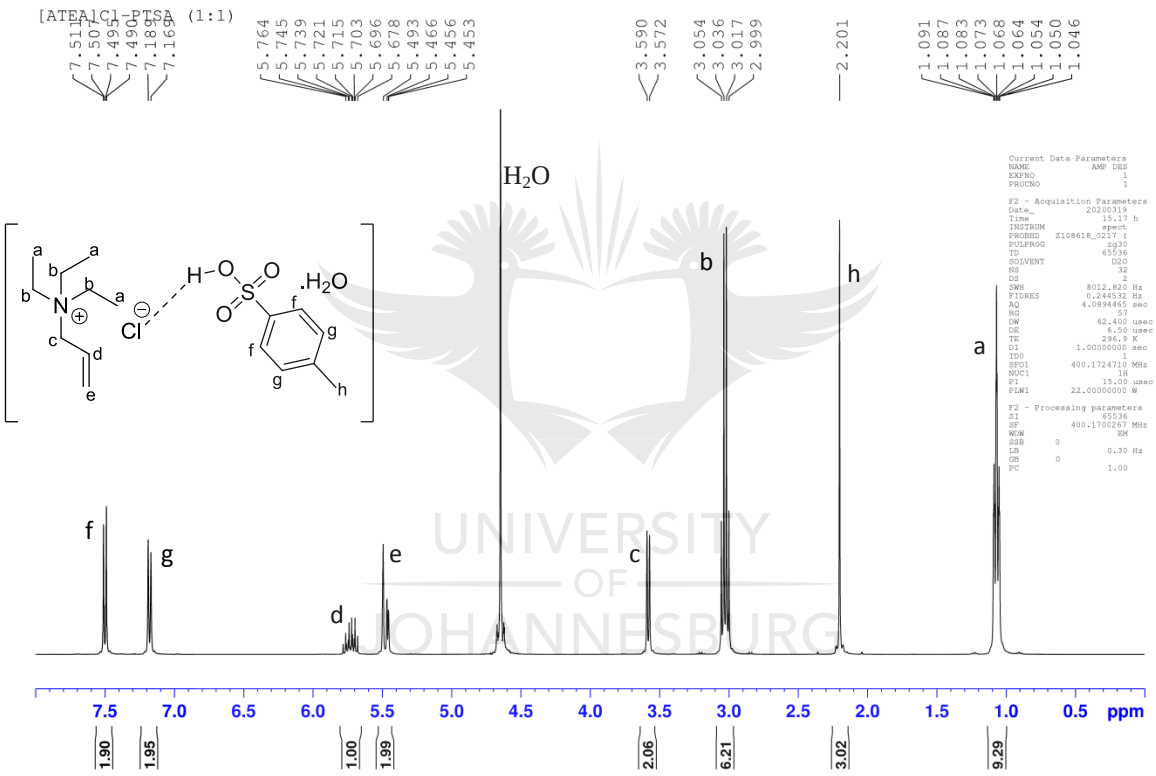

Figure 2.10: ^{1}H NMR spectrum of DES 3 recorded in D_2O

The ^{1}H NMR for **DES 4** is seen to be exactly as observed for **HBA 2**. Oxalic acid has no protons aside from its OH protons and hence no peaks are observed. The slight shift in ppm values of **HBA 2** peaks is still however observed. The presence of oxalic acid was hence observed by ^{13}C

{^{1}H} NMR where the chemically equivalent carboxylic acid carbons of the acid are seen at 160.9ppm at position **f**. (**Figure 2.11**)

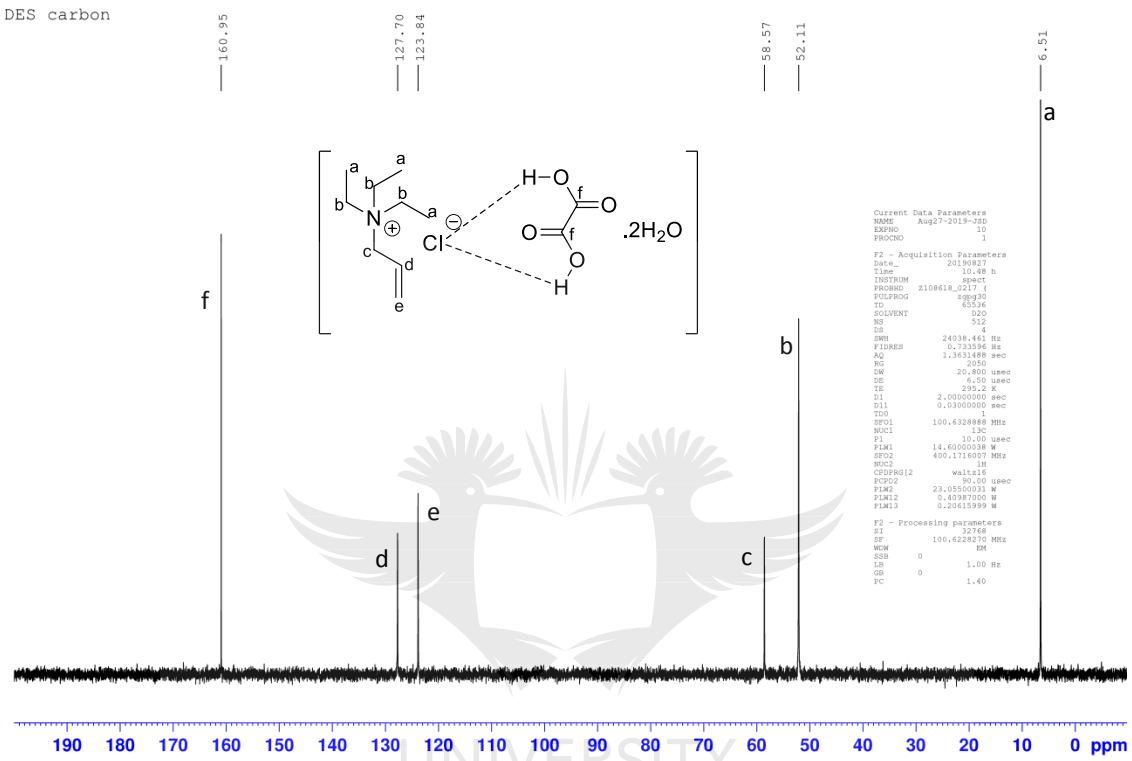

Figure 2.11: ^{13}C {^{1}H} NMR spectrum of DES 4 recorded in D_2O

2.4. Molecular weight calculations of deep eutectic solvents

The average molecular weights of the synthesized DES were also calculated according to **Eqn. 2.1** as reported by Ghaedi *et al*.[9] The values of the molecular weights of the DES are reported in **Table 2.1** below

$$M = \frac{X_{HBA}M_{HBA}+X_{HBD}M_{HBD}}{X_{HBA}+M_{HBD}} \quad \text{..... (Eqn. 2.1)}$$

Where M is the molecular weight of DES, X_{HBA} is the molar ratio and M_{HBA} is the molecular weight of the salt (HBA) in g.mol^{-1} and X_{HBD} is the molar ratio and M_{HBD} is the molecular weight of the HBDs.

Table 2.1: Calculated molecular weights of DESs

Salt		HBD		Molar ratio		DES	
Name	**M_s**	**Name**	**M_{HBD}**	**Salt**	**HBD**	**Name**	**M_{DES}**
HBA 1	282.70	lactic acid	90.08	1	10	DES 1	107.52
HBA 2	177.71	msa	96.10	1	1	DES 2	136.91
HBA 2	177.71	ptsa	190.22	1	1	DES 3	183.97
HBA 2	177.71	oxa	126.07	1	1	DES 4	151.89

2.5. Melting temperature of synthesized deep eutectic solvents

Concerning ILs and DESs, the terms melting point and freezing point are usually interchanged. The "freezing point" of the solid components of DESs is the same as its "melting point" while the "melting point" of the eutectic mixture is the same as its "freezing point". The melting temperatures of the synthesized DESs were measured and estimated using a conventional method. The melting points of DESs are usually measured using a differential scanning calorimeter (DSC). In this method, used by Torres and coworkers,[10] the DESs were frozen at a temperature of -78^{0}C in liquid nitrogen and the mixtures were then left to cool slowly at room temperature. The estimated range of melting temperature of the DESs was then recorded using a thermometer (-100^{0}C to 50^{0}C). The melting point of the bis (hydroxymethyl) diphenyl phosphonium chloride (**HBA 1**) was recorded using a melting point apparatus while that of allyl triethylammonium chloride (368^{o}C) was reported based on literature findings.[6] The measured melting temperatures of the DESs were observed to be lower than their individual components.

This method of determining the melting temperature of the DES was only used to estimate their melting temperature range. A more accurate result may be obtained using appropriate instrumentation. The observed reduced melting temperature is a result of the complexation of the HBA and the HBD at their specific mole ratios.

The values of the melting temperature of the DESs and their individual components are reported in **Table 2.2** below;

Table 2.2: Measured melting temperatures of DESs

HBA	mp (^{0}C)	HBD	mp (^{0}C)	DES	mp (^{0}C)
Bis(hydroxymethyl) diphenyl phosphonium chloride	158-160	Lactic acid	18	1	13-14
Allyltriethylammonium chloride	368	Methanesulfonic acid	17-19	2	13-14
Allyltriethylammonium chloride	368	P-toluenesulfonic acid monohydrate	103-106	3	14-16
Allyltriethylammonium chloride	368	Oxalic acid dihydrate	101.5	4	9-10

2.6. Viscosity measurement of synthesized deep eutectic solvents

The viscosities of the various synthesized DESs (freshly prepared) were measured. The measurements were recorded at a temperature of 22^{0}C. In the procedure, a pipette was filled with about 0.3mL of sample and mounted into the viscometer. The sample is run within a few minutes and the viscosity value is displayed. The results of the viscosities are shown in **Table 2.3** below. **DES 3** was seen to be the most viscous (3320mPa.s) followed by **DES 2** (161.5mPa.s), **DES 4** (154.2mPa.s) and **DES 1** (42.8mPa.s). Theoretically, low viscosity is necessary for pretreatment as solute to solvent interaction is enhanced.

2.7. Water content measurements: Karl Fischer titration results of synthesized deep eutectic solvents

The amount of water in freshly prepared samples was measured using a Karl Fischer titrator. The catholyte and anolyte were injected into the measuring cell of the titrator and the samples were analyzed. Results are reported in percentage in **Table 2.3** below. Some components used in the preparation of the DESs are hygroscopic and hence water may be present in the DESs formed. **DES 1** showed very high water content (12.74%) possibly due to a large amount of lactic acid (1:10) which is hygroscopic, used in making the DES. The DESs formed from hydrated HBAs (**DES 3** and **DES 4**) also showed significant amounts of water with 6.08% for **DES 3** having one molecule of water in its HBD and 11.30% for **DES 4** which has two molecules of water in its HBD. The least amount of water was seen for **DES 2** (1.25%).

2.8. pH of synthesized deep eutectic solvents

The pH of the DESs was measured using a pH meter. The pH meter was calibrated using standard 4, 7, and 10 buffers. The samples were weighed and an amount of water was added to each of them to prepare a concentration. The concentrations of the solutions prepared were 0.06mol/L, 0.4mol/L, 0.3mol/L and 0.4mol/L for **DES**s **1**, **2**, **3**, and **4** respectively. The pH was measured at 25^0C. The pH values are reported in **Table 2.3** below.

Table 2.3: Some measured physical properties of synthesized DESs

DES	HBA	HBD	Molar ratio (HBA:HBD)	pH ± 0.02 (25^0C)	Viscosity (mPa.s) 22^0C	Water content (%)
1	Bis(hydroxymethyl) diphenyl phosphonium chloride	Lactic acid	1 : 10	1.50	42.8	12.74
2	Allyltriethylammonium chloride	Methanesulfonic acid	1 : 1	1.23	161.5	1.25

3	Allyltriethylammonium chloride	P-toluenesulfonic acid monohydrate	1 : 1	1.38	3320	6.08
4	Allyltriethylammonium chloride	Oxalic acid dihydrate	1 : 1	1.33	154.2	11.30

2.9. Conclusion

A new phosphonium-based deep eutectic solvent and three ammonium-based deep eutectic solvents (two of which are new) have successfully been synthesized and characterized. The HBDs of the DESs are Bronsted acids and contribute to the acidity of their mixtures. The pH of the mixtures was measured as well as their viscosities. The components of the DES are also known to be hygroscopic and hence, the water content of the DESs was measured. Aside from the determinations of some physical properties, DESs were also characterized by different spectroscopic techniques including FT-IR spectroscopy and NMR spectroscopy, and their molecular weights were calculated. The melting temperatures of the DES were also estimated using a conventional method. These DESs have been assessed as solvents and catalysts in the fractionation and dissolution of biomass and cellulose (and its hydrolysis) and the dehydration of sugars, of which the results are, discussed in Chapters 3 and 4.

2.10. Experimental section

2.10.1. Materials and instrumentation

All chemicals used were of reagent grade purchased from Sigma Aldrich and used without further purification. Diphenylphosphine, triethylamine, allyl chloride, methanesulfonic acid, para-toluenesulfonic acid monohydrate, oxalic acid dihydrate, lactic acid, aqueous formaldehyde (40%), HCl (32%), acetone. Bis (hydroxymethyl) diphenyl phosphonium chloride (**HBA 1**) and allyl triethylammonium chloride (**HBA 2**) were synthesized according to literature procedures.

All DESs were synthesized according to the described methods in the literature. DESs were freshly prepared prior to characterization and used and obtained and without further purification. Elemental analysis was performed on a Thermo Scientific FLASH 2000 CHNS-O analyzer. The melting point was determined using a Gallenkamp digital melting apparatus.

2.10.2. Fourier-Transform-Infrared Spectroscopy

FT-IR data were obtained neat using a Perkin Elmer Spectrum BX II fitted with an ATR probe at the University of Johannesburg, Department of Chemical Sciences. The absorption intensities were recorded in percentage (%) and the absorption frequencies in wavenumbers (cm^{-1}) in the range of 400-4000 at a resolution of 16 and the number of scans of 32.

2.10.3. Nuclear Magnetic Resonance Spectroscopy

NMR data were recorded on Brucker Avance III 400 MHz NMR spectrometer at the University of Johannesburg, Department of Chemical Sciences. All samples were dissolved in deuterium oxide (D_2O) and ran at room temperature. Chemical shift signals were reported in ppm values relative to the internal standard trimethylsilane (δ= 0.00) and referenced to the residual protons of the deuterated solvent, D_2O (4.65ppm). The resonance multiplicity or splitting pattern of signals is reported as follows: s = singlet, d = doublet, t = triplet, q = quartet, m = multiplet, dd = doublet of doublets, bs = broad signal, bm = broad multiplet. Coupling constants (*J* constant), are reported in Hertz (Hz)

2.10.4. pH

The pH of the DESs was measured at 25^0C using a Labotec Orion pH meter (model 520A). The pH meter was calibrated using standard pH buffers of 4, 7, and 10. The instrument's average uncertainty was estimated at ±0.02.

2.10.5 Viscosity

The viscosities of the synthesized DESs were measured at a temperature of 22^0C ± 0.2 using a RheoSense microVISC portable viscometer. The rheometer was used in auto mode with an average uncertainty of ±2. The flow rate of the instrument is in the range of 0.5µl/min to 450µl/min. Viscosity values were reported in millipascal seconds (mPa.s).

2.10.6 Water Content

The amount of water was measured on freshly prepared DESs using a Mettler Toledo Karl Fischer coulometric titrator (C20/C30). The catholyte used was Hydranal-coulomat CG. KF water standard 1.0 was first measured before the samples. Water content values were recorded in ppm and percentage.

2.11. Synthesis

2.11.1. Synthesis of bis(hydroxymethyl)diphenylphosphonium chloride (HBA 1)

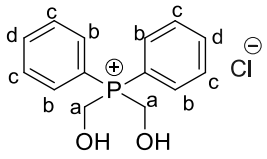

A solution of formaldehyde, HCHO ($9cm^3$, 40% solution) and HCl ($5cm^3$, 32% solution) was added to diphenylphosphine, Ph_2PH (10g, 54mmol) in a 250ml flask equipped with a magnetic stirrer. The hot homogenous solution was allowed to stir at room temperature. Upon cooling, a white solid (yield: 11.7g, 77%) crystallized out and was filtered. Solubility: soluble in polar solvents (water, methanol, ethanol). Melting point range: 158^0C-160^0C. FT-IR (ν_{max}/cm^{-1}) = 3325 (O-H), 3109 (sp^2 C-H), 2877 (sp^3 C-H). ^{1}H NMR (400 MHz D_2O 30^0C, ppm) = 5.01 (d, $^3J_{HH}$= 1.20 Hz 4H, H_a), 7.54-7.60 (m, $^3J_{HH}$= 1.60 Hz 4H, H_c), 7.66-7.74 (bm, $^3J_{HH}$= 1.20 Hz 2H, 4H, H_d, H_b). ^{13}C {^{1}H} NMR (100 MHz D_2O 30^0C, ppm) = 53.86; 114.72; 130.25; 133.53;

135.52. ^{31}P-{^{1}H} NMR (162 MHz, D_2O 30^{0}C, ppm) = 16.59. Elemental Analysis: Anal calcd for $C_{14}H_{16}ClO_2P$: C, 59.48%; H, 5.70%; Found: C, 59.75%; H, 5.48%.

2.11.2. Synthesis of *allyl triethylammonium chloride* (HBA 2)

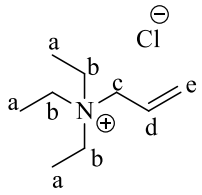

The synthesis of the allyl triethylammoniun chloride salt ($C_9H_{18}ClN$) was performed from the procedure by Ren et al.[6] Triethylamine, Et_3N (59.4mmol, 8.3mL) was added to allyl chloride (65.3mmol, 5.32mL) in acetone in a 250mL round bottom flask and heated at 55^{0}C for 6hours. A white hygroscopic crystalline solid (14% yield) was filtered and washed with clean acetone and dried under vacuum at room temperature. Solubility: soluble in water, chloroform. FT-IR (ν_{max}/cm^{-1}): 3345 (sp^2 C-H), 2978 (sp^3 C-H), 1650 (C=C), 1350-1000 (C-N)**,** ^{1}H NMR (400 MHz, D_2O, 30^{0}C, ppm): 1.14 (m, $^3J_{HH}$= 1.60 Hz, 9H, H_a), 3.12 (q, $^3J_{HH}$= 7.60 Hz, 6H, H_b), 3.67 (d, $^3J_{HH}$= 7.20 Hz, 2H, H_c), 5.81 (m, $^3J_{HH}$= 7.20 Hz, 1H, H_d), 5.54 (d, $^3J_{HH}$= 1.20 Hz, 1H, H_e), 5.55 (d, $^3J_{HH}$= 1.20 Hz, 1H, H_e). ^{13}C {^{1}H} NMR (100 MHz D_2O 30^{0}C, ppm): 6.70, 52.47, 59.01, 124.14, 127.98.

2.11.3. Synthesis of DES 1

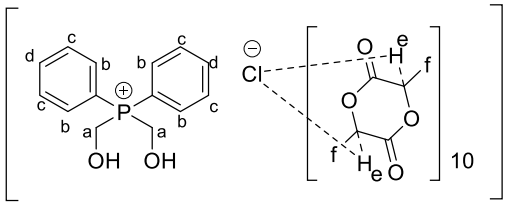

To a 100ml round bottom flask was added phosphonium salt, **HBA 1**(2g, 7.1mmol) and lactic acid (5.3mL, 71mmol) under stirring at 60^0C for 30mins under stirring. A clear and viscous homogenous mixture as formed and sealed in a clean vial and stored in a desiccator. Solubility: polar solvents. Melting temperature range (^{0}C): 13 -14. FT-IR (ν_{max}/cm^{-1}) = 3311 (COOH), 2985 (sp^3 C-H). ^{1}H NMR (400 MHz, D_2O, 30^0C, ppm) = 1.28ppm (q, $^3J_{HH}$= 7.0 Hz, 3H, H_f), 1.39ppm (q, $^3J_{HH}$= 7.0 Hz, 3H, H_f), 4.22-4.29ppm (m, $^3J_{HH}$= 7.0 Hz, 1H, H_e), 4.93-4.99ppm (m, $^3J_{HH}$= 7.0 Hz, 1H, H_e). 4.99 (d, $^3J_{HH}$= 1.20 Hz, 4H, H_a), 7.54-7.60 (bm, $^3J_{HH}$= 7.0 Hz, 4H, 2H, H_b, H_d), 7.55 (bs, 4H, H_c). ^{13}C {^{1}H} NMR (100 MHz D_2O 30^0C, ppm) = 15.97; 19.19; 53.71; 66.38; 70.01; 114.64; 130.13; 133.43; 135.40; 175.67; 178.47 . Molecular weight= 107.52gmol^{-1} pH (± 0.02) = 1.50. Viscosity (mPa.s) = 42.8, Water content (%) = 12.74

2.11.4. Synthesis of DES 2

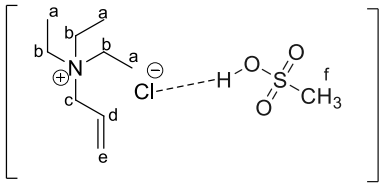

Allyl triethylammonium chloride, **HBA 2** (2g, 12mmol) was weighed into a 100mL round bottom flask containing methanesulfonic acid (0.74mL, 12mmol). The mixture was heated while stirring at 60^0C for 60mins until a clear homogenous mixture was formed. Melting temperature range (^{0}C): 13 -14. FT-IR (ν_{max}/cm^{-1}) = 3400 (O-H), 2978 (sp^3 C-H), 1634 (C=C). ^{1}H NMR (400 MHz, D_2O, 30^0C, ppm) = 1.11 (m, $^3J_{HH}$= 1.60 Hz, 9H, H_a), 3.11 (q, $^3J_{HH}$= 7.20 Hz, 6H, H_b), 3.65 (d, $^3J_{HH}$= 7.60 Hz, 2H, H_c), 5.76 (m, $^3J_{HH}$= 7.20 Hz, 1H, H_d), 5.48 (d, $^3J_{HH}$= 1.20 Hz, 1H, H_e), 5.52 (d, $^3J_{HH}$= 1.20 Hz, 1H, H_e), 2.62 (s, 3H, H_f) . ^{13}C {^{1}H} NMR (100 MHz D_2O 30^0C, ppm) =

6.59; 38.41; 52.33; 58.84; 124.01; 127.88. Molecular weight = 136.91 $gmol^{-1}$. pH (± 0.02) = 1.23, Viscosity (mPa.s) = 161.5, Water content (%) = 1.25

2.11.5. Synthesis of DES 3

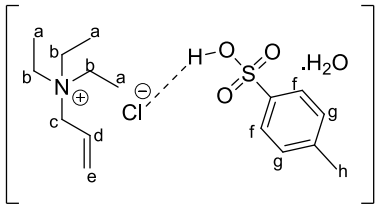

Allyl triethylammonium chloride, **HBA 2** (2g, 12mmol) was weighed into a 100mL round bottom flask containing para toluenesulfonic acid (2.3g, 12mmol). The mixture was heated at 60^0C for 60mins while stirring until a clear homogenous mixture was formed. Melting temperature range (^{0}C): 14 -16. FT-IR (ν_{max}/cm^{-1}) = 3400 (O-H), 2978 (sp^3 C-H), 1589 (C=C), 1300-1000(C-N). ^{1}H NMR (400 MHz, D_2O, 30^0C, ppm) = 1.07 (m, $^3J_{HH}$= 1.60 Hz, 9H, H_a), 3.04 (q, $^3J_{HH}$= 7.20 Hz, 6H, H_b), 3.59 (d, $^3J_{HH}$= 7.20 Hz, 2H, H_c), 5.71 (m, $^3J_{HH}$= 7.60 Hz, 1H, H_d), 5.49 (d, $^3J_{HH}$= 1.20 Hz, 1H, H_e), 5.45 (d, $^3J_{HH}$= 1.20 Hz, 1H, H_e), 7.50 (dd, $^3J_{HH}$= 1.6 Hz, 2H, H_f), 7.18 (d, $^3J_{HH}$= 8 Hz, 2H, H_g), 2.20 (s, 3H, H_h). ^{13}C {^{1}H} NMR (100 MHz D_2O 30^0C, ppm) = 6.57; 20.43; 52.30; 58.80; 123.94; 125.33; 127.90; 129.41; 139.49; 142.39. Molecular weight = 183.87 $gmol^{-1}$. pH (± 0.02) = 1.38, Viscosity (mPa.s) = 3320, Water content (%) = 6.08

2.11.6. Synthesis of DES 4

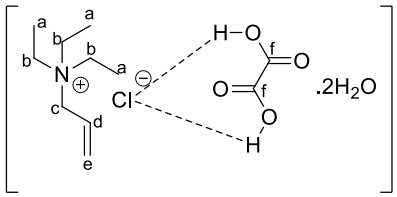

Allyl triethylammonium chloride, **HBA 2** (2g, 12mmol) was weighed into a 100mL round bottom flask containing oxalic acid dihydrate (1.5g, 12mmol). The mixture was heated at 60^0C for 60mins while stirring until a clear homogenous mixture was formed. Solubility: polar solvents. Melting temperature range (^{0}C): 9 -10. FT-IR (ν_{max}/cm^{-1}): 3400 (COOH), 2978 (sp^3 C-H), 1720 (C=O), 1300-1000(C-N). ^{1}H NMR (400 MHz, D_2O, 30^0C, ppm) = 1.09 (t, $^3J_{HH}$= 7.20 Hz, 9H, H_a), 3.06 (q, $^3J_{HH}$= 3.60 Hz, 6H, H_b), 3.63 (d, $^3J_{HH}$= 7.20 Hz, 2H, H_c), 5.73 (m, $^3J_{HH}$= 7.60 Hz, 1H, H_d), 5.31 (d, $^3J_{HH}$= 1.20 Hz, 1H, H_e), 5.27 (d, $^3J_{HH}$= 1.20 Hz, 1H, H_e). ^{13}C {^{1}H} NMR (100 MHz D_2O 30^0C, ppm) = 6.51; 52.11; 58.57; 123.84; 127.70; 160.95. Molecular weight = 151.90gmol^{-1}.pH (± 0.02) = 1.33, Viscosity (mPa.s) = 154.2, Water content (%) = 11.3

2.12. References

1 M. Hayyan, C. Y. Looi, A. Hayyan and W. F. Wong, *PLoS One*, 2015, **10**, 1–18.

2 Y. Dai, J. Van Spronsen and G. Witkamp, *Anal. Chim. Acta*, 2013, **766**, 61–68.

3 C. Florindo, F. S. Oliveira, L. P. N. Rebelo, A. M. Fernandes and I. M. Marrucho, *ACS Sustain. Chem. Eng.*, 2014, **2**, 2416–2425.

4 G. C. Maria, L. Ferrer, C. R. Mateo and F. Monte, *Langmuir*, 2009, **25**, 5509–5515.

5 T. El, S. Fourmentin and H. Greige-gerges, *J. Mol. Liq.*, 2019, **288**, 111028.

6 H. Ren, C. Chen, S. Guo, D. Zhao and Q. Wang, *BioResources*, 2016, **11**, 8457–8469.

7 J. Fawcett, P. A. T. Hoye, R. D. W. Kemmitt, a D. J. Law and D. R. Russell, *J. Chem. Soc. Dalt. Trans.*, 1993, 2563–2568.

8 M. Epstein and S. A. Buckler, *Tetrahedron*, 1962, **18**, 1231–1242.

9 H. Ghaedi, M. Ayoub, S. Sufian, A. M. Shariff and B. Lal, *Preprints*, 2017, 1–25.

10 P. Torres, M. Balcells, E. Cequier and R. Canela-Garayoa, *Molecules*, , DOI:10.3390/molecules25092157.

CHAPTER THREE

Fractionation of biomass and dissolution of cellulose in deep eutectic solvent

3. Introduction

The pretreatment of biomass is primarily aimed at disrupting its complex structure and increasing the accessibility of catalysts such as enzymes and acids to the biopolymers of biomass to obtain fermentable sugars.[1,2] The use of DESs in lignocellulosic biomass pretreatment has gained considerable attention due to their "green" properties.[3]

Arundo donax (also called giant reed or cane), one of several reed species, is a tall perennial bamboo-like herbaceous grass belonging to the Poaceae family and is usually suited to warm-temperature to subtropical climates.[4] *A. donax* is considered a promising energy crop because, compared to other energy crops, it is produced in great yields even when cropped in low input conditions resulting in its high potential in EROEI value (energy returned on energy invested).[5] It has therefore found a wide application in energy production including its fermentation to produce bioethanol, the production of biogas by anaerobic digestion[6] and its use as a solid biofuel in direct combustion, pyrolysis and gasification.[7]

Prior to the fractionation or pretreatment of biomass, quantitative methods of analysis are necessarily performed to determine the composition of biomass in terms of extractives, ash, lignin (acid-soluble and acid-insoluble), hemicellulose and cellulose. Extractives (extractable ash) refer to the non-structural material in biomass that includes inorganic materials such as soil, fertilizer, non-structural sugars and nitrogenous materials that are either water-soluble or ethanol soluble.[8] Extractives are removed to avoid any interference in subsequent analysis. Unlike extractable ash (extractives), structural ash refers to inorganic materials that are bound to the

physical structure of biomass and cannot be removed by washing with water or ethanol.[9] The quantity of ash measures the mineral content and other inorganic matter left in the biomass. The composition of biomass that makes up lignin, cellulose and hemicellulose is the largest; hence its determination/analysis before fractionation is of the essence. The determination of these components is reported on an Oven Dry Weight (ODW) basis. The amount of total solids and moisture content is hence determined. In the quantification of these fractions, a two- step acid hydrolysis process is employed to fractionate the extractives-free biomass. Lignin fractionates into acid-soluble and acid-insoluble material. These procedures are repeated on the pretreated biomass to determine the effect of pretreatment on the removal of the biomass fractions. A scheme of the chemical analysis of biomass is shown below (**Figure 3.1**).

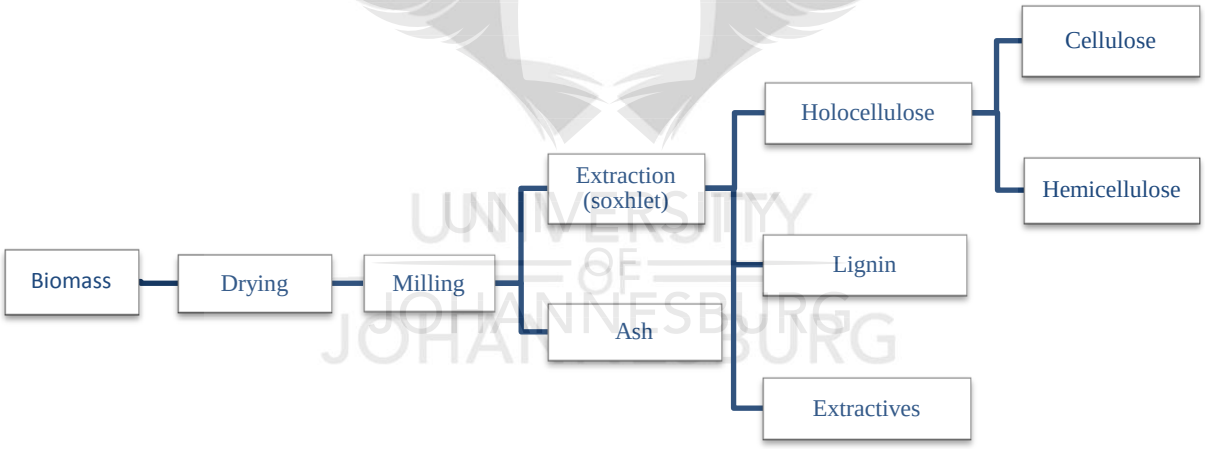

Figure 3.1: Scheme of chemical analysis of biomass

3.1. Compositional analysis of *Arundo donax*

Before chemical analysis of *A.donax*, dried stems of the biomass (obtained from the Centre for Synthesis and Catalysis, Department of Chemical Sciences, University of Johannesburg, South Africa) were milled and passed through a 0.4mm mesh and then sealed in air-tight containers and

stored at 4^0C. Moisture content was determined using NREL methods "determination of total solids". Determination of extractives, ash and acid-soluble lignin was performed using procedures from the National Renewable Energy Laboratory (NREL) methods. Determination of acid-insoluble lignin, hemicellulose and cellulose were performed using the proposed Designer Energy Limited (DE) methods. The DE Limited methods in determination of acid-insoluble lignin, cellulose and hemicellulose were employed to overcome the inadequacies of the conventional methods. In this method, the centrifugation technique (rather than vacuum filtration method) is used which has been reported to prevent the loss of lignin particles. The determination of acid-insoluble lignin in biomass using the improved DE limited method showed that the lignin particles completely settle and the supernatant is a clear solution under the used centrifugation conditions. This minimizes the loss of lignin, hence reduced lignin content, as lignin particles do not penetrate filters. The NREL method of determining polysaccharides, however simple and accurate also presents certain drawbacks including (i) partial degradation of carbohydrates at high hydrolysis temperature and (ii) adsorption of sugars on the surface of precipitated calcium sulfate.[10]. The chemical analyses were performed in duplicate.

3.1.1. Determination of extractives

As described by the NREL methods [8], a two-step procedure for the removal and determination of water-soluble and ethanol-soluble extractives is described. A known amount of *Arundo donax* (milled) was weighed into a thimble and extracted with 190mL of water for 24hours to determine the amount of water extractives. After which the heat was turned off and left to cool to room temperature. The solution was transferred into a 200mL volumetric flask and topped up to make 200mL. A 10mL aliquot was taken and kept for sucrose analysis. The water was removed *in vacuo* to determine the amount of water-soluble extractives. An ethanol extraction was

subsequently performed using 190mL ethanol for another 24hours. After which the system was allowed to cool to room temperature and the solvent was removed by evaporation to determine the amount of ethanol extractives.

Percent total extractives was determined using the formula,

$$\%Extractives = \frac{\text{Weight}_{\text{flask and extractives}} - \text{Weight}_{\text{flask}}}{\text{ODW}_{\text{sample}}} x100 \ldots\ldots\ldots\ldots\ldots\ldots\ldots \text{(Eqn. 3.1)}$$

For percent water extractives, the formula below was used

$$\%Extractives = \frac{\text{Weight}_{\text{flask and extractives}} - \text{Weight}_{\text{flask}}}{\text{ODW}_{\text{sample}}} x \frac{\text{Volume}_{\text{total}}}{\text{Volume}_{\text{total}} - \text{Volume}_{\text{aliquot removed}}} x\ 100 \ldots$$

(**Eqn.3.2**)

3.1.2. Determination of total solids

As further described by the NREL methods[11], 1g of biomass was kept in an oven at a temperature of 105 ^{0}C for a minimum of 4hours. The sample was allowed to cool to room temperature in a desiccator. The weight was recorded and the sample was put back into the oven for 1hour. This was repeated until a constant weight was obtained.

%Total solids and %Moisture was determined by the following calculations,

$$\%Total\ solids = \frac{Weight_{dry\ pan+\ dry\ sample} - Weight_{dry\ pan}}{Weight_{sample\ as\ received}} x100 \ldots\ldots\ldots \text{(Eqn. 3.3)}$$

$$\%Moisture = 100 - \left(\frac{Weight_{dry\ pan+\ dry\ sample} - Weight_{dry\ pan}}{Weight_{sample\ as\ received}}\right) x100 \ldots\ldots\ldots \text{(Eqn. 3.4)}$$

3.1.3 Determination of ash

As described by the NREL methods[9], 1g of biomass sample was weighed into marked crucibles and placed into a muffle furnace. The crucibles were oven-dried for a few hours and weighed to

constant weight before analysis. The samples were then ashed using the muffle furnace equipped with a ramping system as described. The samples were dried in a desiccator, weighed and put back into the furnace to obtain constant weight. The analysis was done in duplicate.

Amount of ash was determined by the following calculations,

$$\%Ash = \frac{Weight_{crucible+ash} - Weight_{crucible}}{ODW_{sample}} x\ 100 \ldots\ldots\ldots\ldots\ldots \text{(Eqn. 3.5)}$$

3.1.4. Determination of acid-soluble lignin (ASL)

As described by the NREL methods[12] in this procedure, 150mg of biomass sample (extractives-free) was weighed into a pressure tube. 1.50mL 72% sulfuric acid was added and the mixture was stirred thoroughly for 1min. The pressure tube was then put into an oil bath set at 30 ^{0}C for 1hour, stirring every 5-10mins. At the end of the 1hour, the acid was diluted to 4% by adding 42mL of water and the solution was mixed thoroughly. The mixture was further incubated for 1hour at 121 ^{0}C. 10mL aliquot of the liquid was collected to analyze acid-soluble lignin. On a UV-VIS Spectrometer, water was used to run the background and the absorbance of the sample was measured at a wavelength of 240nm. The sample was diluted with enough deionized water to obtain an absorbance between 0.7 and 1. The amount of acid-soluble lignin was then calculated.

The amount of ASL was determined using the following calculations,

$$\%ASL = \frac{UV_{abs}\ x\ Vol_{filtrate}\ x\ Dilution}{\varepsilon\ x\ ODW_{sample} x\ Pathlength} x\ 100 \ldots\ldots\ldots\ldots\ldots \text{(Eqn.3.6)}$$

3.1.5. Determination of acid-insoluble lignin (AIL)

As described by the DE Limited methods for determination of acid-insoluble lignin,[10] 0.3g of extractives-free biomass was mixed with 5mL of 72% sulfuric acid and pre-hydrolyzed at 25^{0}C

for 2hours in a 100mL round bottom flask. The acid was then diluted with 45mL of distilled water and hydrolyzed again at a boiling temperature under reflux for additional 2hours in an oil bath. The mixture was allowed to cool at room temperature for 30mins and the acidic mixture was transferred in 50mL falcon tubes (PP tubes) and centrifuged at RCF of 4500 for 15mins. The solid residue was washed with hot water (50^0C), 5wt% sodium bicarbonate and distilled water to reach a pH of 7. The solids were separated by centrifugation and dried in the falcon tubes at 105^0C to constant weight. The percent AIL was calculated by the following equation;

$$\%AIL = 100\% \frac{(P-Pt)}{Ps} \quad \text{(Eqn.3.7)}$$

Where P is the weight of residue with falcon tube, Pt is the weight of empty falcon tube and Ps is the weight of dry extractives-free biomass.

3.1.6. Determination of holocellulose

In the determination of holocellulose (that is, the total polysaccharides made up of both cellulose and hemicellulose),[10] 40mL of distilled water, followed by 0.5g of sodium chlorite ($NaClO_2$) and 1mL of glacial acetic acid was added to 0.5g of the extractives-free biomass in a 100mL round bottom flask. The mixture is treated at 90^0C for 45mins in an oil bath while stirring. An additional portion of 0.5g of sodium chlorite and 1mL acetate buffer was added and treated again for 45mins. The mixture was then allowed to cool for 30mins and then transferred into a 50mL falcon tube and centrifuged for 10mins. The residue was washed with hot water until a pH of 7 was obtained. The residue was then dried at 105^0C to constant weight. The percent holocellulose (HC) was calculated by the following equation;

$$\%HC = 100\% \frac{(P-Pt)}{Ps} \quad \text{(Eqn.3.8)}$$

Where P is the weight of residue together with falcon tube, Pt is the weight of empty falcon tube and Ps is the weight of dry extractives-free biomass.

3.1.7 Determination of cellulose and hemicellulose

In finding the amount of cellulose and hemicellulose in holocellulose,[10] the hemicellulose was removed from the obtained holocellulose by hydrolyzing at boiling temperature for 2hours under reflux with 45mL of 2wt% HCl in a 100mL round bottom flask. The mixture was then allowed to cool for 30mins and transferred into 50mL PP tubes and centrifuged for 10mins. The residue was washed with hot water, 1wt% sodium bicarbonate and distilled water to reach a pH of 7. The washed residue was dried at 105^0C to constant weight. The percent cellulose (C) and hemicellulose was calculated by the equation below;

$$\%C=\%HC\frac{(P-Pt)}{Ps} \quad \text{(Eqn. 3.9)}$$

$$\%H=\%HC-\%C \quad \text{(Eqn. 3.10)}$$

Where HC is the percentage of holocellulose, P is the weight of residue together with falcon tube, Pt is the weight of empty falcon tube and Ps is the weight of holocellulose.

3.2. Fractionation of *Arundo donax*

In a typical procedure, 5wt% (per mass of DES) of *A.donax* was added into an autoclave reactor containing DES and treated at a specific temperature for a period of time under stirring. After which ethanol was added to the mixture and the undissolved residue (pulp/solid I) was separated by vacuum filtration using nylon 66 membrane filters (0.2µm) to obtain a clear DES-biomass-ethanol mixture (liquid I). The undissolved pulp/solid I was oven-dried overnight at 70^0C following analysis. Ethanol was then removed by rotary evaporation and water was added to the

DES-biomass mixture to precipitate the dissolved biomass fraction (solid II). The mixture was washed repeatedly and decanted to remove the DES and water solution to obtain the biomass-rich phase which was dried under vacuum prior to analysis.

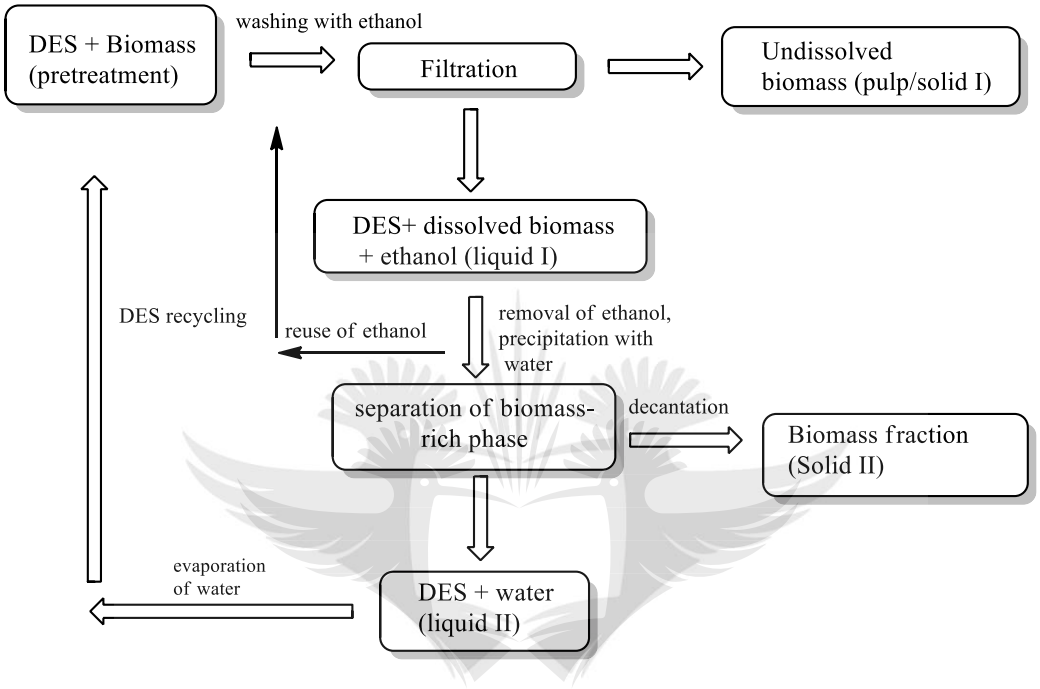

Scheme 3.1: Scheme of the fractionation process

3.3. Dissolution of cellulose

The dissolution (or swelling) of cellulose using DESs has seen massive development over the years. Navard and co-workers describe the swelling of cellulose fibres as the disruption or disordering of the structure of cellulose and is followed by its dissolution.[13] The swelling of cellulose fibres is also described by the "ballooning" phenomenon, where the secondary cell wall of plants swells so much resulting in the bursting of the primary cell wall within the cellulose structure.[14] Currently, the highest amount of cellulose dissolved in a deep eutectic solvent has been reported by Ren and co-workers (6.48 wt% in an allyl-functionalized DES).[15]

The synthesized phosphonium based DES (**DES 1**) was then tested in the dissolution of cellulose. The dissolution of cellulose in deep eutectic solvent was performed according to previously described methods.[15] In this procedure, a known amount of cellulose was gradually added into **DES 1** in a round bottom flask with stirring for a specific amount of time. After stirring for a few hours the mixture was allowed to stand the DES overnight. The dissolution was carried out within a temperature range of 80^0C to 120^0C after which the cellulosic mixture was washed with ethanol and filtered by vacuum to obtain the undissolved cellulose. Water was then used to regenerate the dissolved cellulose. The regenerated cellulose was dried at 80^0C and analyzed by FT-IR, P-XRD and SEM-EDX. The solubility of cellulose was calculated by a percentage of the mass of cellulose (dissolved) per mass of DES.

3.4. Hydrolysis of cellulose in deep eutectic solvents using other catalysts

In an attempt to hydrolyse cellulose using other catalysts (DES and zeolite), the catalyst (**DES 2** and zeolite Y) was added to the **DES 1**-cellulose mixture and allowed to stir at 100^0C for between 24-30 hours after which the sample was analysed by ^{1}H NMR in D_2O.

In this chapter, we describe and report on the fractionation of *A. donax*, as well as the dissolution of cellulose in a deep eutectic solvent (**DES 1**). **DES 1** was employed in the fractionation of biomass and the dissolution of cellulose mainly to examine the effect of phosphonium-based DESs on biomass feedstock. The attempted hydrolysis of cellulose is also investigated. The results of this work are analyzed by FT-IR spectroscopy, Powder-Xray diffraction and Scanning electron microscopy.

3.5. Results and discussion

The compositional analysis for the untreated biomass was found as follows (graphically represented in **Figure 3.2**);

%Water extractive was found to be 16.09% and %Ethanol Extractives was found to be 1.11%. Hence, %total extractives were calculated to be 17.2% ± 0.1%. %Total solids was calculated to be 94.4% and %Moisture was found to be 6.6%. The %Ash was found to be 1.66% ± 0.4%. The %ASL was found to be 3.35% ± 0.07%, the %AIL was found to be 11.51% ± 0.7%. The amount of holocellulose was found to be 66.27% ± 0.01%. The amount of cellulose and hemicellulose was calculated to be 35.30% ± 0.01% and 30.97% ± 0.01% respectively.

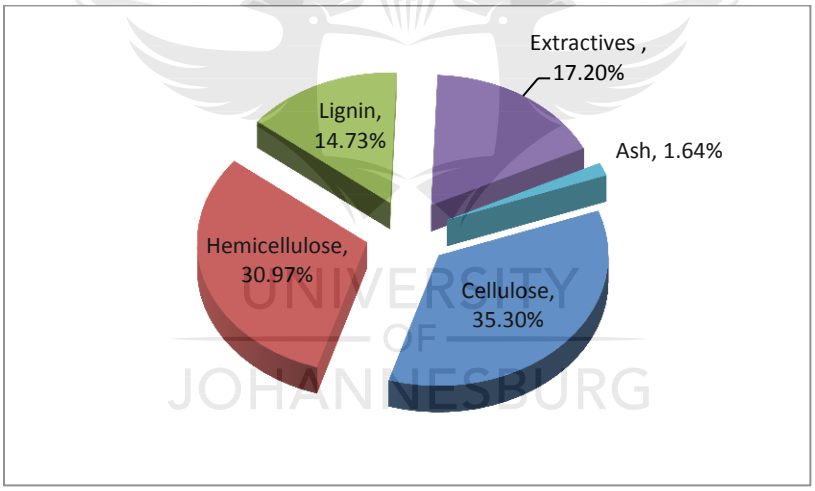

Figure 3.2: Graphical representation of the chemical compositional of *A. donax*.

Arundo donax was treated with a phosphonium salt-lactic acid deep eutectic solvent (**DES 1**) at various biomass loadings, pretreatment time and temperatures. The percent amount of biomass dissolved and the yield of solid residue with respect to these parameters was explored. The process yielded an undissolved solid residue and an extracted oily material. The structural changes of the pretreated biomass were analyzed by FT-IR analysis, while crystallinity was

judged by P-XRD analysis. The surface morphology of the treated and untreated biomass was observed by SEM-EDX analysis. The extracted material which precipitated was analyzed by FT-IR. The recovered DES was analyzed by ^{1}H NMR to investigate the formation of other by-products of hydrolysis of the biopolymers and dehydration of sugars during fractionation. A recyclability study to test its potential for reuse was performed on the DES.

3.5.1. Mass recovery and compositional analysis of cellulosic pulp

As a reference sample, cellulose cotton linters obtained from sigma Aldrich was analyzed by FT-IR (**Figure 3.3**) to establish and identify the characteristic peaks of cellulose functional groups and comparing them with that of the treated and untreated biomass. The broad peak in the region of 3660cm^{-1} and 3100cm^{-1} is characteristic of the O-H stretching vibrations including vibrations of inter-and intra-molecular hydrogen bonding of cellulose.[16] The peak in the region of 2900cm^{-1} and 2800cm^{-1} corresponds to the C-H stretching vibration. The distinctive bands assigned to cellulose are observed in the region of 1630cm^{-1} to 900cm^{-1}. According to the data given by Xu *et al*,[17] the intense peak at 1033cm^{-1} corresponds to the stretching in the C-O bonds. The medium peaks at 1157cm^{-1} and 1334cm^{-1} represent the C-O-C asymmetrical stretching and O-H in-plane vibration respectively.

Obtaining a reference sample for lignin, being a more complex biopolymer of biomass with several different bonds, for comparison is more of a challenge as chemical processes tend to cleave different bonds, altering the structure of lignin obtained.[18] Data collected from the literature was used to assign peaks for the biomass components. *A. donax* residue, analyzed by Licursi *et al*[19] showed that *A. donax* lignin had the broad O-H absorption stretch between 3500cm^{-1} and 3300cm^{-1}. The peaks at 2850cm^{-1} and 2930cm^{-1} represent the C-H stretching in aromatic methoxyl groups and methyl groups in the lignin side chains. *A. donax* residue also

showed a C=O stretching of unconjugated ketones, carbonyls and ester groups as well as C=O stretching of conjugated p-substituent carbonyl and carboxyl groups at absorption bands in the region of 1705 cm^{-1} and 1605 cm^{-1} respectively. An absorption band at 1220 cm^{-1} due to C-C and C-O stretching vibrations of guaiacyl lignin units is also observed.

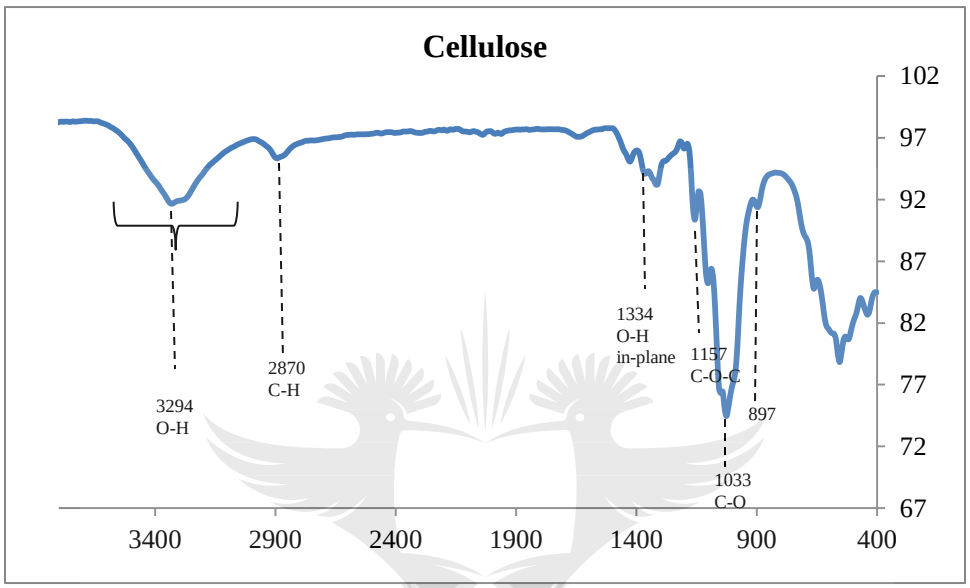

Figure 3.3: FT-IR spectrum of pure cellulose

A reference sample for hemicellulose was also not obtained for comparison; however, the functional groups of hemicellulose are thought to usually overlap with those of cellulose.[20] From literature data, a summary of the functional groups' assignment is given below.

Table 3.1: Summary of functional groups of biomass components

Wavenumber (cm^{-1})	**Assignment/functional group**	**Biopolymer**	**Ref**
3660-3100	O-H stretching vibrations	Cellulose, Lignin	16,19
2930-2800	C-H stretching vibrations	Cellulose, Lignin	16,19
1730, 1705	C=O stretching vibrations (unconjugated ketones, carbonyls	Cellulose, hemicellulose, lignin	16,17,20

	and esters)		
1605	C=O (conjugated p-substituent carbonyl, carboxyl groups)	Lignin	[16]
1440	O-H (in-plane bending)	Cellulose, hemicellulose, lignin	[17]
1380	C-H bending	Cellulose, hemicellulose, lignin	[17]
1220	C-C + C-O stretching	Lignin (guaiacyl)	[16]
1035	C-O, C=C, C-C-O stretching	Cellulose, hemicellulose, lignin	[17]
1160	C-O-C asymmetrical stretching	Cellulose, hemicellulose	[17]
930	Glycosidic linkage	Hemicellulose	[20]
875	Glycosidic linkage	Hemicellulose	[20]

According to studies on the acid pretreatment of biomass, the severity of pretreatment conditions may lead to the formation of a new lignin-like structure called pseudo-lignin [21]. This new lignin-like material has been thought to be formed from the acid-catalyzed condensation and re-polymerization reactions of dehydration products of polysaccharides such as furfural and HMF into aromatic structures of carbon which are then deposited onto the pulp.[22,23] The formation of pseudo-lignin is also investigated.

3.5.2. Effect of pretreatment time on biomass dissolution

The recovery yield of solid residues obtained from the biomass with respect to pretreatment time at a biomass loading of 5.0wt% and temperature of 100^0C was analyzed (**Figure 3.4**). The dissolution of biomass was seen to increase with a rise in treatment time from 1 hour to 12 hours, resulting in the gradual reduction in the yield of cellulosic material within that time; however, after 18 hours to 24 hours, there is an observed slight decrease in the amount of biomass that

dissolved corresponding to a slight relative increase in the recovery yield of the cellulosic pulp. The solid residues obtained were smaller and finer by observation for pretreated samples. From this observation, it could be assumed that the size of biomass particles reduces with increasing pretreatment time, hence facilitating dissolution.

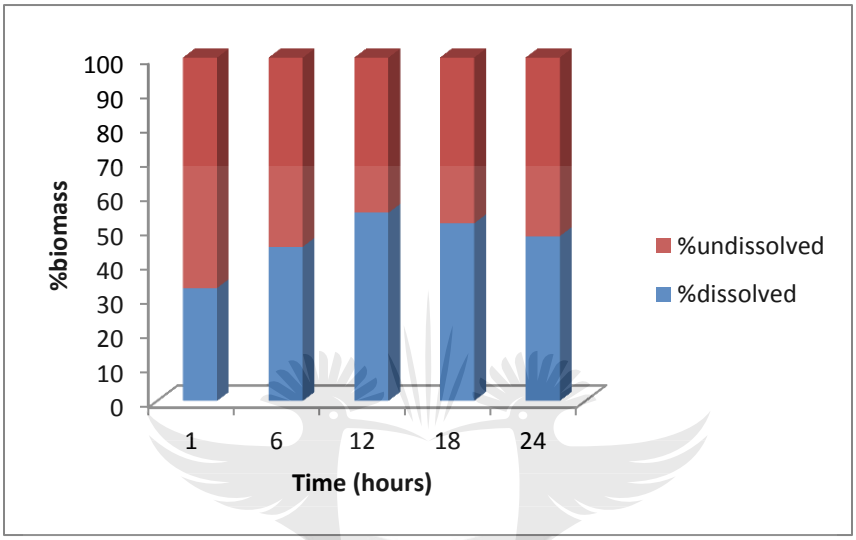

Figure 3.4: Yields of undissolved and dissolved biomass as a function of pretreatment time (Operating conditions: 5wt% biomass of DES, 100^{0}C)

The increase in the amount of undissolved biomass obtained after long pretreatment times (18 hours-24 hours) is assumed to be due to the formation and deposition of pseudo-lignin onto the cellulosic pulp. Evidence of the formation of pseudo-lignin was confirmed by FT-IR analysis by comparing the surface changes of the biomass with respect to pretreatment time. The fingerprint regions (<1800cm^{-1}) of the IR spectra were analyzed to find evidence of pseudo-lignin formation (**Figure 3.6**). FT-IR data of pseudo-lignin (**Table 3.2**) collected by Shinde *at al* was used as a comparison in confirming the formation of pseudo-lignin.

Table 3.2: FT-IR absorbance bands for pseudo-lignin.[24]

Wavenumber (cm^{-1})	Assignment/ functional groups
3238	O-H stretching in alcohols, phenols or carboxylic acids
2923	Aliphatic C-H stretching
1697	C=O stretching in carboxylic acids, conjugated aldehydes or ketones
1611, 1512	Aromatic C=C stretching (in ring)
1360	Aliphatic C-H rocking
1299,1203, 1020	C-O stretching in alcohols, ethers, or carboxylic acids
867, 800	Aromatic C-H out-of-plane bending

The effect of pretreatment time on biomass dissolution was also studied using FT-IR, with a keen eye on structural changes on the pretreated samples. Notably, the FT-IR analysis does not only reflect the result of the removal of the biomass fractions under discussion but also a result of the relative amounts of biomass fractions present in samples before and after pretreatment. A chemical analysis of the pretreated sample is necessary to investigate what fractions of biomass are removed during pretreatment.

According to Mamilla *et al*, the shape of the O-H stretch in the IR spectrum between $3600cm^{-1}$ and $3200cm^{-1}$ is usually deeper in cellulose (due to intermolecular hydrogen bonds) and wider in lignin (due to OH groups in phenols).

From the spectra (**Figure 3.5**), there is an observed sharpening of the O-H stretch at $3294cm^{-1}$ in the 1 hour, 6hour, and 12hours treated samples with a high intensity of the peak seen in the 12hour treated sample. The observed increased narrowing or deepening of the O-H stretch seen for the 1 hour, 6 hours and 12 hours pretreated sample depicts the presence of more cellulose, relative to the amount of lignin and hemicellulose. The O-H stretch of the 18 hour and 24 hour

pretreated samples are however less deep and broader, likely due to the presence of pseudo-lignin. These results could be indicative of the increasing amount of cellulose relative to hemicellulose and lignin in the samples from the beginning of pretreatment to 12 hours. The decrease in the intensity at 18 hours and 24 hours is likely as a result of the presence of pseudo-lignin. In the fingerprint region, the peak at 1219 cm^{-1} in the untreated biomass which is also visible in the 1 hour and 6 hours treated samples is characteristic of lignin C-C, C-O stretching. At this point, it can be assumed that relative amount of lignin compared to cellulose and hemicellulose in the samples is still significant (in terms of amount) to appear in the spectrum, and as time progressed, the lignin peak is seen to be suppressed or disappear in the 12 hours, 18 hours and 24 hours treated samples as the amount of cellulose increases and the cellulosic peaks increase. The peak at 1035 cm^{-1} seen for all pretreated samples which is characteristic of the C-O stretching of cellulose is seen to increase significantly from 1 hour to 12 hours indicating the gradual increase in the amount of cellulose in the treated samples and the decrease in the amount of the other biopolymers. The decrease in its intensity at higher pretreatment time (18 hours to 24 hours) could again be attributed to the deposition of pseudo-lignin on the pulp, compensating for the decrease in cellulose amount.

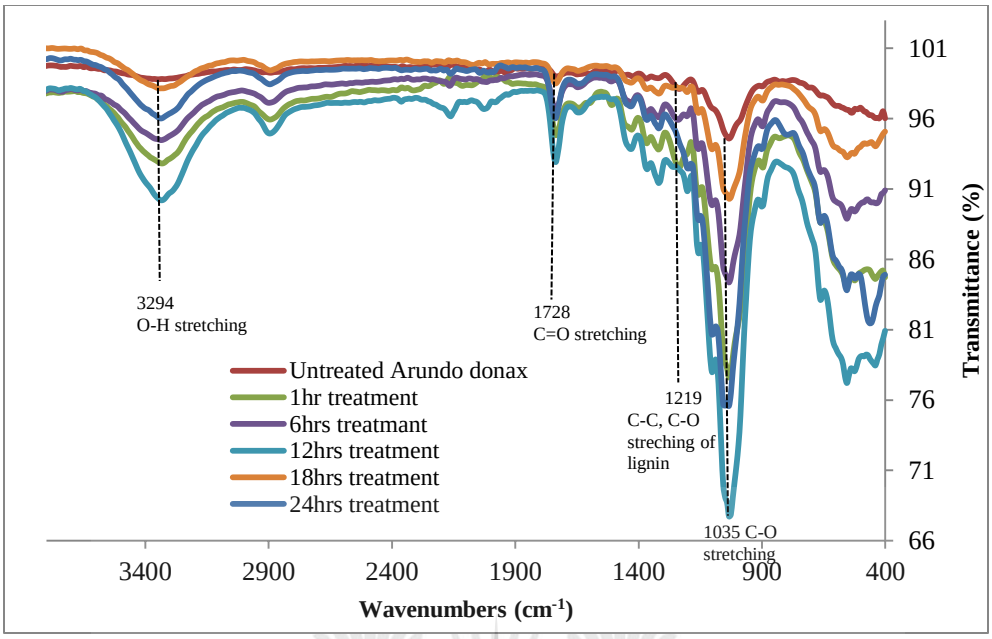

Figure 3.5: FT-IR spectrum of biomass pretreatment as an effect of time (Operating conditions: 5wt% biomass of DES, 100^{0}C)

From the FT-IR spectrum of the fingerprint region of the pretreated samples, very little evidence of the formation and deposition of pseudo-lignin is observed. The appearance of a new peak is however seen for sample pretreated for the 24 hours at 802 cm^{-1}. This peak is similar to the peak position found by Shinde *et al* at 800 cm^{-1} representing aromatic C-H out-of-plane bending but is however not enough evidence of pseudo-lignin deposition.

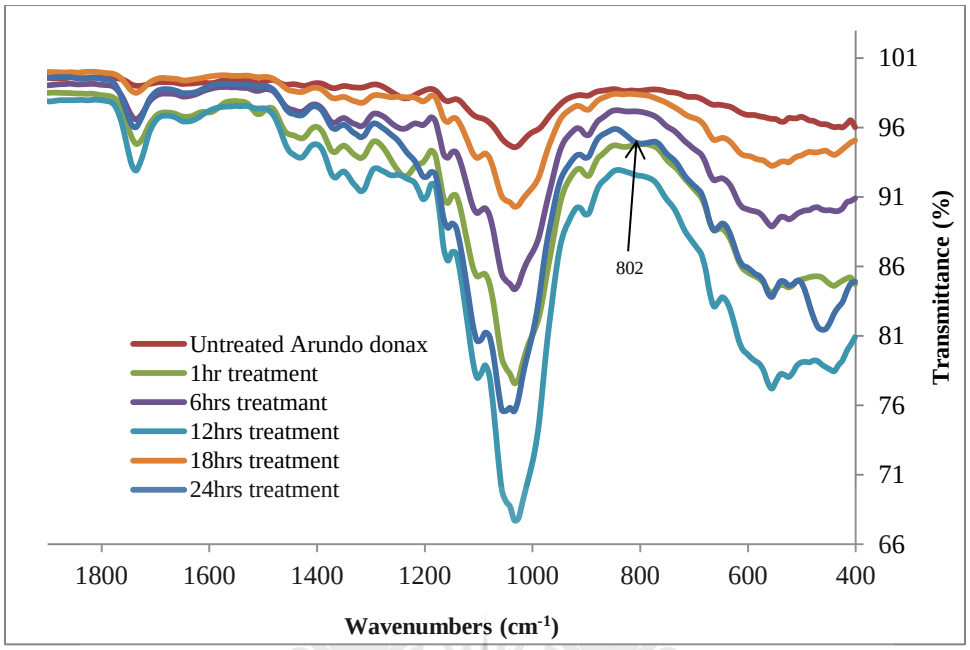

Figure 3.6: IR spectra of the fingerprint region for treated and untreated *A.donax*

3.5.3. Effect of biomass loading on biomass dissolution

The effect of biomass loading on the dissolution of biomass was analyzed. The yields of undissolved solid residues were assessed at different biomass loading of 2.5wt%, 5.0wt%, 10wt%, pretreatment temperature of 100^{0}C and time of 12 hours (**Figure 3.7**). The particle size of biomass was also observed to decrease with lower biomass loading (**Figure 3.8**). The biomass particles tend to look finer after pretreatment signifying dissolution. The percentage amount of biomass dissolved was observed to increase at a biomass loading of 5wt% under the same conditions. The amount of dissolved biomass for the 2.5wt% (43%) was slightly lower than that of 5wt% (54.8%). This is possibly as a result of poor recovery of the undissolved residue affecting its yield. The decrease in the amount of dissolved biomass with respect to increasing biomass loading from 5wt% to 10wt% (54.8% to 49.7%) can be attributed to the reduced level of interaction between the biomass particles and the solvent. With more solvent and less biomass, the solute-solvent interaction is increased thereby increasing dissolution. A higher biomass

loading in a given amount of solvent also increases the viscosity of the mixture. Lower viscosity is beneficial to biomass dissolution as it enhances solute-solvent interaction and eases mass transfer by increasing and promoting the diffusion of the solvent molecules into the pores of the biomass.

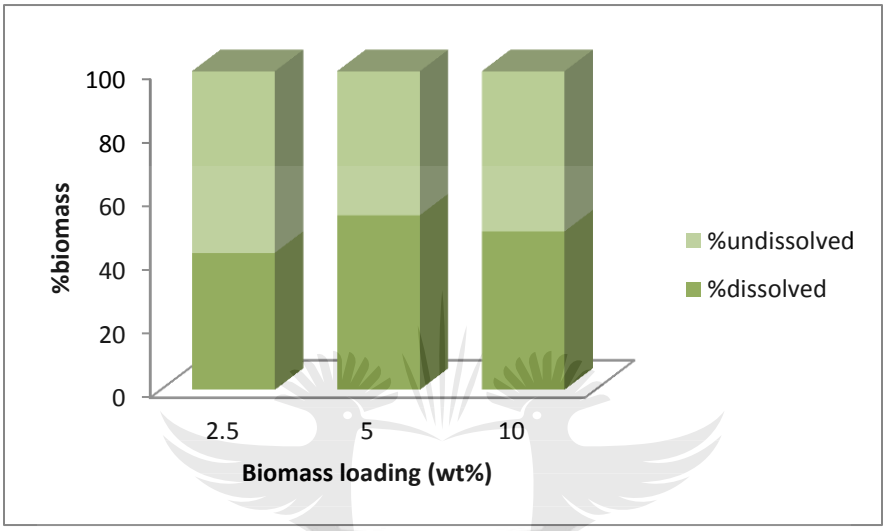

Figure 3.7: Yield of undissolved and dissolved biomass as a function of biomass loading
(Operating conditions: 12hrs, 100^{0}C)

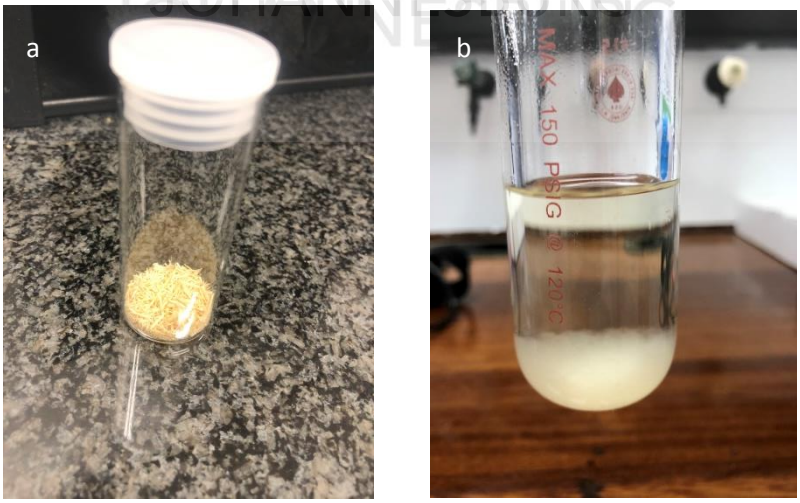

Figure 3.8: Biomass particle size before (a) and after pretreatment (b)

FT-IR analysis was used to measure the structural changes of solid yield with respect to biomass loading (**Figure 3.9**). The yield of cellulosic material is seen to correspond with the intensity of the characteristic cellulose peaks increasing from 2.5wt% to 10wt% to 5wt%. Accordingly, the relative amount of cellulose is more than hemicellulose and lignin in the sample treatment of 5wt% biomass loading, followed by the treatment of 10wt% and then 2.5wt%.

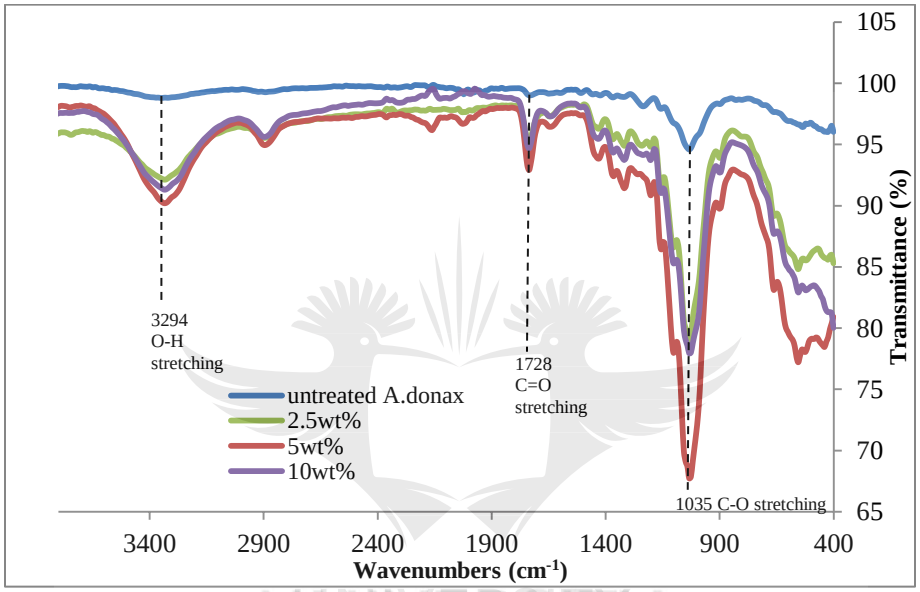

Figure 3.9: FT-IR spectra of *A.donax* as an effect of biomass loading (Operating conditions: 12hrs, 100^{0}C)

3.5.4. Effect of temperature on biomass dissolution

The effect of temperature on the dissolution of biomass was investigated. 5wt% of biomass was pretreated for 12 hours at temperatures of 80^{0}C, 100^{0}C and 120^{0}C. The yield of biomass residues obtained was found to be 1.2%, 45.2% and 46.3% at pretreatment temperatures of 80^{0}C, 100^{0}C and 120^{0}C respectively (**Figure 3.10**). Higher pretreatment temperature is observed to lower the viscosity of the mixture thereby enhancing biomass dissolution by easing mass transfer. There is an observed increase in the yield of solid residue for the treatment at 120^{0}C from that of 100^{0}C. Again, this may be attributed to the formation and deposition of pseudo-lignin at such a high

temperature and the biomass is assumed to be over-treated. The particle size of biomass residues was also observed to reduce with increasing pretreatment temperature.

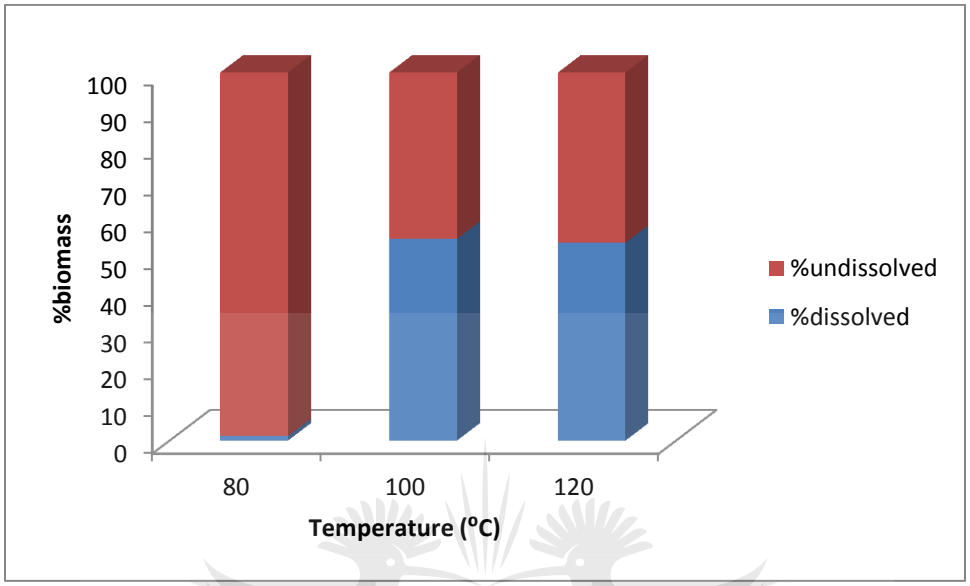

Figure 3.10: Yield of undissolved and dissolved biomass as a function of temperature
(Operating conditions: 12hrs, 5wt% biomass of DES)

The biomass dissolution was again measured by FT-IR analysis (**Figure 3.11**) to observe any structural changes and evidence of the formation of pseudo-lignin.

From the FT-IR spectra of the pretreated samples, it is observed that there is no significant structural modification of the 80^0C pretreated sample compared to the untreated sample. However, the shape of the O-H stretch, as well as the peak at 1219cm^{-1} (C-O stretch of lignin) as seen in the spectrum of the 80^0C treated sample and the untreated sample again indicates the significant amount of lignin present in the sample, relative to the others as stated earlier. The peaks are then seen to disappear or be suppressed (in the case of the O-H peak, the shape is changed) with the increase in pretreatment temperature implying the increase in cellulose in both the 100^0C and 120^0C treated samples. The intensity of the peaks at 3340cm^{-1} as well 1033cm^{-1}

corresponding to the O-H stretch and C-O stretch of cellulose for the 120^{0}C pretreated sample are seen to reduce while the same peaks for the 100^{0}C pretreated sample are increased. This implies that the amount of cellulose in the 100^{0}C pretreated sample is higher than that of the 120^{0}C pretreated sample. This is possible if there is a formation and deposition of pseudo-lignin on the pulp of the 120^{0}C pretreated sample.

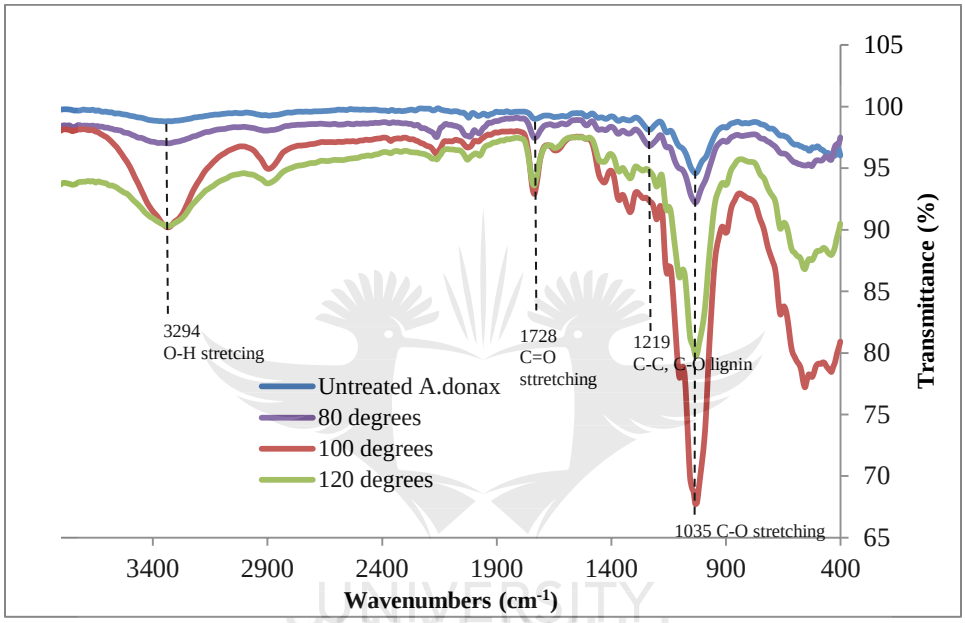

Figure 3.11: FT-IR spectra of *A. donax* as an effect of temperature (Operating conditions: 12hrs, 5wt% biomass of DES)

3.5.5. Compositional analysis of pretreated *Arundo donax*

The pretreated sample obtained under optimum conditions (5wt%, 12 hours, and 100^{0}C) was considered for compositional analysis in comparison to the untreated *A. donax*. The NREL methods were used in the determination of acid-soluble lignin, while the DE limited methods were used in the determination of acid-insoluble lignin (Klason lignin), cellulose and hemicellulose.

The amount of holocellulose was first analyzed using the DE limited methods. The amount of cellulose and hemicellulose was found to be 61.3% and 19.4%. The acid-insoluble lignin content of the pretreated sample was also found to be 12%. Acid soluble lignin content was also found to be 3.94% giving a total lignin amount of 15.94% (**Figure 3.12**). These results correspond with the hypothesis that under these conditions, the relative amount of cellulose is significantly increased as that of lignin is only slightly increased and hemicellulose decreases. This indicates that mostly hemicellulose is extracted from the biomass with some small amount of lignin. This correlates with reports in the literature that under acidic conditions, hemicellulose is easily removed because it has a less crystalline structure compared to cellulose.[25]

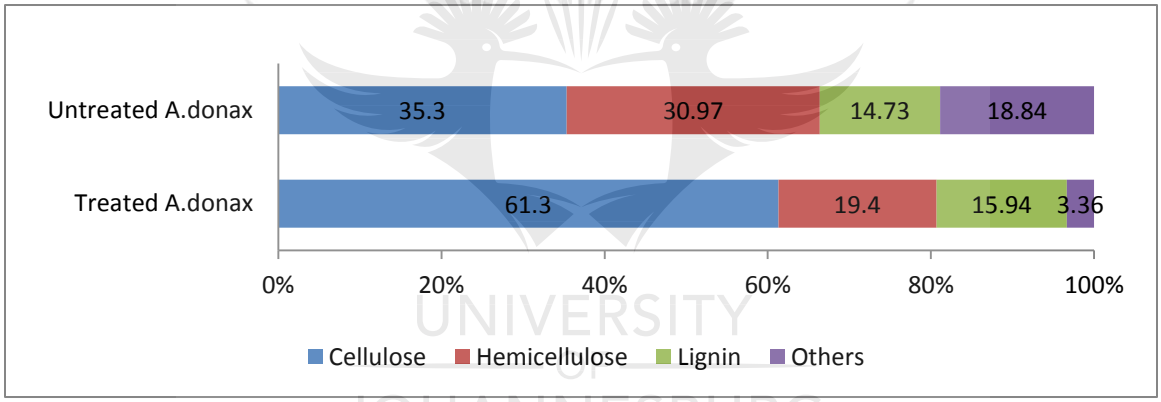

Figure 3.12: Compositional analysis of treated and untreated *A.donax*

3.5.6. P-XRD analysis of undissolved solid residue and untreated biomass

Powder-X-ray diffraction was also used to analyze the crystallinity of the pretreated biomass with respect to the untreated biomass. **Figure 3.13** shows the X-ray diffractograms of untreated *A. donax* and the 12 hours treated *A.donax*. The spectra of both samples show similar diffraction patterns of native cellulose (cellulose I allomorph). This implies that the DES pretreatment did not in any way modify or alter the structure of cellulose in the biomass. The major peaks observed at 15.5 -17, 22.3 and 34.8 2θ degrees depict that the crystalline structure of cellulose in

A.donax remained unchanged even after DES treatment. Certain minor peaks were also observed in both treated and untreated samples at 26.7, 28.2, 29.5, 32.1 2θ degrees. These minor peaks are suspected to be from other crystalline compounds or inorganic materials in the original *A.donax* as they are seen to be carried into the pretreated sample.

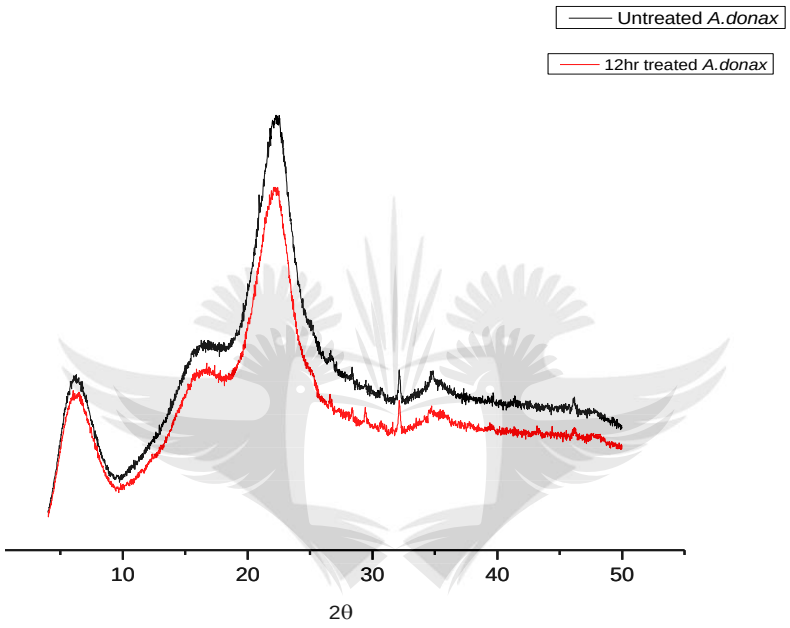

Figure 3.13: P-XRD diffractograms of untreated *A.donax* and the 12hour treated *A.donax* showing cellulose reflections

Using the Segal method for rapid determination of crystallinity of cellulose,[26] the Crystallinity Index (CrI) of the treated and untreated biomass was calculated. The mathematical expression of CrI according to the Segal method is represented by equation 3.11 below. The CrI compares the content crystalline fractions in cellulose samples.[27] It gives information on which samples have higher crystallinity and which samples do not. It does not necessarily give results of the amount of cellulose present in samples because the value of CrI for the sample may be different depending on the method of calculation and measuring technique. Interestingly, the CrI of the pretreated sample was slightly lower than that of the untreated biomass (**Table 3.3**). It was

expected that the crystallinity of cellulose in the pretreated sample would be higher than in the untreated sample due to the increase in the amount of cellulose. However, that was not seen from the X-ray diffraction results. It is hence, possible that the cellulose is in a way exposed to swelling and the DES breaks the crystalline regions of cellulose during pretreatment leading to reduced crystallinity.

$$CrI = \frac{(I_{002} - I_{am})}{I_{002}} x100 \ldots\ldots\ldots\ldots\ldots \text{(Eqn. 3.11)}$$

Where I_{002} is the highest intensity of the 002 lattice diffraction (in arbitrary units) and I_{am} is the intensity of diffraction at $2\theta = 18^0$ (in arbitrary units).

Table 3.3: Crystallinity Index of treated and untreated *A. donax*

Sample	%Crystallinity Index (CrI)
Untreated *A.donax*	53.6
12 hour treated *A.donax*	51.4

3.5.7. FT-IR analysis of precipitated biomass fraction (dissolved biomass)

The biomass fraction obtained from precipitation with water after the 12-hour treatment was analyzed by FT-IR spectroscopy to observe its structural properties (**Figure 3.14**). From the spectrum, a very intense C=O stretching peak is seen at 1735 cm^{-1}. This peak, as discussed earlier is characteristic of the carbonyl group of unconjugated ketones, carbonyls and esters of cellulose, hemicellulose or lignin. However, from the structural nature of the sample observed in the spectrum, other attributes of cellulosic peaks (such as the shape of O-H stretch and cellulosic C-O stretch at 1033 cm^{-1}) are not observed. Also from the results of the chemical analysis of the pretreated sample (which depicts the removal of hemicellulose), this fraction is most likely to be

hemicellulose and possibly some amount of lignin. The above results suggest that the DES system extracts a larger amount of hemicellulose and some lignin from *A.donax*.

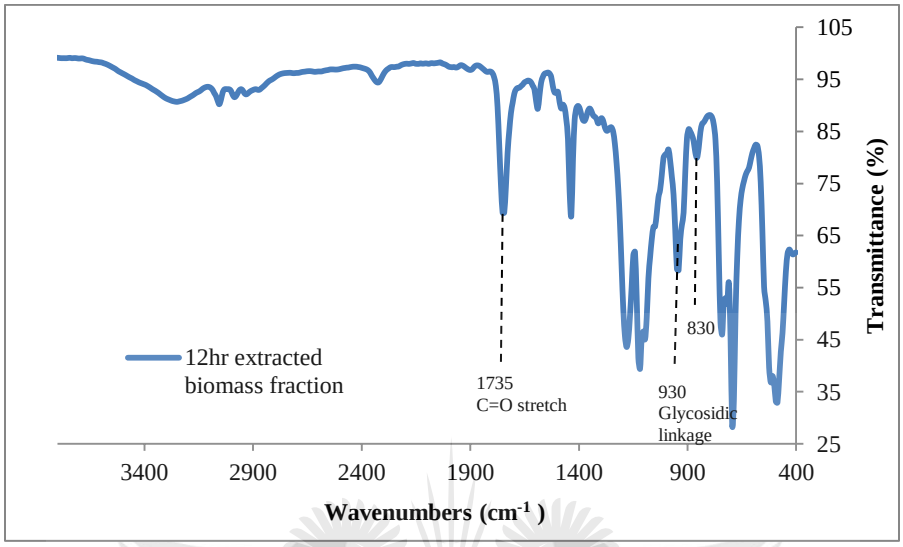

Figure 3.14: FT-IR spectrum of 12hour treated *A. donax* extract

3.5.8. SEM analysis of undissolved solid residue and untreated biomass

SEM analysis of the solid residues of both untreated and treated biomass was analyzed. It is expected that the structure of the fibres of the treated biomass would be rougher by the action of the DES interacting with it, giving it a looser surface compared to the untreated biomass. However, the surface of the treated biomass is rather observed to be smoother and more ordered than that of the untreated biomass. The tiny fibres seen on the untreated biomass are observed to be absent in the surface structure of the treated biomass. This suggests that the DES possibly works on the outer surface of biomass. There are currently different reports on the structure of biomass and the arrangement of the biopolymers in its cell wall. According to Qin et al, the primary cell wall (outer layer of the cell wall) is a heterogeneous mixture of cellulose, hemicellulose and pectin whereas the secondary cell wall (which is inside the primary cell wall) contains majorly, cellulose, hemicellulose and lignin (**Figure 3.15**).[25] Hemicellulose is also

reported to be attached to cellulose fibrils by hydrogen bonds and Van der Waal's interactions while also been cross-linked with lignin accounting for the strength of the plant cell wall.[28] Based on these reports, it would suggest that mainly hemicellulose in the primary cell wall of the biomass was removed resulting in the smoothening of the surface of the treated biomass.

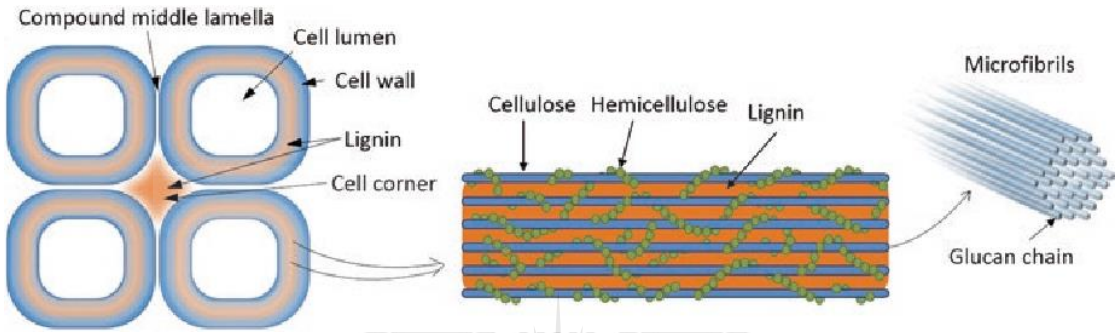

Figure 3.15: Visualisation of plant cell wall structure[25]

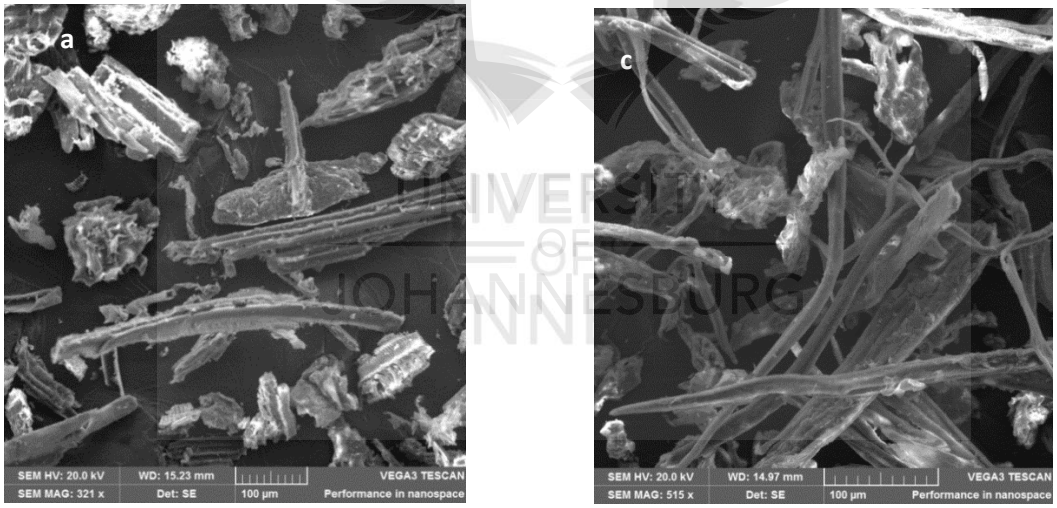

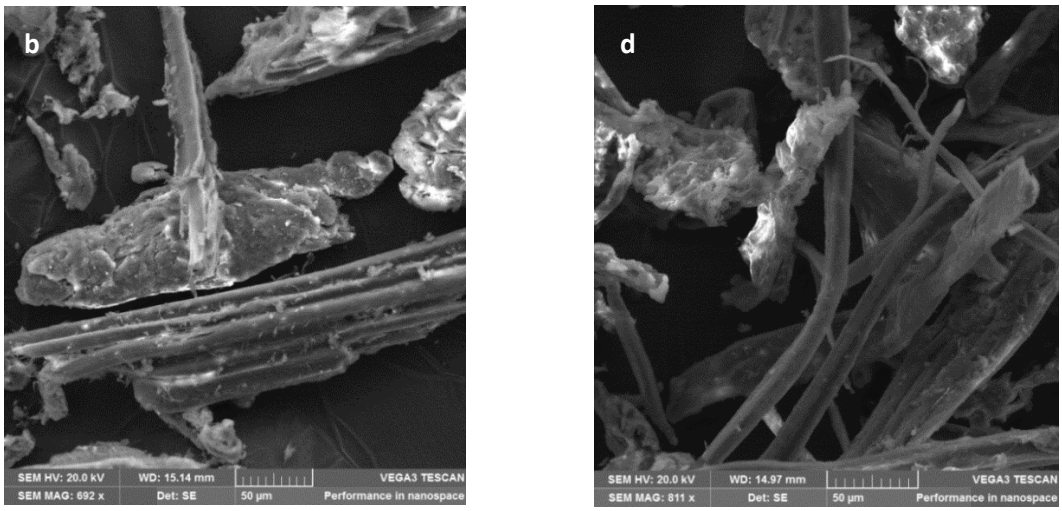

Figure 3.16: SEM micrographs of untreated *A. donax* (a & b) and DES-treated *A. donax* (c & d)

3.6. DES Recovery

After precipitation of the dissolved biomass from the mixture by washing severally with water, the DES-water mixture was left in a vacuum oven at 60^0C for more than 12 hours to evaporate the water. The amount of DES recovered was found to be less than 20%. The small yield of DES recovered could be attributed to loss as a result of several washing steps.

3.7. Regeneration and yield of dissolved cellulose

The amount of cellulose dissolved as observed to increase as temperature as increased. However at temperatures above 130^0C, the mixture was observed to decompose after a few hours of stirring. At higher temperatures, the cellulose in the reaction mixture began to gradually turn dark, signifying its decomposition. The increase in the rate of dissolution with increase in temperature can be attributed to the reduced viscosity of the system as temperature increase which leads to a higher interaction of the solute and the solvent. The DES is able to penetrate the pores of the biomass and facilitate dissolution.

Table 3.4: Dissolution of cellulose at various temperatures in DES 1

Dissolution temperature (^{0}C)	80	100	120
Solubility (wt %)	0.50	0.60	0.83

3.7.1. FT-IR analysis of dissolved cellulose

The DES-dissolved cellulose (regenerated cellulose) was analyzed by FT-IR spectroscopy (**Figure 3.17**) to observe any structural changes that might have occurred.

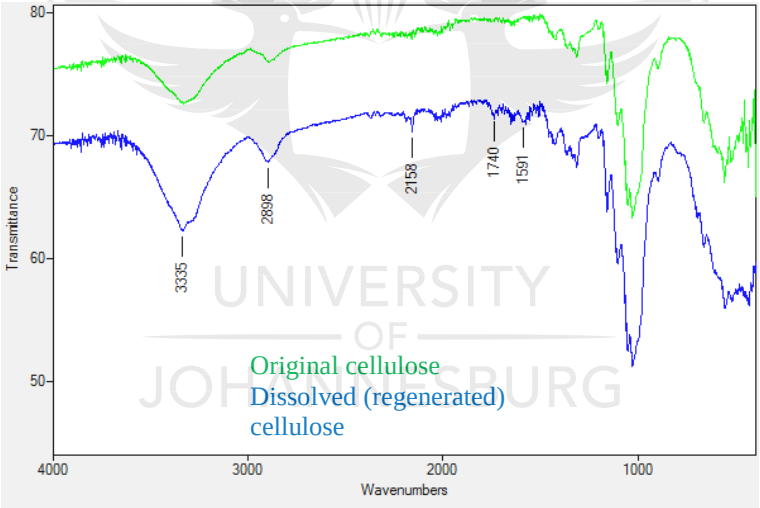

Figure 3.17: FT-IR spectrum of the regenerated and original cellulose

From the spectrum in **Figure 3.17**, it can be seen that the structure of cellulose remains unchanged and hence there is no derivatization whatsoever of the regenerated cellulose. There is however an observed sharpening of the O-H stretch of dissolved cellulose indicative of free OH groups and partial breaking of intermolecular hydrogen-bonding

3.7.2. P-XRD analysis of dissolved cellulose

The diffraction patterns of the untreated and treated cellulose (both the undissolved and regenerated cellulose) were analysed by P-XRD (**Figure 3.18**). The spectra show the diffraction pattern of native cellulose I and not amorphous cellulose (cellulose II). The major diffractions peaks of cellulose were observed at 15.5 -17, 22.3 and 34.8 2θ degrees for all samples including the treated samples suggestive of unchanged crystalline nature of cellulose by DES treatment.

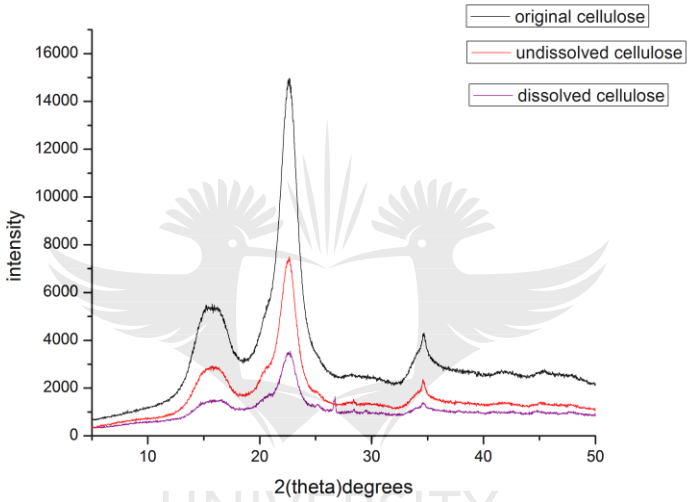

Figure 3.18: P-XRD spectra of treated and untreated cellulose samples

The intensity of the peaks in a way gives us information on the crystallinity of the samples. However, the Segal method for rapid determination of the crystallinity index (CrI) (**Eqn. 3.11**) was used to estimate the CrI of the samples (**Table 3.4**). The crystallinity index of cellulose was observed to decrease from 78.8% to 67.1%. The spectrum of the undissolved cellulose suggests that the DES swells the cellulose fibres as it is also observed to have a decreased crystallinity. The decrease in the cellulose crystallinity as a result of DES treatment could facilitate the easy hydrolysis of regenerated cellulose either by enzymes or acids to produce sugars.

Table 3.5: Crystallinity index of treated and untreated cellulose samples

Sample	Crystallinity index (%)
Original cellulose	78.8
Undissolved cellulose	76.2
Dissolved (regenerated) cellulose	67.1

3.7.3. SEM Analysis of treated and untreated cellulose

The SEM micrographs of both the untreated and treated cellulose as also analyzed to observe surface changes caused by pretreatment. The fibres of the treated cellulose seemed to have been compacted by the action of DES treatment hence showing clusters of the fibres. However, a closer look at the surface of the fibres of the treated cellulose shows a rough surface compared to that of the untreated cellulose which shows a smooth surface. The roughness of the surface of the treated cellulose is suggested to be as a result of DES penetrating the fibres and breaking the bonds, giving it a looser surface compared to the untreated cellulose and causing decrystallization in the cellulose as observed.

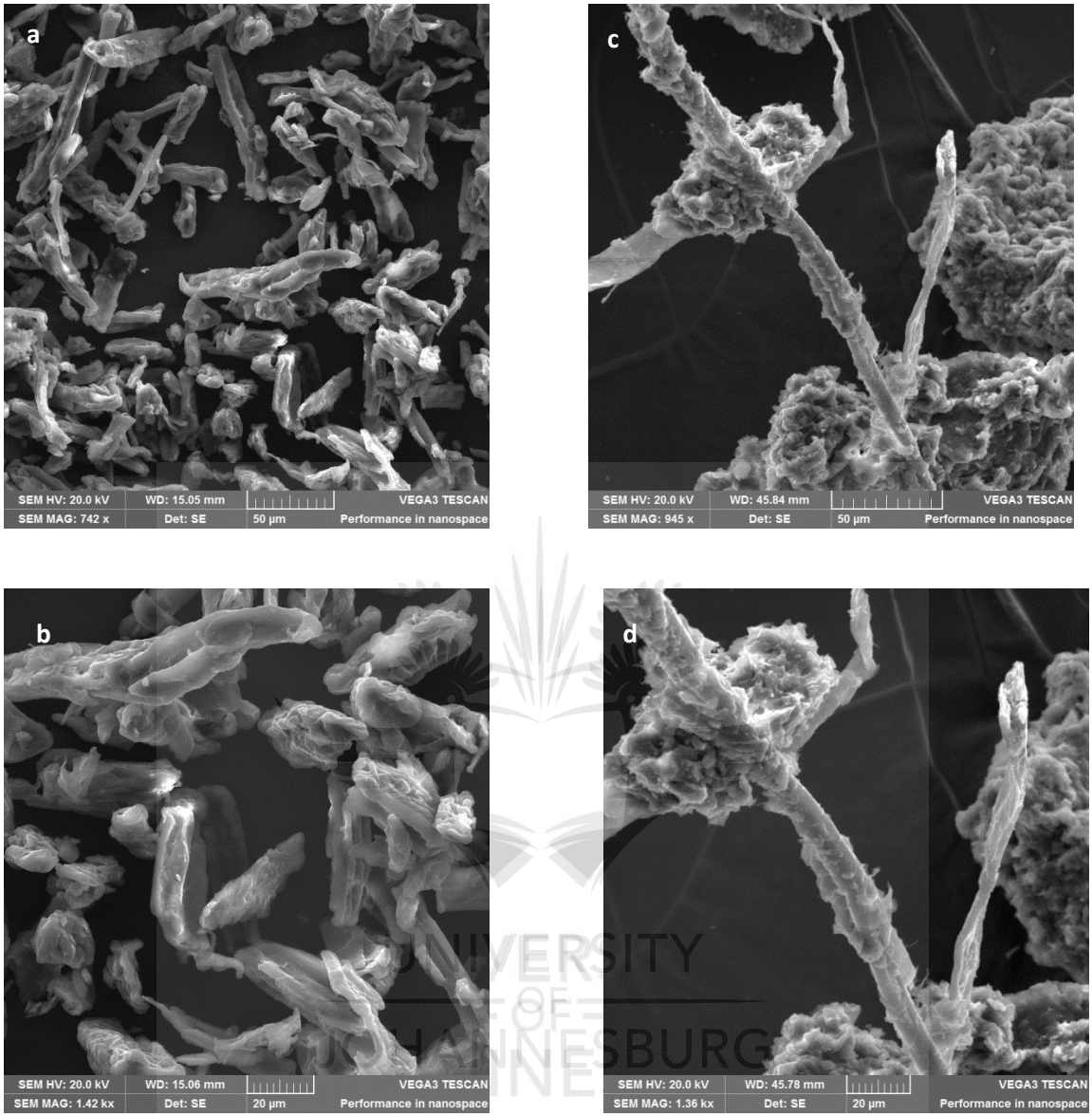

Figure 3.19: SEM micrographs of untreated cellulose (a & b) and DES-treated cellulose (c & d)

3.8. Attempted direct dissolution and hydrolysis of cellulose

The dissolved cellulose obtained from the dissolution in **DES 1** was then directly hydrolyzed using various catalysts in **DES 1** as a solvent. In this procedure, the undissolved cellulose from the dissolution process was separated from the dissolved cellulose by washing with ethanol and

filtering. The ethanol was then removed from the DES-cellulose mixture and a catalyst was added to hydrolyze the dissolved cellulose.

3.8.1. Hydrolysis of cellulose using DES 2 as catalyst

The ^{1}H NMR of the crude mixture from the hydrolysis reaction (**Figure 3.20**) showed peaks of the two DESs as well as the appearance of new peaks in the region of 3.0-4.0 ppm. The NMR solvent peak is seen at 4.6ppm. Comparing the spectrum to that of pure glucose shows a similarity in the peaks, suggesting that some of the dissolved cellulose has been hydrolysed to glucose. New peaks are also observed at approximately 2.0 ppm. Further studies are underway to ascertain and quantify the glucose formed by HPLC and to further optimize for increased yields

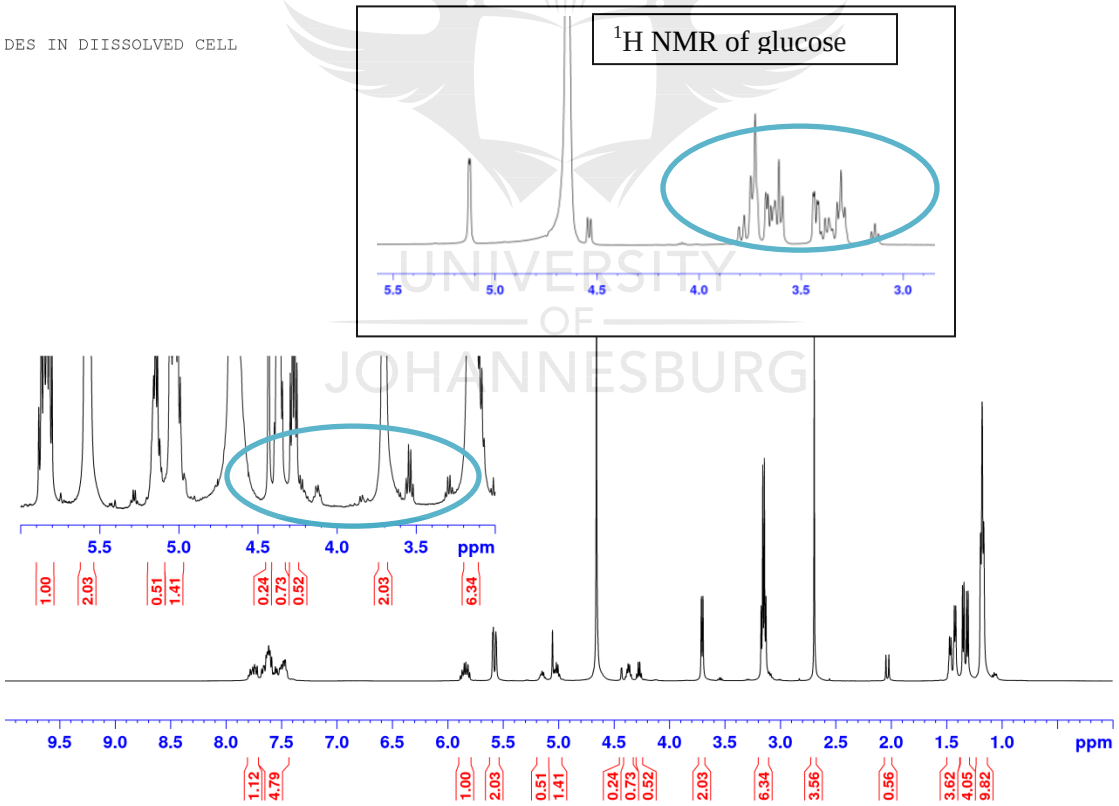

Figure 3.20: ^{1}H NMR of the crude mixture of cellulose hydrolysis using DES 2

3.8.2. Hydrolysis of cellulose using a zeolite

Figure 3.21 shows the ^{1}H NMR spectrum of the crude mixture of cellulose hydrolysis using zeolites. The DES 1 peaks are seen between 1.0ppm and 1.5pmm as well as between 4.0ppm and 5.0ppm and in the aromatic region. The NMR solvent peak is seen at 4.6ppm. The appearance of new peaks in the ^{1}H NMR spectrum of the crude mixture is not direct evidence of the presence of glucose. However, there is an increase in the intensity of the peak at 2.0 ppm. Further studies are underway to ascertain and quantify the glucose formed by HPLC and to further optimize for increased yields.

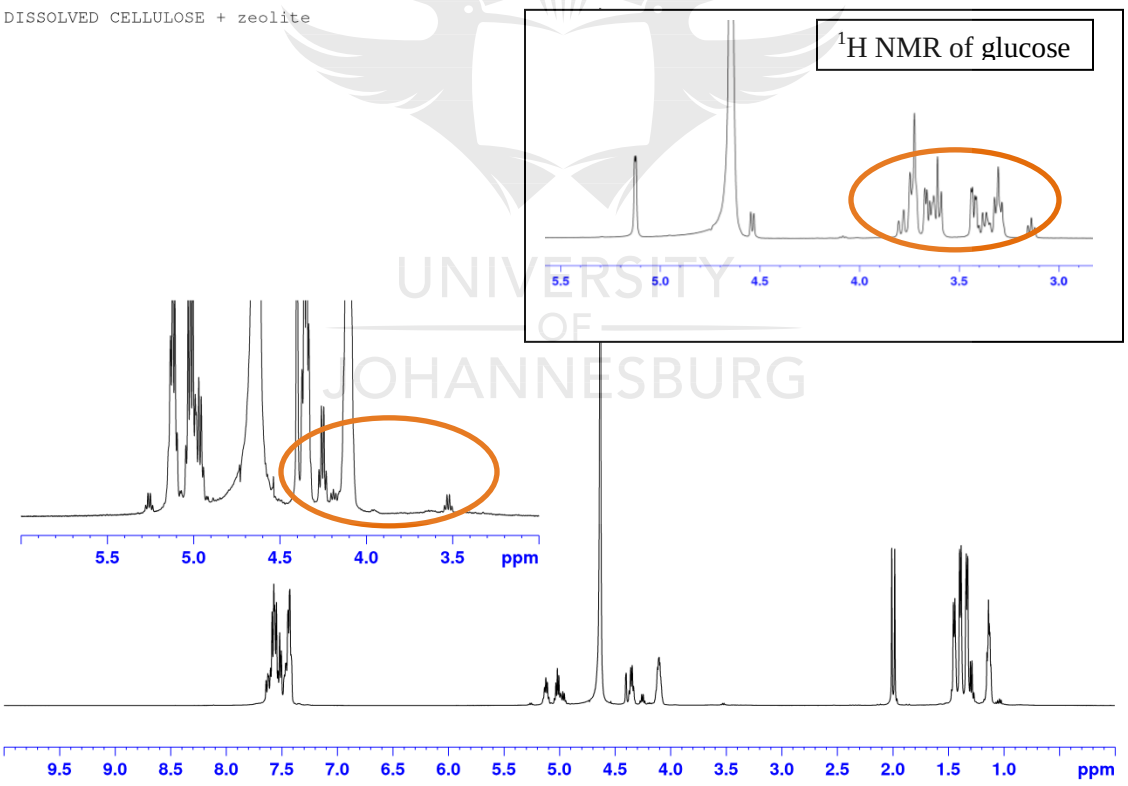

Figure 3.21: ^{1}H NMR of the crude mixture of cellulose hydrolysis using zeolites recorded in D_2O

3.9. Summary and conclusions

The use of a phosphonium-based DES in biomass fractionation and cellulose dissolution has been explored. The optimum conditions for biomass dissolution were achieved at 100^0C for 12hrs and at a biomass loading of 5wt%. Biomass samples were analyzed using SEM and FT-IR before and after pretreatment. Compositional analysis of the pretreated biomass sample suggested that hemicellulose was mostly solubilized during pretreatment. Concerning cellulose dissolution, the highest amount of cellulose dissolved was obtained at 120^0C. The hydrolysis of the dissolved cellulose was also attempted using DES and zeolite as catalysts.

3.10. Experimental section

3.10.1 Materials, methods and instrumentation

All chemicals and solvents used were of reagent grade purchased from Sigma Aldrich and used without further purification. Cellulose cotton linters (type 20, 20µm), sodium chlorite ($NaClO_2$), sodium bicarbonate ($NaHCO_3$), glacial acetic acid (CH_3COOH), hydrochloric acid (HCl), sulfuric acid (H_2SO_4) and ethanol. Nylon 66 membrane filters were also purchased from Sigma Aldrich. DESs and IL used were freshly synthesized prior to use.

3.10.2. Ultra-Violet-Visible Spectroscopy

UV-Visible spectrophotometry data were collected on a Shimadzu UV 2540 spectrophotometer at the University of Johannesburg, Department of Chemical Sciences Measurements were recorded within the absorbance range of 200-800nm. The absorbance of the blank (water) was initially measured prior to sample measurements.

3.10.3. Fourier-Transform-Infrared Spectroscopy

FT-IR data were obtained neat using a Perkin Elmer Spectrum BX II fitted with an ATR probe at the University of Johannesburg, Department of Chemical Sciences. The absorption intensities

were recorded in percentage (%) and the absorption frequencies in wavenumbers (cm^{-1}) in the range of 400-4000.

3.10.4. Scanning Electron Microscopy (SEM)

SEM micrographs were recorded on a Tescan Scanning Electron Microscope equipped with an Oxford INCA Electron Dispersive System detector at the University of Johannesburg, Analytical facility, Spectrau. The type of electron signal used was that of the secondary electron (SE). The Vega software was used in capturing images.

3.10.5. Powder X-ray Diffraction (P-XRD)

P-XRD diffractions were recorded on a PANalytical X'PertPro X-Ray diffractometer at the University of Johannesburg, Analytical facility, Spectrau. Diffraction patterns were reported in arbitrary units [a.u] on the vertical axis and position [2 θ (^{0})] on the horizontal axis within a range of 4-50 2θ (^{0}). The Highscore software was used to match the crystalline phase of the samples.

3.11. References

1 B. Yang and C. E. Wyman, *Biofuels, Bioprod. Biorefining*, 2008, **2**, 26–40.

2 I. M. O'Hara, Z. Zhang, W. O. S. Doherty and C. M. Fellows, in *Green Chemistry for Environmental Remediation*, 2012, pp. 505–560.

3 M. Francisco, A. Van Den Bruinhorst and M. C. Kroon, *Green Chem.*, 2012, **14**, 2153–2157.

4 R. Pilu, A. Bucci, F. C. Badone and M. Landoni, *African J. Biotechnol.*, 2012, **11**, 9163–9174.

5 R. Pilu, A. Manca, M. Landoni and S. Agrarie, *Maydica*, 2013, **58**, 54–59.

6 Y. J. Jeon, Z. Xun and P. L. Rogers, *Lett. Appl. Microbiol.*, 2010, **51**, 518–524.

7 P. Ghetti, L. Ricca and L. Angelini, *Fuel*, 1996, **75**, 565–573.

8 A. Sluiter, R. Ruiz, C. Scarlata, J. Sluiter, D. Templeton, A. Sluiter, R. Ruiz, C. Scarlata,

J. Sluiter and D. Templeton, *Determination of Extractives in Biomass Laboratory Analytical Procedure (LAP)*, Colorado, 2008.

9 A. Sluiter, B. Hames, R. Ruiz, C. Scarlata, J. Sluiter and D. Templeton, *Determination of Ash in Biomass Laboratory Analytical Procedure (LAP)*, Colorado, 2008.

10 M. Ioelovich, *J. SITA*, 2015, **4**, 208–214.

11 A. Sluiter, B. Hames, D. Hyman, C. Payne, R. Ruiz, C. Scarlata, J. Sluiter, D. Templeton and J. W. Nrel, *Determination of Total Solids in Biomass and Total Dissolved Solids in Liquid Process Samples Biomass and Total Dissolved Solids in Liquid Process Samples*, Colorado, 2008.

12 A. Sluiter, B. Hames, R. Ruiz, C. Scarlata, J. Sluiter, D. Templeton and D. C. Nrel, *Determination of Structural Carbohydrates and Lignin in Biomass*, Colorado, 2012.

13 P. Navard and C. Cuissinat, in *7th International Symposium 'alternative Cellulose: Manufacturing, Forming, Properties'.*, 2011, pp. 1–8.

14 A. Geffert, O. Vacek and A. Jankech, *BioResources*, 2017, **12**, 5017–5030.

15 H. Ren, C. Chen, S. Guo, D. Zhao and Q. Wang, *BioResources*, 2016, **11**, 8457–8469.

16 M. Popescu, C. Popescu, G. Lisa and Y. Sakata, *J. Mol. Struct.*, 2011, **988**, 65–72.

17 F. Xu, J. Yu, T. Tesso, F. Dowell and D. Wang, *Appl. Energy*, 2013, **104**, 801–809.

18 A. Galia, B. Schiavo, C. Antonetti, A. Maria, R. Galletti, L. Interrante, M. Lessi, O. Scialdone and M. G. Valenti, *Biotechnol. Biofuels*, 2015, **8**, 1–19.

19 D. Licursi, C. Antonetti, J. Bernardini, P. Cinelli, M. Beatrice, A. Lazzeri, M. Martinelli, A. Maria and R. Galletti, *Ind. Crop. Prod.*, 2015, **76**, 1008–1024.

20 J. L. K. Mamilla, U. Novak, M. Grilc and B. Likozar, *Biomass and Bioenergy*, 2019, **120**, 417–425.

21 F. Hu, S. Jung and A. Ragauskas, *Bioresour. Technol.*, 2012, **117**, 7–12.

22 X. Qian, M. R. Nimlos and D. K. Johnson, *Appl. Biochem. Biotechnol.*, 2005, 1–4.

23 P. Sannigrahi, D. H. Kim, S. Jung and Arthur Ragauskas, *Energy Environ. Sci.*, 2011, **4**, 1306–1310.

24 S. D. Shinde, X. Meng, R. Kumar and A. J. Ragauskas, *Green Chem.*, 2011, 1–14.

25 L. Qin, W. Li, J. Zhu, B. Li and Y. Yuan, *Production of Platform Chemicals from Sustainable Resources*, 2017.

26 L. Segal, J. J. Creely, A. E. Martin and C. M. Conrad, *Text. Res. J.*, 1959, 786–794.

27 M. Y. Ioelovich and G. P. Veveris, *J. Wood Chem.*, 1987, **5**, 72–80.

28 P. Phanthong, P. Reubroycharoen, X. Hao and G. Xu, *Carbon Resour. Convers.*, 2018, **1**, 32–43.

CHAPTER FOUR

Dehydration of carbohydrates to 5-HMF

4. 1 Introduction

In the efficient valorization of biomass to produce fuels and platform chemicals, the abundance of hexoses and pentoses in the biopolymers of biomass (cellulose and hemicellulose) has created an avenue for the making of these platform chemicals (examples, furfural, 5-hydroxymethyl furfural, 5-chloromethyl furfural) mainly through acid-catalyzed dehydration of sugars.[1] The production of HMF has gained increasing attention over the years as HMF is a significant building block for the production of polymers, fuel additives, and other chemicals.[2] HMF can be obtained from fructose as well as glucose (by isomerization of fructose), sucrose, and directly from cellulose.[3]

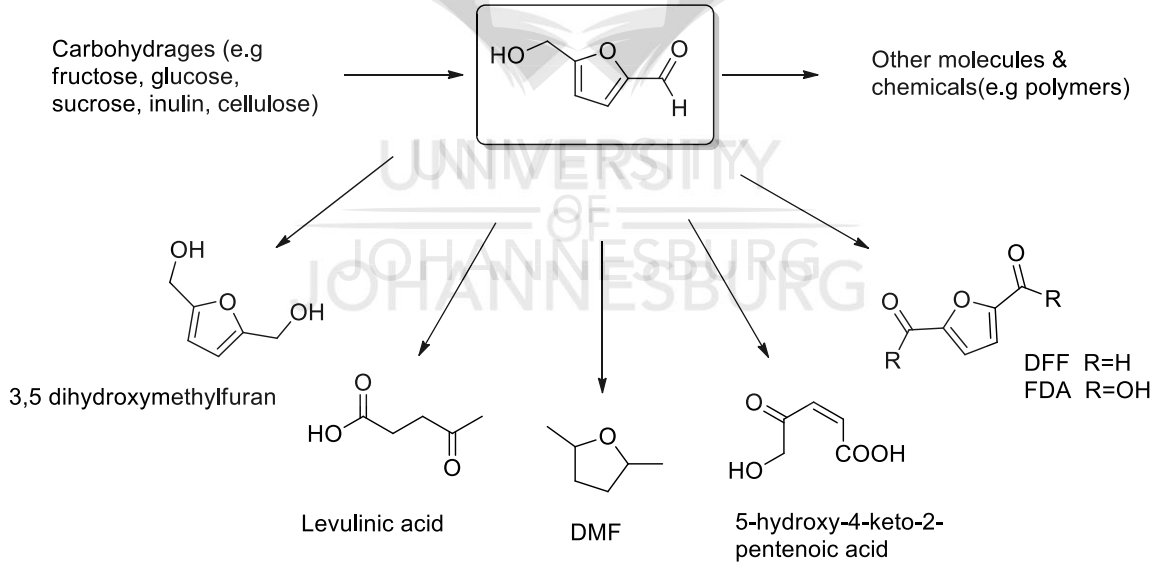

Scheme 4.1: Examples of chemicals obtained from HMF[3]

The formation of HMF is reported to proceed by the acid-catalyzed dehydration of monosaccharides by the loss of water molecules hence, its production from polysaccharides such

as cellulose will first require depolymerization by hydrolysis to breakdown the complex glycosidic bonds present in cellulose thereby liberating sugar monomers that can easily be converted by dehydration.[3] Having observed the formation of some amounts of glucose in the hydrolysis of cellulose by a DES (Chapter 3.5) we are interested to see if direct degradation of cellulose to HMF might be affected in the future by first separately studying carbohydrate (fructose, glucose, and molasses) dehydration by the DESs.

The synthesis of HMF by acid dehydration at high temperatures has been reported to be followed by the formation of side products[4] including humins and levulinic acid.[5] The low reactivity of glucose compared to fructose (due to fructose ability to form less stable ring structures and hence easily enolise) makes fructose react faster than glucose in converting to HMF.[6]

Molasses obtained from sugarcane have been used in different applications including the production of alcohol, yeast as well as feed for livestock.[7] Molasses could however be a viable feedstock for the production of sugar-derived platform chemicals such as 5-HMF. Final molasses or C molasses or blackstrap molasses is obtained from the final boiling of sugarcane juice to obtain sugar crystals.[8,9] The C molasses are the least in sugar quality as most of the sucrose has been removed. An approximate amount of sucrose left in C molasses is about 32-42% which is currently not removed or utilized.[9]

4.2. Results and discussion

4.2.1 Dehydration of fructose in deep eutectic solvents

The dehydration reactions were performed using DES as both solvent and catalyst. The dehydration of fructose, glucose, and molasses was evaluated with respect to time, temperature, and substrate loading. The mass of humins formed was quantified in milligrams and the yields of known products were reported in percentage. The dehydration of these substrates yielded 5-HMF

as the major product and 5-CMF as a by-product. The formation of 5-CMF was assumed to be as a result of the presence of chloride ions in the DES. The hydroxyl group of HMF undergoes a halogen substitution reaction as it is being produced to give 5-CMF.[10] The percent amount of HMF formed was calculated by the mathematical expression below (**Eqn 4.1**). The yields of products are also summarized and reported in **Table 4.1** below.

$$\%HMF\ yield = \frac{\text{moles of HMF}}{initial\ moles\ of\ sugar}\ x\ 100 \quad \text{(Eqn 4.1)}$$

4.2.2. Screening of DESs for the dehydration of fructose

The procedure for the reaction was adding 5wt% (per mass of DES, that is, between 70mg-120mg) of fructose into a round bottom flask containing deep eutectic solvent (**DESs 2-4**) at 80^0C for 60mins under stirring after which the reaction is quenched using cold water. Deionized water was added to the reaction mixture and the crude mixture was analyzed by ^{1}H NMR spectroscopy using DMF as an internal standard. Three DESs were screened for the dehydration reactions (**Figure 4.1**). The yield of 5-HMF was highest in **DES 4** (45.4%), followed by **DES 2** (34%) and then **DES 3** (25.3%). **DES 2** and **DES 3** were observed to be more selective to 5-HMF under these conditions however the yields were poor. **DES 4** was hence chosen to be the best DES for the dehydration of fructose.

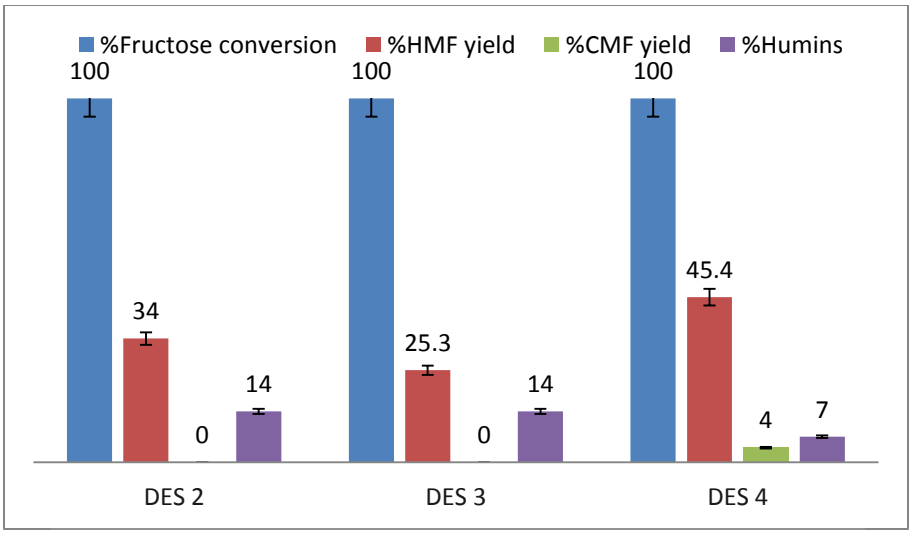

Figure 4.1: Screening of DESs for fructose dehydration (Operating conditions: T=80^{0}C, t=60mins, amount of fructose= 5wt% of DES)

The acidity and pH of the DES are known to influence the dehydration of sugars. According to Rosatella *et al*, the formation of HMF was favored by increased acidity (lower pH).[3] However, according to the work done by Korner and coworkers, the DES with weaker acidity gave a higher yield of HMF, suggesting that faster kinetics and higher yield of dehydration products is as a result of the molecular interactions of the solvent and not necessarily the acidic strength.[11] It is hence not surprising that **DES 4** gave a higher yield of HMF even though it is not the most acidic. The presence of a suitable amount of water is also known to be beneficial to the formation of HMF in DESs.[12] The increase in the yield of HMF in **DES 4** is possibly a result of the presence of water molecules in the DES produced by the oxalic acid dihydrate used. The water present in the DES reduces the viscosity of the mixture and enhances mass transfer, hence, promoting the yield of the product.

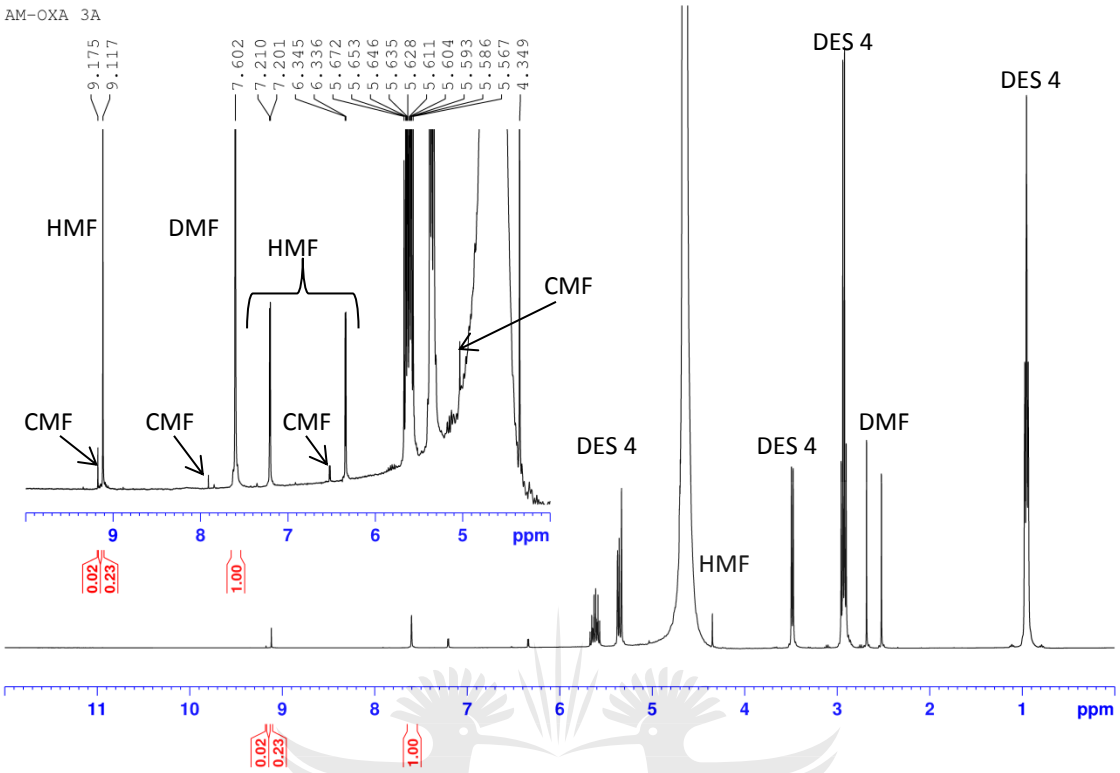

Figure 4.2: ^{1}H NMR of the crude mixture of fructose dehydration in DES 4

Figure 4.2 above shows the ^{1}H NMR spectrum of the crude mixture of the dehydration of fructose in **DES 4**. The peaks belonging to HMF as well as the DES are represented. As seen, there is an appearance of a second aldehyde proton peak at 9.17ppm which is suspected to be CMF. This is possible because of the presence of chloride ions in the DES.

4.2.3. Conversion as a function of temperature

Using **DES 4** as the best DES for fructose dehydration, the reactions were performed at 60^{0}C, 80^{0}C, and 100^{0}C for 60mins. The mass of fructose used (5wt %) was approx. 88mg. The %HMF yield was 2% at 60^{0}C, 45.4% at 80 ^{0}C, and 27.7% at 100^{0}C (**Figure 4.2**). At increasing temperatures, an increase in the amount of humins was observed, resulting in a decrease in product yield at 100^{0}C (8.8mg of humins). At 60^{0}C however, a small amount of humins (5.2mg)

formed and the conversion of fructose was less than 100% while 6.1mg of humins was formed at 80^0C. Increasing temperature increases the rate of reaction of reactants. This increase is suggested to result in the formation of humins by the increased reaction of reaction intermediates and products resulting in decreased yields at high temperatures.[13]

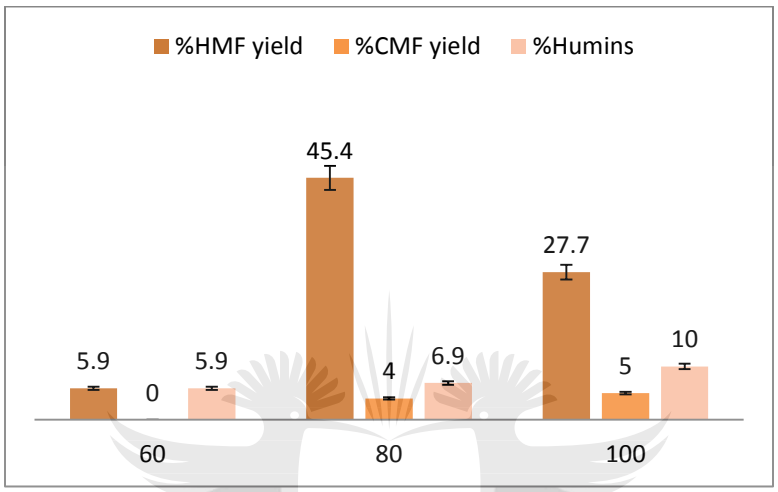

Figure 4.3: Effect of temperature on HMF yield. (Operating conditions: DES=DES 4, t=60mins, amount of fructose= 5wt% of DES)

4.2.4 Conversion as a function of time

The effect of time on the dehydration of fructose was determined by performing the reactions using **DES 4** at 80^0C and within the times of 30mins, 45mins and 60mins. The mass of fructose used (5wt %) ca. 88mg. The amount of humins formed was observed to increase with an increase in time (despite the full conversion of fructose) thereby affecting the yield of HMF. The %HMF yield after 30mins was 43.6%, after 45mins, 61.1% and after 60mins, 45.4% (**Figure 4.3**). The optimum time for the reaction was hence 45mins. The influence of reaction time on the yield of product is such that, as products stay longer in the reaction mixture, they react with themselves and with intermediates formed to produce insoluble humins and hence decrease the yield of the

products. The amount of humins formed after 60mins was highest (6.1mg) followed by 45mins (5.0mg) and then 30mins (4.9mg).

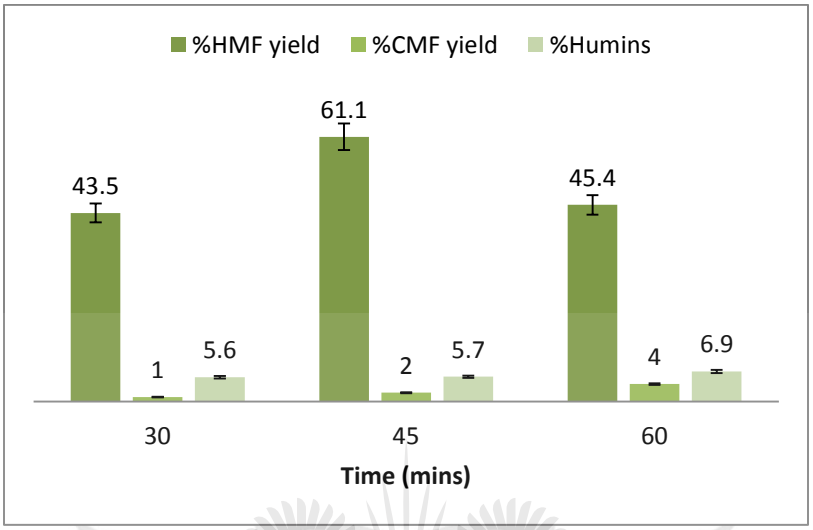

Figure 4.4: Effect of time on HMF yield. (Operating conditions: DES=DES 4, Temperature= 80^{0}C, amount of fructose= 5wt% of DES)

4.2.5 Conversion as an effect of substrate loading (fructose)

The dehydration reactions were performed at 80 ^{0}C for 45mins using different amounts of substrates, 2.5wt% (ca. 44mg of fructose), 5.0wt% (ca. 88mg of fructose) .and 10.0wt% (ca. 176mg of fructose) per mass of DES used (**DES 4**). The highest yield of HMF was observed for 5.0wt% fructose (61.1%) (**Figure 4.4**). A larger amount of humins was seen to be formed for the reaction with 10wt% substrate loading as the yield of HMF was reduced (48.7%) with an increase in the amount of CMF formed. While fewer humins was observed in the reaction with the substrate loading of 2.5wt%, more HMF (58.7%) was however produced. The increase in the formation of humins with higher substrate loading is suggested to be as a result of the reactions of the products produced, intermediates, and starting material.[3] The high substrate loading also

affects the viscosity of the reaction mixture and hence affects the yield of products by reducing mass transfer.

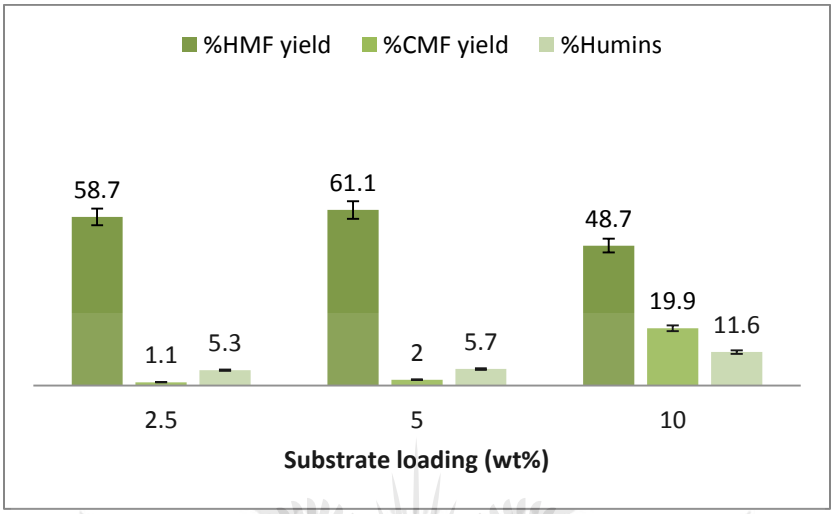

Figure 4.5: Effect of substrate loading on HMF yield. (Operating conditions: DES=DES 4, t=45mins, Temperature=80^{0}C)

4.3. Dehydration of glucose

Glucose (anhydrous) was also employed as an alternative substrate for the production of HMF. As stated previously, glucose has a low reactivity rate as compared to fructose due to the formation of a more stable ring structure. Its reactivity was hence tested in the three DESs. In this procedure, 5wt% of glucose (ca.70mg-120mg depending on the DES used) was added to the DESs at 80^{0}C and stirred for some time, after which the reaction is quenched under cold water. Deionized water is then added to the mixture and the yield of the product is analyzed by ^{1}H NMR spectroscopy using an internal standard.

From **Table 4.1**, the highest conversion of glucose to HMF was seen in **DES 2** (6.8%). This was accompanied by the formation of humins and the presence of some unreacted glucose. The conversion of glucose in **DES 3** was found to be 3.1% also with the formation of a small amount

of humins and unreacted glucose. There was no observed conversion of glucose to HMF in **DES 4** however even after 60mins of the reaction. In this case, a high yield of HMF was observed with high acidity.

4.4. Dehydration of molasses

As an alternative feedstock, molasses were used under the optimum conditions (5wt%, 45mins, and 80^{0}C) to produce HMF. In this procedure, 5wt% of blackstrap molasses (ca. 70mg-120mg) were added to DES in a 50mL round bottom flask. The reaction mixture was allowed to stir for 45mins at 80^{0}C. The reaction is quenched under cold water and water is added to the reaction mixture. The amount of sugars in 5wt% of molasses is calculated based on the amount of total sugars in 100g of molasses. The yield of the desired product is analyzed by ^{1}H NMR spectroscopy using an internal standard. The reaction in **DES 2**, gave an HMF yield of 33.5%, 33.7% for **DES 3,** and 31.4% for **DES 4**.

Table 4.1: Conversion of sugars in deep eutectic solvents: (a) Glucose, (b) Molasses [0.37g of sugars is in 1g of molasses]

Entry	DES	Temperature (^{0}C)	Time (mins)	Substrate loading (wt %)	HMF yield (%)	CMF yield (%)	Mass of humins (mg)
1	[ATEA]Cl-Msa	80	60	5	34	-	10.9
2	[ATEA]Cl-Ptsa	80	60	5	25.3	-	14
3	[ATEA]Cl-Oxa	80	60	5	45.4	4	6.1
4	[ATEA]Cl-Oxa	100	60	5	27.7	5	8.8
5	[ATEA]Cl-Oxa	60	60	5	2	-	5.2
6	[ATEA]Cl-Oxa	80	30	5	43.6	1	4.9

7	[ATEA]Cl-Oxa	80	45	5	61.1	2	5.0
8	[ATEA]Cl-Oxa	80	45	10	48.7	19.9	10.2
9	[ATEA]Cl-Oxa	80	45	2.5	58.7	1.1	4.7
10[a]	[ATEA]Cl-Msa	80	60	5	6.8	-	9.4
11[a]	[ATEA]Cl-Ptsa	80	60	5	3.1	-	5.3
12[a]	[ATEA]Cl-Oxa	80	45	5	-	-	-
13[b]	[ATEA]Cl-Msa	80	45	5	33.5	-	18.2
14[b]	[ATEA]Cl-Ptsa	80	45	5	33.7	-	20.6
15[b]	[ATEA]Cl-Oxa	80	45	5	31.4	-	8

4.5. Conclusion

Deep eutectic solvents have successfully been used as both solvent and catalyst in the conversion of sugars to platform chemicals. Good yields of 5-HMF were obtained in short time and mild temperature. With the observation of the formation of humins in these reactions, the yield of 5-HMF could be enhanced by the extraction of HMF as it is being produced. This could be accomplished by the use of a solvent system that readily dissolves 5-HMF (and other products) and sparingly dissolves the DES to form a biphasic system. The highest yield of HMF recorded (61.1%) was obtained using **DES 4** at a temperature of 80^0C, time of 45mins, and fructose loading of 5wt%. Good dehydration potential for molasses (up to 61% HMF yield) is also demonstrated in this section meaning in the future DESs can be further developed into effective catalysts valorization of molasses, a by-product, of the sugar refining process.

4.6. References

1 R. A. Sheldon, *Green Chem.*, 2014, **16**, 950–963.

2 Q. Zhang, K. De Oliveira Vigier, S. Royer and F. Jérôme, *Chem. Soc. Rev.*, 2012, **41**, 7108–46.

3 A. A. Rosatella, S. P. Simeonov, R. F. M. Frade and C. A. M. Afonso, *Green Chem.*, 2011, **13**, 754–793.

4 C. Zhou, J. Zhao, A. E. G. A. Yagoub, H. Ma, X. Yu, J. Hu, X. Bao and S. Liu, *Egypt. J. Pet.*, 2017, **26**, 477–487.

5 F. Ilgen, D. Ott, D. Kralisch, C. Reil and K. Burkhard, *Green Chem.*, 2009, **11**, 1948–1954.

6 B. F. M. Kuster, *Starch*, 1990, **42**, 314–321.

7 T. Hashizume, S. Higa, Y. Sasaki, H. Yamazaki, H. Iwamura and H. Matsuda, *Agric. Biol. Chem.*, 1966, **30**, 319–329.

8 H. V. De Amorim and M. L. Lopes, *Chemistry (Easton).*, 2009, **Vi**, 39–46.

9 R. Perez, in *Tropical Feeds and Feeding Systems*, 1995, pp. 233–239.

10 W. Gao, Y. Li, Z. Xiang, K. Chen, R. Yang and D. S. Argyropoulos, *Molecules*, 2013, **18**, 7675–7685.

11 S. Körner, J. Albert and C. Held, *Front. Chem.*, 2019, **7**, 1–11.

12 S. Hu, Z. Zhang, Y. Zhou, B. Han, H. Fan, W. Li, J. Song and Y. Xie, *Green Chem.*, 2008, **10**, 1280–1283.

13 A. Assanosi, M. M. Farah, J. Wood and B. Al-Duri, *Comptes Rendus Chim.*, 2016, **19**, 450–456.

CHAPTER FIVE

Overall conclusions and future outlook

5.1. General conclusions

Three new deep eutectic solvents (one phosphonium-based and two ammonium-based) **DES1**, **DES 2** and **DES 3** as well as one already reported (**DES 4**) have been successfully synthesized and characterized by various spectroscopic techniques.

The phosphonium-based DES (**DES 1**) has proven to be effective in the fractionation of biomass (*Arundo donax*) and the dissolution and decrystallization of cellulose. The fractionation of *A. donax* at 12 hours with a biomass loading of 5wt% and temperature of 100^0C resulted in the highest dissolution of biomass. Compositional analysis suggested that hemicellulose was mostly extracted from the biomass, leaving behind cellulose fibers and lignin. The solid residues obtained after pretreatment showed slight changes in the morphology of the fibres (as evidenced by SEM analysis) of the treated and untreated biomass proving that the DES disrupts the bonds in biomass to enhance its dissolution. P-XRD analysis and calculation of the crystallinity index (CrI) of treated biomass showed a slight decrease in its crystallinity as compared to that of the untreated biomass suggesting that the DES also disrupts the bonds in cellulose and enhances amorphization.

Cellulose was also treated with **DES 1** to study its dissolving and swelling ability. The CrI of the dissolved cellulose was seen to be considerably lower than the original cellulose. The highest amount of cellulose dissolved (0.83wt%) was achieved at 120^0C in **DES 1**.

The cellulose dissolved in the **DES 1** could be hydrolyzed using a DES and zeolite as catalysts to produce glucose. Further studies to quantify and further corroborate the glucose formed are underway. This will also be coupled with optimization for higher glucose yields.

DES 2, **DES 3** and **DES 4** were effective in dehydration of carbohydrates to mainly HMF. The DESs were employed both as solvents and catalysts thereby proving their versatility and need for use of additional solvent. The dehydration of fructose resulted in the formation of 5-HMF and other side products including 5-CMF and humins. The highest yield of 5-HMF obtained was observed for **DES 4** at 80^0C and substrate loading (fructose) of 5wt%. The formation of humins was observed for the reactions with increasing temperature, time, and substrate loading.

5.2. Future outlook

The use of DESs in biomass fractionation or pretreatment and its mechanism is still at its infancy and phosphonium-based DESs have not seriously been explored as solvents for biomass pretreatment. This project proves that they have the potential of being effective in the pretreatment of biomass, dissolution of cellulose and in selective extraction of hemicellulose from biomass.

The structure of the alkyl side-chain of the HBAs play a role in the DESs interaction with biomass components, hence, other derivatives of phosphonium-based DES with varying side chains could be explored in biomass pretreatment or fractionation as well as cellulose dissolution.

The chemistry and interaction between the phosphonium-based DES and biomass as well as cellulose is not yet known and a study in this line is necessary and underway.

In the dehydration of sugars, the amount of humins (and other side product) formed was observed to increase with time and temperature. The humins are formed as a result of the polymerization of products and intermediates formed during the reaction. This occurrence can be minimized by the continuous or intermittent extraction of the product during the reaction. A biphasic system with a solvent that sparingly dissolves the DES but also readily dissolves the products could promote the increase in the yield of products.

APPENDIX

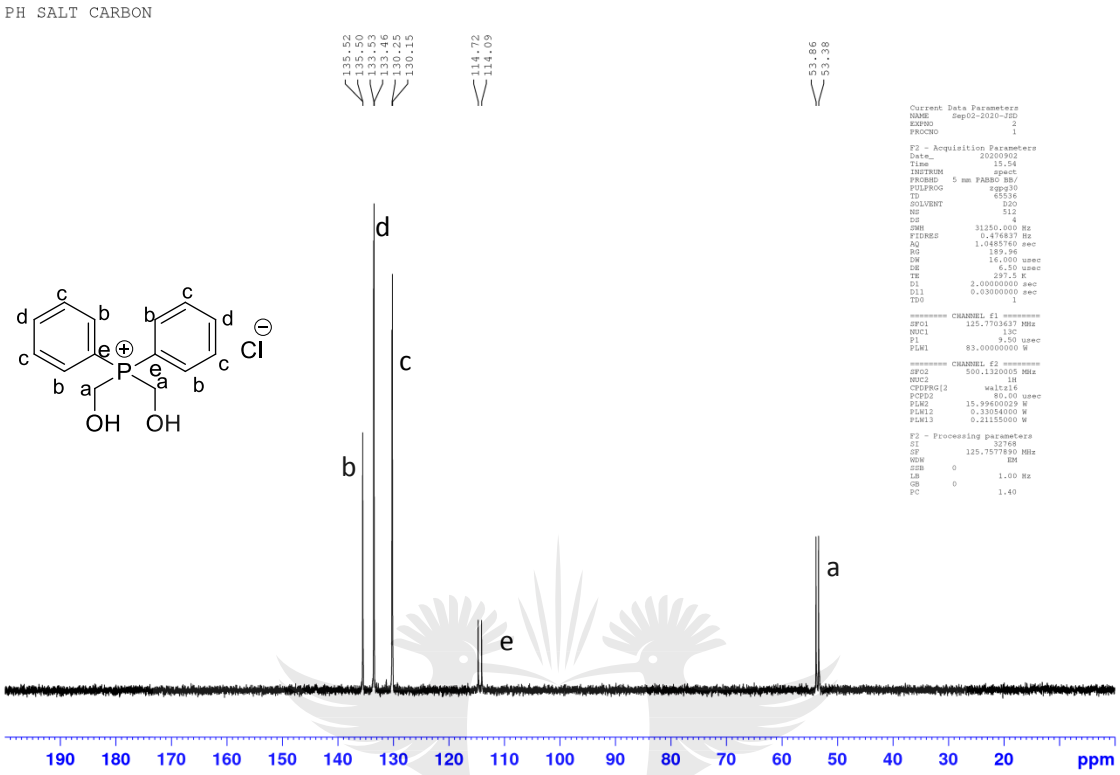

Figure A1: $^{13}C\{^{1}H\}$NMR of HBA 1 recorded in D_2O

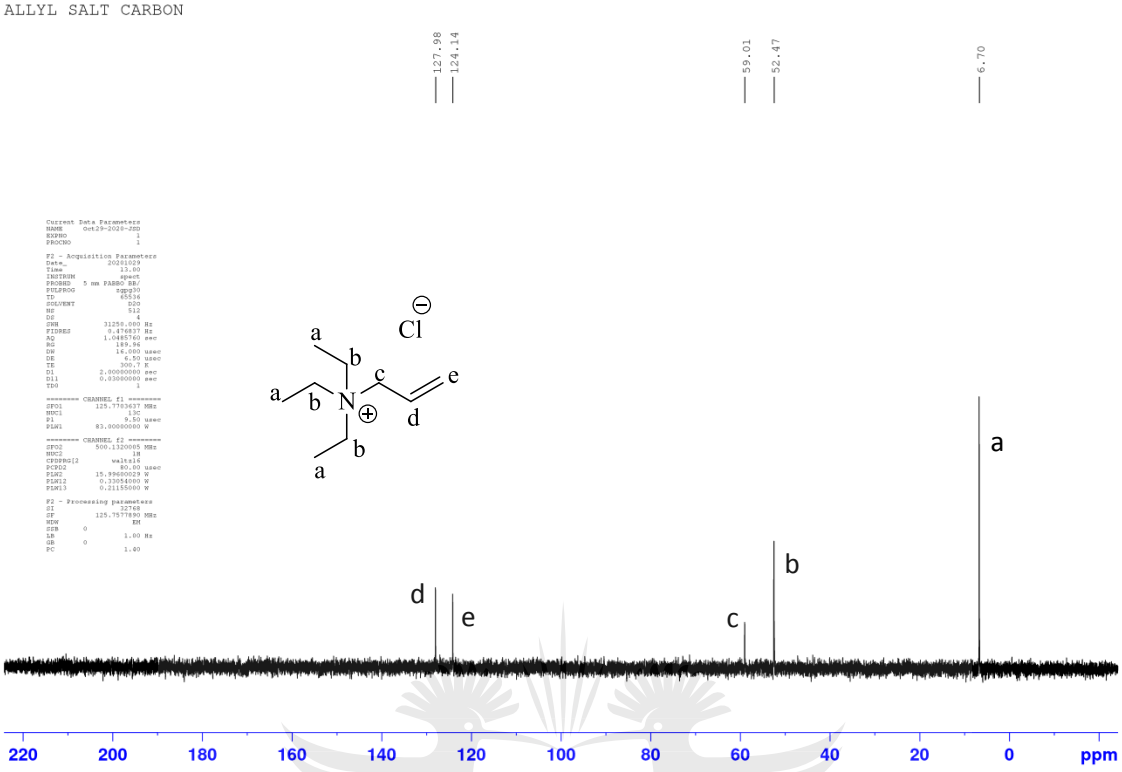

Figure A2: ^{13}C-{^{1}H}-NMR of HBA 2 recorded in D_2O

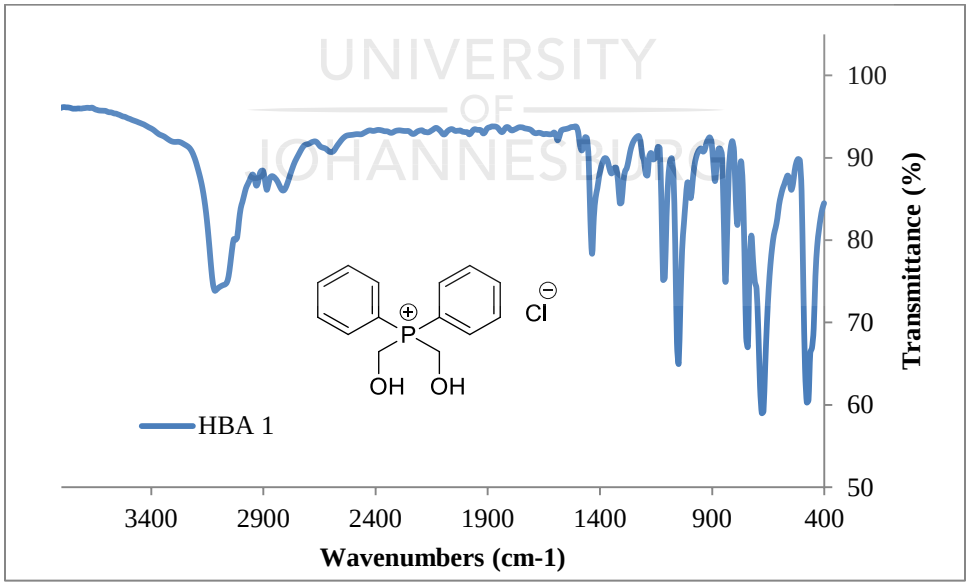

Figure A3: FT-IR spectrum of HBA 1

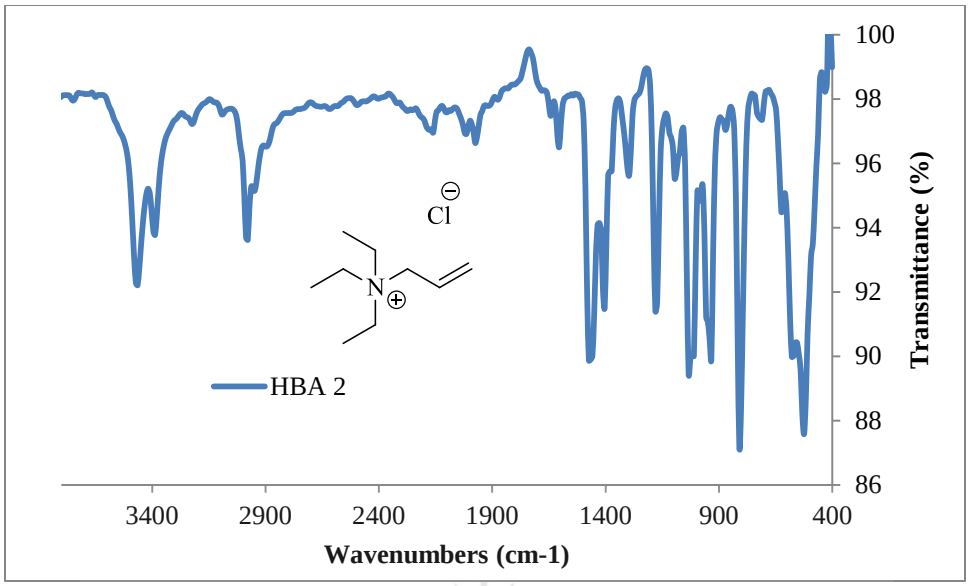

Figure A4: FT-IR spectrum of HBA 2

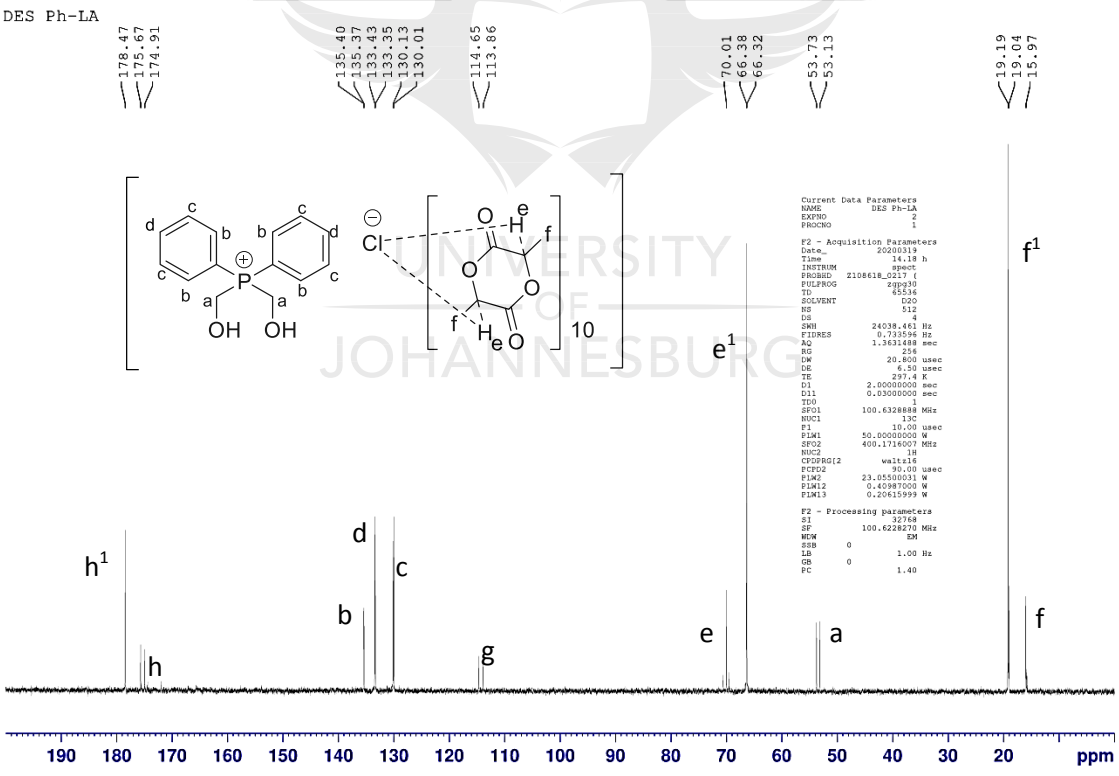

Figure A5: ^{13}C-{^{1}H}-NMR of DES 1 recorded in D_2O

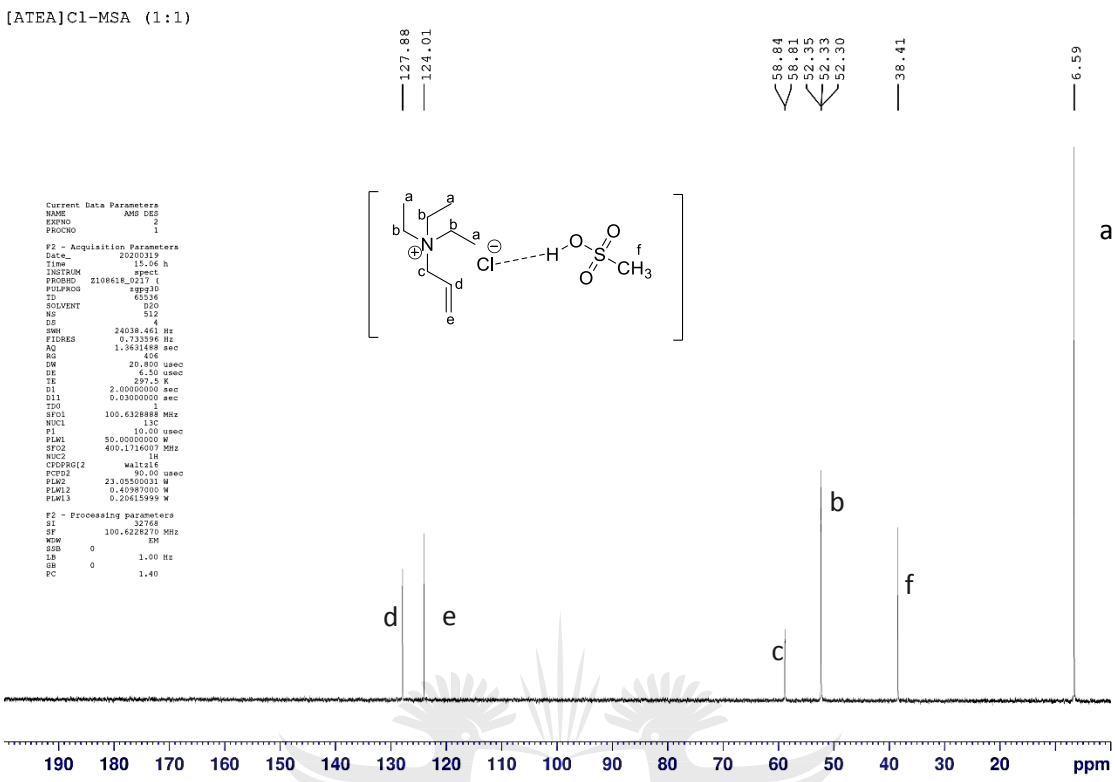

Figure A6: ^{13}C-{^{1}H}-NMR of DES 2 recorded in D_2O

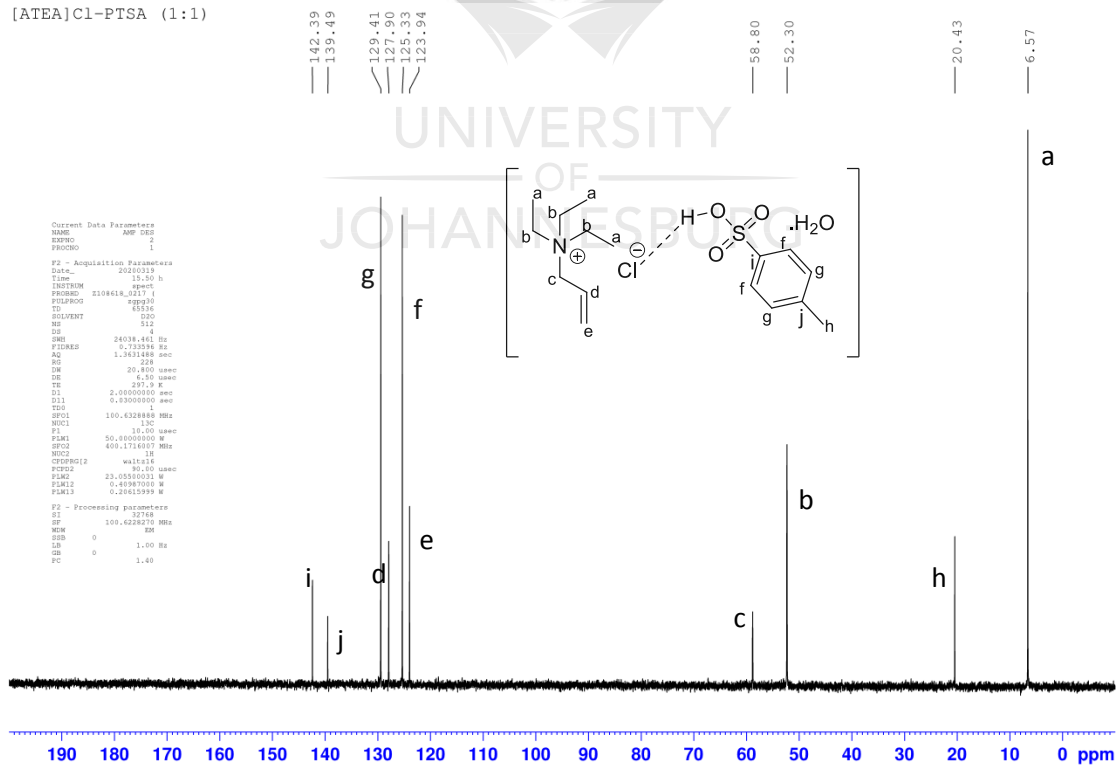

Figure A7: ^{13}C-{^{1}H}-NMR of DES 3 recorded in D_2O

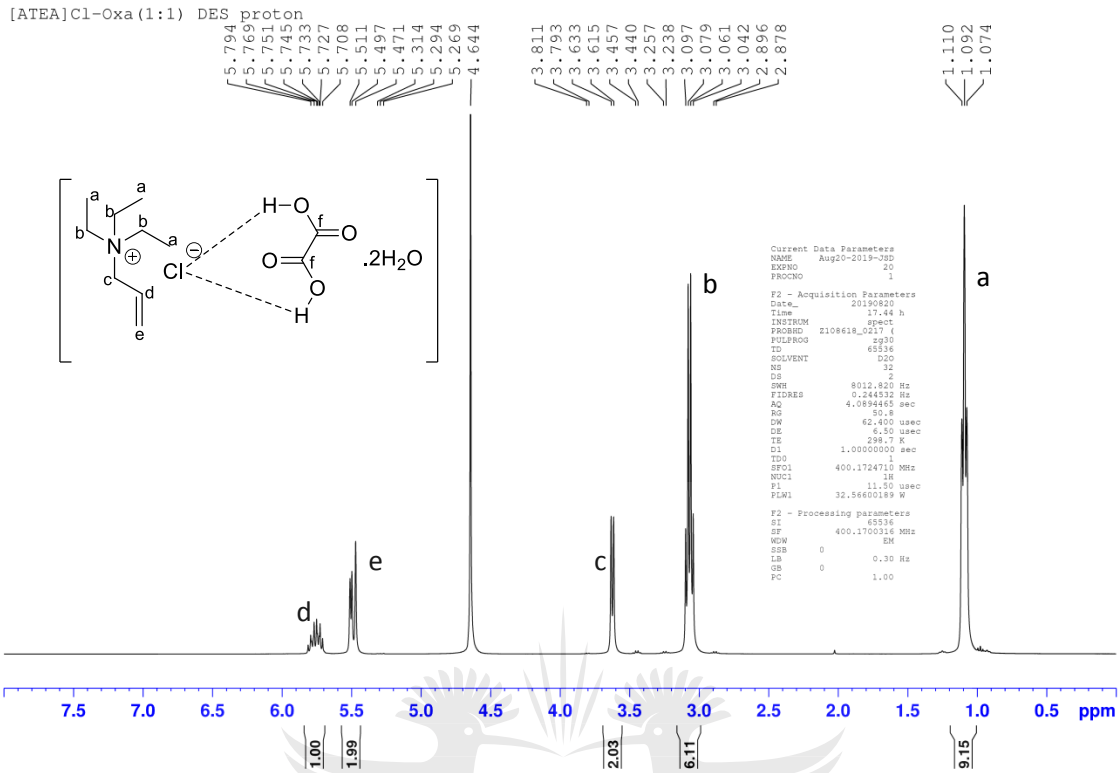

Figure A8: ^{1}H-NMR of DES 4 recorded in D_2O